Chem Soc Rev

REVIEW ARTICLE

View Article Online
View Journal | View Issue

Cite this: *Chem. Soc. Rev.*, 2026, **55**, 3380

Molecular innovations in nanofiltration *via* interfacial polymerization: from monomer design to membrane performance

Wenxing Cheng,†[a] Qipeng Zhao, †[ab] Huaqiang Chu,*[ab] Xuefei Zhou, [ab] Yalei Zhang *[abc] and Tai-Shung Chung *[de]

Membrane technology plays a crucial role in solving global water scarcity, where high-performance semipermeable membranes, such as nanofiltration (NF) membranes, are essential elements for efficient water treatment. The performance of NF membranes is largely determined by both the molecular structures of the monomers and the mechanisms of interfacial polymerization, which ultimately influence their permeability, selectivity, and stability. In recent years, significant progress has been made in the development of NF membranes using novel monomers. This review aims to provide a comprehensive overview on the synthesis methods for these novel monomers and NF membranes, with a particular emphasis on the modern interfacial polymerization techniques to fabricate NF membranes. We will also examine the detailed surface chemistry and structural characteristics of these novel membranes, elucidating the underlying mechanisms and sciences governing their separation performance. Finally, we will discuss the current challenges associated with the novel monomer-based NF membranes and offer potential solutions to develop next-generation NF membranes. By addressing these key aspects, this critical review may provide valuable insights to molecularly design novel NF membranes and to explore their applications in the field of wastewater treatment and resource recovery.

Received 20th October 2025

DOI: 10.1039/d5cs00787a

rsc.li/chem-soc-rev

[a] *State Key Laboratory of Water Pollution Control and Green Resources Recycling, College of Environmental Science and Engineering, Tongji University, Shanghai, 200092, China. E-mail: chuhuaqiang@tongji.edu.cn, zhangyalei@tongji.edu.cn*
[b] *Shanghai Institute of Pollution Control and Ecological Security, Tongji University, Shanghai, 200092, China*
[c] *College of Environment and Safety Engineering, Fuzhou University, Fuzhou, 350108, China*
[d] *Department of Chemical and Biomolecular Engineering, National University of, Singapore, 117585, Singapore. E-mail: chencts@nus.edu.sg*
[e] *Graduate Institute of Applied Science and Technology, National Taiwan University of Science and Technology, 10607, Taipei, Taiwan*
† These authors contributed equally to this work.

Wenxing Cheng

Wenxing Cheng received her Master's degree in Environmental Science and Engineering from Hunan University in 2024. She is currently pursuing a PhD at the School of Environmental Science and Engineering, Tongji University, under the supervision of Prof. Huaqiang Chu. Her research focuses on the development of high-performance nanofiltration membranes for water treatment.

Qipeng Zhao

Qipeng Zhao is an Associate Professor at Tongji University. He received his PhD degree in Chemical Engineering from National University of Singapore in 2016. In 2019, he worked as a postdoctoral research fellow in Prof. Tai-Shung Chung's group, followed by joining Tongji University in 2024. His research focuses on developing reverse osmosis and nanofiltration membranes for applications in desalination and wastewater treatment.

Introduction

Water is essential for the growth of all terrestrial organisms, intricately tied to human survival and ecological sustainability. However, rapid urbanization and industrialization have led to severe water pollution and clean water shortages.[1,2] Hence, it is imperative to develop advanced and efficient technologies to address these challenges. Innovative approaches leveraging advanced functional materials have been extensively explored for water purification and resource recovery, particularly through membrane-based separation and adsorption.[3] Membrane separation technology has emerged as a leading solution for seawater desalination and wastewater treatment due to its cost-effectiveness, energy efficiency, environmental sustainability, small footprint, minimal secondary pollution, and long-term durability.[4–12]

Generally, depending on pore sizes and separation mechanisms, membranes for water use and seawater desalination can be classified as microfiltration (MF) membranes,[13] ultrafiltration (UF) membranes,[14] reverse osmosis (RO) membranes,[15–20] and nanofiltration (NF) membranes.[11] Among them, NF membranes have recently gained the most prominence due to their unique and important applications as a result of possessing distinctive surface properties (*e.g.* contact angle, roughness, and charge) and structural properties (*e.g.* thickness, porosity, and pore size) (Fig. 1). These characteristics endow NF membranes with excellent separation performance and broad environmental adaptability under relatively low operating pressures compared to RO, owing to the key separation mechanisms (*e.g.* size exclusion and the Donnan effect) (Fig. 1).[6] Although commercial NF membranes, such as NF90 and NF270, have been available for years, they often fail to meet the increasingly complex and dynamic requirements for industrial water recycling. Thus, many laboratory-developed NF membranes with superior separation properties have been explored under industrial demands. These new membranes were fabricated by various advanced techniques, such as layer-by-layer self-assembly,[21–25] surface graft polymerization,[26–29] phase inversion,[30–36] deposition,[37–39] and interfacial polymerization (IP) (Fig. 1).[40–44] Among them, IP is the most widely adopted method, typically involving the formation of an active layer *via* polycondensation reactions between aqueous-phase monomers (*e.g.* diamines) and oil-phase monomers (*e.g.* acyl chlorides) at their interface.[45] The newly invented NF membranes have

Huaqiang Chu

Huaqiang Chu is a Tenured Professor at Tongji University. He received his PhD in Municipal Engineering from Tongji University in 2010. He is a recipient of the National Science Fund for Excellent Young Scholars and the All-China Environment Federation Outstanding Young Scientist Award. His research focuses on membrane materials and near-zero liquid discharge technologies.

Xuefei Zhou

Xuefei Zhou is a Full Professor at the College of Environmental Science and Engineering, Tongji University. She received her PhD degree from the Harbin Institute of Technology in 2001. She was awarded the Leading Talent of Shanghai in 2021. Her research focuses on advanced wastewater treatment and resource utilization.

Yalei Zhang

Yalei Zhang is a Full Professor in Tongji University and also serves as Vice President of Fuzhou University. He received his PhD degree from Tongji University in 1999. He was awarded the National Science Fund for Distinguished Young Scholars in 2016. His research focuses on the development of functional materials and equipment for low-carbon resource recovery from wastewater.

Tai-Shung Chung

Tai-Shung Chung is a Jade Mountain Chair Professor in National Taiwan University of Science and Technology and an Emeritus Professor in National University of Singapore. He received his PhD degree from State University of New York, Buffalo in 1981. He was elected as the Fellow of Academy of Engineering Singapore in 2012 and granted the President's Technology Award (Singapore) in 2015. His research focuses on polymeric membranes for clean water, clear air, clear energy and pharmaceutical separation.

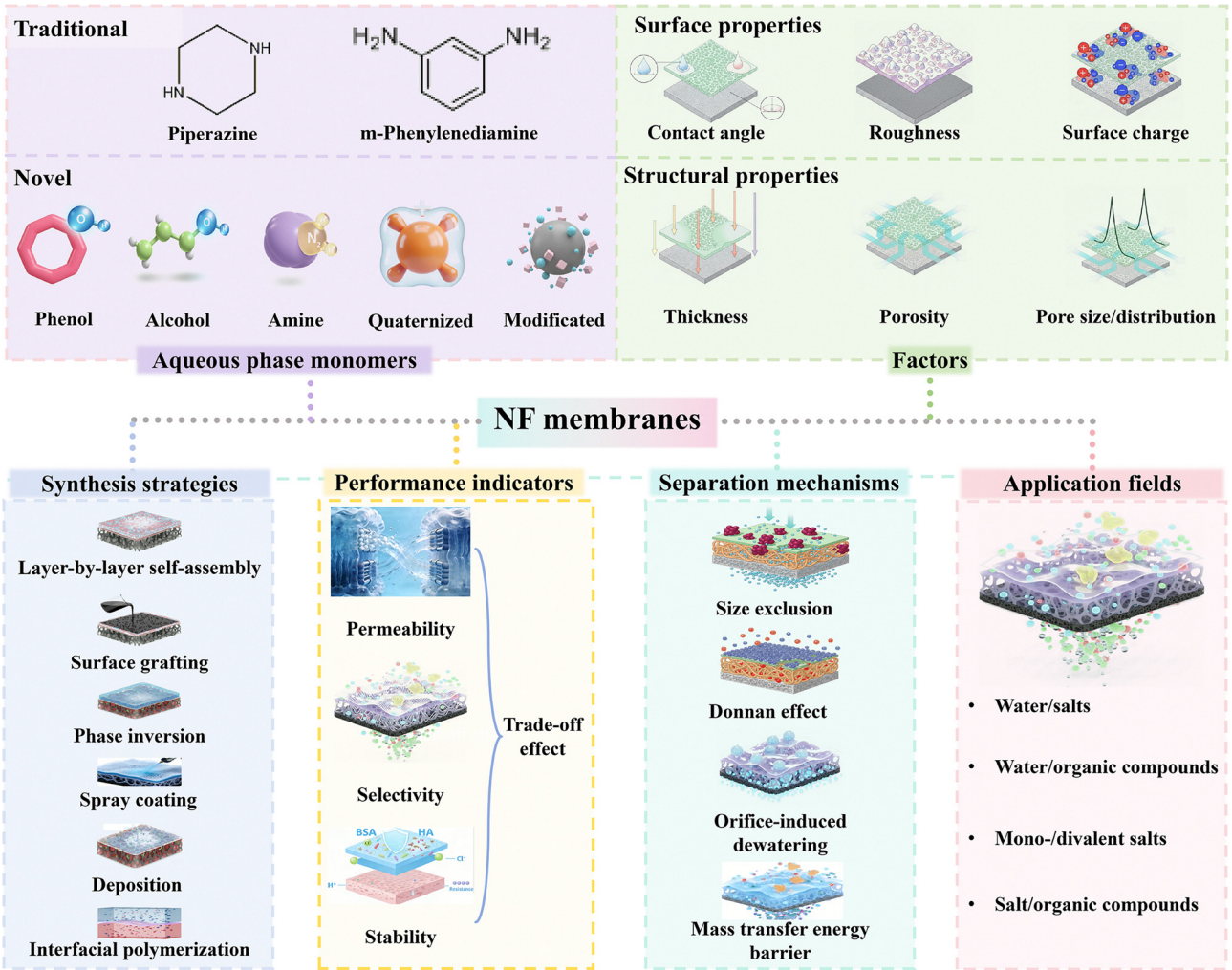

Fig. 1 The aqueous-phase monomers, physicochemical properties, synthesis strategies, performance characteristics, working mechanisms, and application fields of NF membranes.

shown improved permeability, selectivity, and stability because they were prepared by different aqueous-phase monomers, such as amine-based,[46–48] alcohol-based,[49–53] and polyphenol-based monomers from conventional monomers for IP reactions (Fig. 1).[54–57] Therefore, the design of NF membranes with novel monomers has gained global attention and provided a promising strategy to overcome the current limitations of NF membranes with enhanced performance for broader applicability.

To understand the research trend on novel monomer-based NF membranes, a literature search was conducted with the aid of Web of Science using keywords such as ''nanofiltration membrane'' and ''novel monomer'', from January 1, 2000, to December 31, 2025. The results indicate a consistent upward trend in the number of publications on novel monomer-based NF membranes over the years, confirming its importance as an emerging research hotspot (Fig. 2a). Thus, one can anticipate that NF membranes made from novel monomers will attract global attention in the coming years. Additionally, analyses on these publications reveal that research articles constitute most of the works (86.6%), while patents account for only 0.6%, implying that novel monomer-based NF membranes remain primarily at a laboratory stage with limited technological transfer to industrial applications. To further analyze the research themes, VOSviewer 1.6.18 software was employed to extract high-frequency keywords appearing more than 30 times across the 493 collected publications. Fig. 2b summarizes the superimposed visualization of research trends. The initial research phase was primarily focused on fundamental aspects of NF membranes, including ''water flux'', ''preparation'', ''salt rejection'', and ''characterization''. Subsequently, the research shifted towards monomer-based approaches, emphasizing on the preparation of thin-film NF membranes and the analysis of membrane permeability, with key terms such as ''novel'', ''trimesoyl chloride'', ''thin film'', and ''water permeability''. Recently, the focus was expanded to explore the selectivity of polyamide NF membranes in water treatment applications, highlighted by terms like ''monomer'', ''water treatment'', ''polyamide'', ''selectivity'', and ''separation''. These findings indicate that studies on NF membranes have been progressively expanded from basic performance evaluation to monomer-

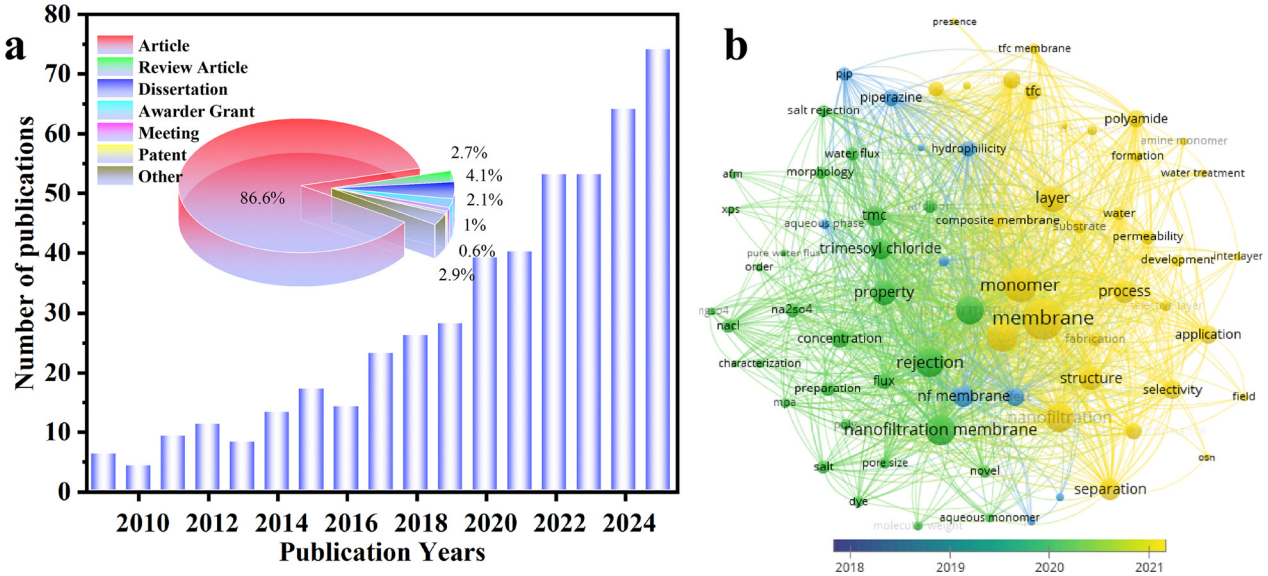

Fig. 2 Research status of NF membranes. (a) The number of publications and the proportion of different types of data from January 1, 2000, to December 31, 2025, as recorded in Web of Science. (b) Superimposed visualization of high-frequency terms in titles and abstracts using VOSviewer 1.6.18 (Note: Only terms occurring more than 30 times were included, but common terms such as "SEM, AFM, XPS, bar, and work" were excluded. The frequency of a term is indicated by the size of its corresponding bubble, whereas its color represents the time of emergence across all occurrences of the term.

driven membrane design and, ultimately, to application-oriented research. Several recent reviews have provided valuable insights.

Wang *et al.* systematically analyzed advancements of NF membranes over the past five years, with a particular focus on interface optimization, solvent/solute transport mechanisms, and solute selectivity.[6] Shao *et al.* reviewed the formation mechanisms of various wrinkled NF membranes and their correlation with enhanced water/solute transport.[7] Additionally, Yu *et al.* discussed the performance and mechanisms of intelligent stimuli-responsive NF membranes, highlighting their capabilities in solute separation, drug delivery, and removal of organic pollutants through microscopic structural changes.[9] Compared to novel monomers such as phenols, alcohols, and amines, which exhibit diverse types and complex molecular structures, traditional aqueous-phase monomers like *m*-phenylenediamine (MPD) and piperazine (PIP) possess relatively simpler molecular architectures. As a result, their roles in the IP process and their impact on membrane structure and performance have been more thoroughly elucidated, leading to a well-established understanding in the field. Although these reviews have provided detailed separation performance and mechanisms, they lack an in-depth assessment of how novel monomers influence the structural and surface properties of NF membranes. Recently, Wu *et al.* also investigated the impact of different monomer structures on the chemical properties of thin-film composite membranes.[46] However, the structural complexity of novel monomers, such as molecular weight, and the types and quantities of functional groups, directly influences critical parameters including their diffusion rate and reactivity during IP, thereby significantly affecting the structure and surface properties of the NF membrane's active layer. This multi-factorial coupling effect renders it highly challenging to derive generalizable structure–property relationships solely from comparisons of molecular designs among different novel monomers. Meanwhile, how and which novel monomers affect solvent/solute transport, anti-fouling properties, and chemical resistance to chlorine, acid, and alkali in NF membranes remain unclear. A systematic understanding of how novel monomers affect the separation mechanisms and which monomers influence membrane properties is essential to design advanced NF membranes. Therefore, the novel monomers discussed in this review specifically refer to those excluding the conventional aqueous-phase monomers such as PIP and MPD. More importantly, future efforts should focus on the development of structurally diverse novel monomer systems, coupled with precisely controlled preparation parameters, to enable more sustainable, environmentally benign, and cost-effective NF membrane fabrication pathways.

To comprehensively understand the latest advancements in NF membranes made from novel monomers, this review focuses on the critical roles and essential contributions of novel monomers in tailoring the pore structures (*e.g.* effective thickness, pore size distribution, porosity) and surface properties (*e.g.* hydrophilicity, chargeability, roughness). By examining the syntheses of novel monomers and IP regulation, this review may provide a systematic understanding of how these factors influence membrane performance. Specifically, Section 2 briefly outlines the design and synthesis strategies for novel monomers. Section 3 presents the preparation methods for novel monomer-based NF membranes. Section 4 comprehensively introduces the key approaches for regulating the IP process. Section 5 delves into the fabrication of novel monomer-based NF membranes *via* IP,

focusing on their performance in terms of permeability, selectivity, and stability across various environmental applications as well as the underlying mechanisms. Finally, the challenges and opportunities associated with novel monomer-based NF membranes will be discussed and the potential solutions to breakthrough performance limitations will be suggested. Overall, this review aims to provide critical insights and references to design advanced novel monomers for the development of high-performance NF membranes in the fields of wastewater reuse and recovery of high value-added substances.

Classification of novel monomers

Synthesizing novel monomers may open up applications of NF membranes for complex environments. Table 1 summarizes the advantages and applications of the developed custom-designed NF membranes utilizing novel monomers. Notably, these novel monomers, particularly aqueous-phase monomers, including non-synthetic novel monomers (*i.e.*, phenol-based, alcohol-based and amine-based) and synthetic novel monomers (*i.e.*, quaternized-based and modified-based), significantly influence the performance of the resultant membranes in terms of permeability, selectivity, and stability. Fig. 3 summarizes the key advantages of the five aforementioned types of novel monomers: (1) phenol-based monomers typically contain multiple benzene rings and phenolic hydroxyl groups (–OH), resulting in relatively high molecular weights and low diffusion rates during IP. Moreover, the low reactivity of the –OH groups leads to slower IP kinetics, favoring the formation of a loosely crosslinked active layer. Similarly, alcohol-based monomers, which also possess hydroxyl groups, exhibit limited reactivity and thus yield low crosslinking density, and structurally loose active layers. Notably, both phenolic-based and alcohol-based monomers are rich in hydrophilic –OH groups. Residual –OH groups within the active layer enhance the surface hydrophilicity of the membrane, thereby mitigating pollutant adhesion and deposition and improving anti-fouling performance. More significantly, the as-formed polyester-based active layer exhibits high resistance to chlorine attack, endowing the membranes with superior chlorine tolerance. (2) Amine-based monomers have relatively low molecular weights and are enriched with highly reactive amino groups ($-NH_2$), which exhibit high reactivity during IP and typically form active layers with a high crosslinking density and compact structure. However, the resulting polyamide networks are vulnerable to attack by chlorine species, leading to chain scission, and consequently, poor chlorine resistance. (3) Quaternary ammonium monomers, synthesized *via* quaternization reactions, possess permanent positive charges that significantly increase the positive charge density of the active layer. This enhanced charge density strengthens electrostatic repulsion, thereby improving the rejection of cationic solutes. (4) Functional group-modified monomers are a class of novel monomers generated through the partial or complete chemical transformation of one functional group into another. Current studies primarily focus on converting less reactive hydroxyl groups (–OH) into more reactive amino groups ($-NH_2$), which enhances monomer diffusion and accelerates IP kinetics. As a result, an active layer with optimal crosslinking density and well-defined pore structure can be achieved. In summary, monomers with varying functional group types and densities impart distinct structural characteristics and performance advantages to the active layer of NF membranes. Therefore, future research should focus on developing novel multifunctional monomers that incorporate multiple functional group architectures, enabling precise structural regulation and performance optimization of the active layer of NF membranes. Herein, we briefly introduce the synthesis strategies of novel monomers to illustrate how their structural characteristics impact performance across various applications.

Non-synthetic novel monomers

Given that the geometric structure and functional groups of novel monomers are critical factors determining the overall performance of NF membranes, a careful selection of suitable novel monomers is therefore essential for the development of advanced NF membranes with enhanced permeability and selectivity. In recent years, polyamide NF membranes prepared from interfacial polymerization of PIP or MPD with TMC have gained considerable attention. However, the inherently rapid and stochastic nature of the crosslinking process often leads to the formation of defective active layers, which are unable to meet the strict requirements for complex and diverse applications. Inspired by the success of PIP and MPD, a broad range of novel monomers containing phenol, alcohol, and amine functional groups have been employed to tailor the surface and structural characteristics of NF membranes. Therefore, a systematic overview of these monomers and their applicability for next-generation NF membranes is elaborated as follows.

Phenol-based monomers

Phenol-based novel monomers are monomers containing phenolic hydroxyl groups. Based on their origins, these monomers can be categorized into two main classes: natural polyphenols and other phenolic derivatives. So far, polyester NF membranes derived from phenolic monomers have been employed in the separation of (1) salt/organic compounds;[54,58,82] (2) monovalent/divalent salts;[76,83] and (3) organic solvent nanofiltration (OSN).[57,84] Driven by the growing emphasis on green and low-carbon approaches, environmentally friendly, non-toxic, and renewable monomers, particularly plant-derived polyphenol monomers, have been utilized to develop high-performance NF membranes. For example, the optimized QE-0.2/TMC-0.2 membrane, prepared from quercetin (QE) and TMC with NaOH regulation, exhibited a remarkable permeance ($\sim$198 L m^{-2} h^{-1} bar^{-1}) and a high NaCl/CR selectivity (123) (Fig. 4a).[54] The low reactivity of QE, combined with its abundant –OH groups, facilitated the formation of a hydrophilic, negatively charged and smooth thin active layer, which not only enhanced solvent distribution and transport but also enabled efficient solute retention.[54] Similarly, phlorotannin-TMC NF membranes synthesized by employing phlorotannins as the aqueous-phase monomer, which possessed abundant –OH groups

Table 1 Preparation and applications of novel monomer-based NF membranes

NF membrane (electrical properties)	Monomers	Novel monomer structure	Regulation strategies	Advantages	Separation	Ref.
QE-0.2/TMC-0.2 (−)	0.2 wt% quercetin, 0.2 wt% TMC	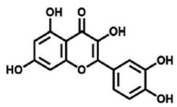	0.2 wt% NaOH	Enhanced hydrophilicity, permeability, and selectivity	Dye/salts	54
$St_{0.1}/TMC_{0.1}$-3 (−)	0.1 wt% stevioside, 0.1 wt% TMC	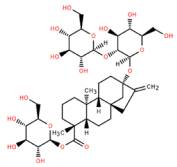	0.05 M NaOH	Enhanced porosity, hydrophilicity and selectivity	Antibiotic/salts	58
Ad-PA-NaOH (−)	0.055 wt% Ad, 0.1 wt% TMC		NaOH (pH = 12.5)	Enhanced porosity and pore size, improved permeability and selectivity	Dye/salts	59
Cyclen-TBB (+)	4.5 mM Cyclen, 6 mM TBB	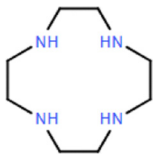	1 M NaOH	Enhanced hydrophilicity, with good permeability, selectivity and acid-alkali resistance	Dye/antibiotic	60
PA-Tg-0.06 (−)	0.06 wt% Tg, 0.1 wt% TMC	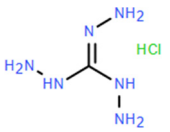	0.8 wt% NaOH	Reduced thickness, and enhanced hydrophilicity, negative charge, permeability, and selectivity	Cl^-/SO_4^{2}	61
M_{MPA} (−)	0.6 wt% MPIP, 0.1 wt% TMC	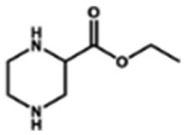	16 mM DTAB, NaOH (pH = 12)	Reduced thickness and pore size, and enhanced connectivity and porosity	Water/TrOCs	62
TET-TMC TFCM (+)	1 wt% TET, 0.3 wt% TMC	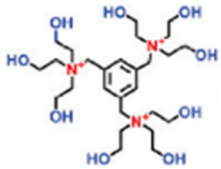	0.06 wt% SDS	Reduced pore size and porosity, and enhanced positive charge density, permeability and chlorine resistance	Li^+/Mg^{2+}	63
QSPIP-TMC TFCM (+)	0.5 wt% QSPIP, 0.1 wt% TMC	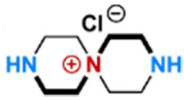	—	Enhanced porosity, positive charge density, permeability and chlorine resistance	Li^+/Mg^{2+}	64
GEM-TMC TFCM (+)	0.5 wt% GEM, 0.3 wt% TMC		pH = 11	Enhanced porosity, positive charge density and selectivity	Li^+/Mg^{2+}	65
PEI-TMC-DAIB TFCM (+)	1 wt% PEI, 0.3 wt% TMC, 2 wt% DAIB		NaOH (pH = 12)	Enhanced positive charge density, hydrophilicity and permeability	Li^+/Mg^{2+}	66
PEI-TMC-DHTAB (+)	0.5 wt% PEI, 0.3 wt% TMC, 0.5 wt% DHTAB	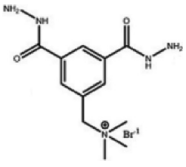	NaOH (pH = 11)	Enhanced positive charge density and selectivity	Li^+/Mg^{2+}	67
QEDTP NFM (+)	0.5 wt% PEI, 0.3 wt% TMC, 3 wt% QEDTP	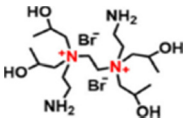	pH = 12	Enhanced positive charge density, permeability and selectivity	Li^+/Mg^{2+}	68
PIP-TMC-QAEP (−)	0.35 wt% PIP, 0.3 wt% TMC, 1 wt% QAEP	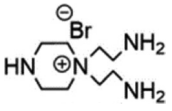	pH = 12	Enhanced hydrophilicity, selectivity, anti-fouling and antibacterial properties	Li^+/Mg^{2+}	69

Table 1 (*continued*)

NF membrane (electrical properties)	Monomers	Novel monomer structure	Regulation strategies	Advantages	Separation	Ref.
PEI-TMC-QTHIM (+)	1 wt% PEI, 0.3 wt% TMC, 2.0 wt% QTHIM	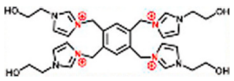	pH = 12	Enhanced positive charge density, permeability and selectivity	Li^+/Mg^{2+}	70
BBD-3 TFC (−)	0.5 wt% PIP, 0.3 wt% TMC, 3 wt% BBD	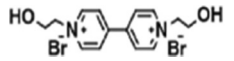	—	Enhanced hydrophilicity, negative charge density and antibacterial properties	Cl^-/SO_4^{2-}	71
PA-QTDEA (−)	0.5 wt% PIP, 2 wt% 4-dimethylaminopyridine, 3 wt% QTDEA	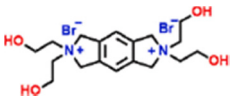	—	Enhanced porosity, hydrophilicity and selectivity	Antibiotic/salts	72
PA-TQTE (−)	0.5 wt% PIP, 0.3 wt% TMC, 3 wt% TQTE	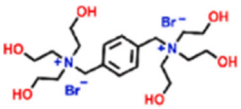	—	Reduced thickness and negative electrical properties, and enhanced hydrophilicity	Antibiotic/salts	73
β-CDA-TPC-0.1 (−)	0.1 wt% β-cyclodextrin, 0.1 wt% TPC	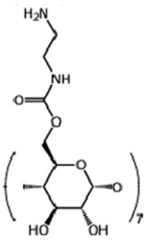	—	Reduced thickness and pore size, and enhanced permeability and selectivity	Ethanol/ cannabidiol oil	74
BAIE-TBB(M-0.1) (+)	0.5 wt% BAIE, 0.1 wt% TBB	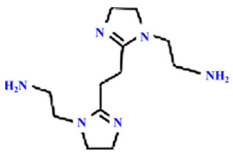	—	Excellent permeability, selectivity and antibacterial properties	Dye/salts	75
Polyarylate (DMAP) (−)	15.0 g L^{-1} BPPZ, 15.0 g L^{-1} TMC	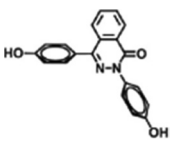	15.0 wt% DMAP	Enhanced hydrophilicity, permeability, chlorine resistance, and thermostability	Cl^-/SO_4^{2-}	76
TFC_{18C6} (—)	20.5 mM 18C6, 2.5 mM TMC	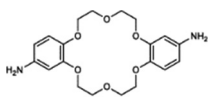	Hexane	Enhanced porosity, hydrophilicity, permeability, and selectivity	Water/ pharmaceuticals	77
LiOH-Am7CD-0.05 TMC (−)	1.23 wt% Am7CD, 0.05 wt% TMC	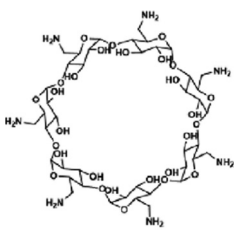	pH = 8.4	Reduced thickness and pore size, and enhanced selectivity	Li^+/Mg^{2+}	78
NF-TPEI (−)	0.075 wt% TPEI, 0.15 wt% TMC	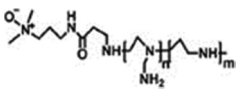	—	Enhanced hydrophilicity, pore size, permeability, selectivity and anti-fouling	Dye/salts	79
TFC-SPVA (−)	2 wt% SPVA, 0.35 wt% TMC	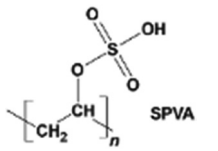	2 M NaOH (pH = 12)	Reduced pore size, and enhanced hydrophilicity, negative charge density, permeability, selectivity, chlorine resistance and anti-fouling	Dye/salts	80
$PE\text{-}PSA_{10000}$ (−)	10 g L^{-1} PEI, 1.5 g L^{-1} NTSC	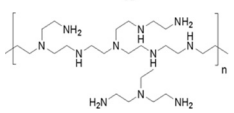	—	Excellent acid resistance	Water/salts	81

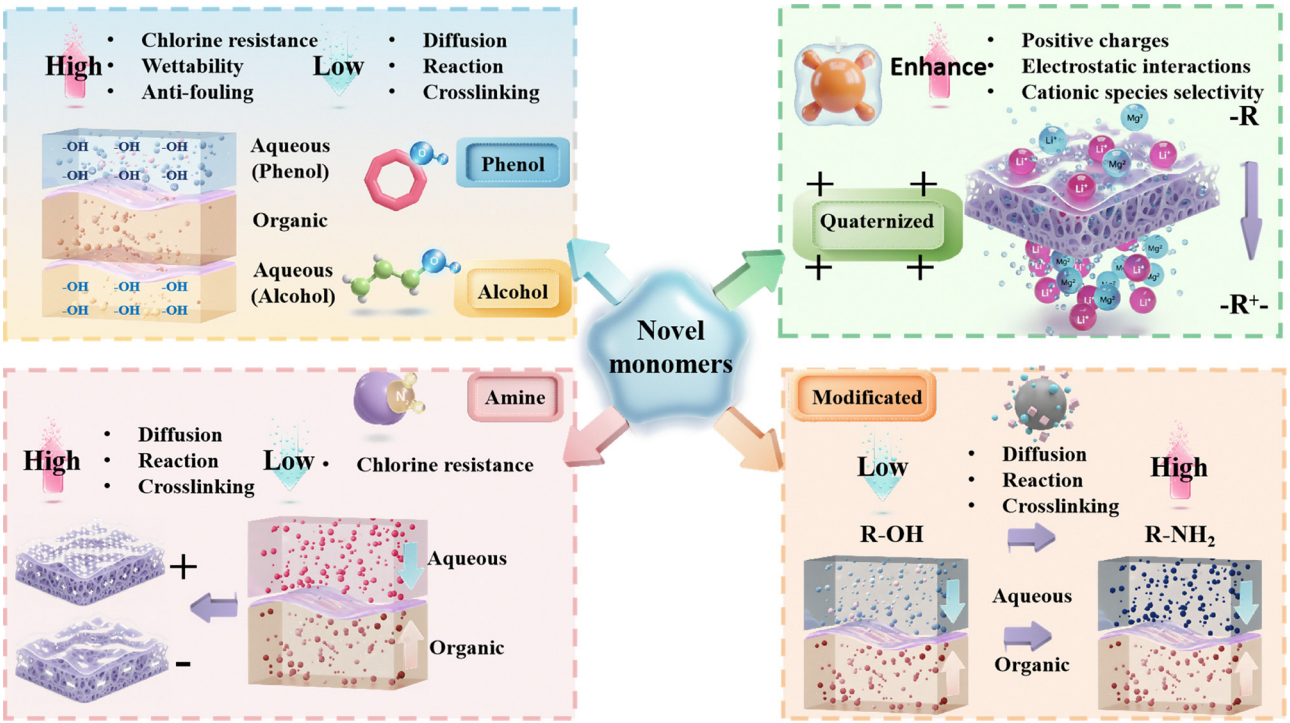

Fig. 3 Key advantages of novel monomers derived from phenolic, alcoholic, amine, quaternary ammonium, and functionally modified groups.

and a twisted biphenyl structure, exhibited a methanol (MeOH) permeance of 10.1 L m^{-2} h^{-1} bar^{-1} and superior rejection capabilities for acid blue 25, Na_2SO_4, and various antibiotics (*e.g.* tetracycline) (Fig. 4b).[57] This was attributed to the smooth surface, high hydrophilicity, high porosity, and negatively charged characteristics of the active layer.[57] Notably, due to the relatively low reactivity of phenolic –OH groups, deprotonation using alkali was essential to increase the reactivity of polyphenolic monomers during IP, enabling enhanced hydrophilicity and negative charge.

In addition to natural polyphenols, synthetic phenolic compounds have also been employed in the fabrication of polyester NF membranes, such as 4,4′-(1-phenylethylidene)bisphenol (PEPB), 4,4′-dihydroxydiphenylmethane (DHDP), *N*-methyl-2-pyrrolidone (NMP), bisphenol A (BPA), and tetramethyl-1,1′-spirobisindane-6,6′diol (SBI).[84] Specifically, the optimized membrane Mem-NaOH-4, prepared *via* activation with SBI and dimethylformamide (DMF), demonstrated a remarkable solvent permeance (DMF: 21.5 L m^{-2} h^{-1} bar^{-1}) and CR rejection rate (94.7%) (Fig. 4c).[84] This superior performance could arise from the enhanced dissolution of the structurally distorted monomer (SBI) facilitated by NaOH, which promoted the formation of an active layer with high porosity, while the efficient rejection of negatively charged dyes was achieved through the Donnan effect (*i.e.*, electrostatic repulsion).[84] In another example, lantern[33]arene, a cage-like oligomer featuring a large macrocyclic cavity and abundant –OH, was employed to construct a hydrophilic intermediate layer for the fabrication of 1L-PA NF membranes.[85] The modified membrane exhibited a Na_2SO_4 rejection rate comparable to that of the pristine membrane, exceeding 99%, while its permeance significantly increased by 28.9 L m^{-2} h^{-1} bar^{-1} relative to the original membrane (10.4 L m^{-2} h^{-1} bar^{-1}), reaching a high value of 39.3 L m^{-2} h^{-1} bar^{-1}.[85] Furthermore, the membrane demonstrated excellent antifouling performance with a flux recovery rate of 96.2% and maintained stable operation over an 8-day continuous filtration test, indicating robust long-term durability.[85] The remarkable enhancement in permeability was primarily attributed to the macrocyclic cavity structure of lantern[33]arene, which enhanced pore connectivity within the polyamide active layer. Simultaneously, the abundant surface –OH groups not only promoted selective adsorption and enrichment of PIP at the intermediate layer interface *via* hydrogen bonding but also elevated the negative charge density on the membrane surface. These effects synergistically regulated the IP process, leading to the formation of a thinner, more uniform, and highly hydrophilic selective layer.[85] By leveraging a functional monomer that integrates well-defined cavities and hydrophilic moieties to engineer a hydrophilic interlayer, this strategy provides an effective approach to overcoming the intrinsic permeability–selectivity trade-off in NF membranes.

Overall, alkali can be employed to modulate the IP reaction when using polyphenolic monomers containing highly hydrophilic functional groups (–OH). This approach enables the customization of active layers with enhanced hydrophilicity and negative charge, facilitating the separation of specific solvent/solute systems.

Alcohol-based monomers

Alcohol-based novel monomers are monomers comprising hydroxyl groups (–OH) attached to the aliphatic groups, such

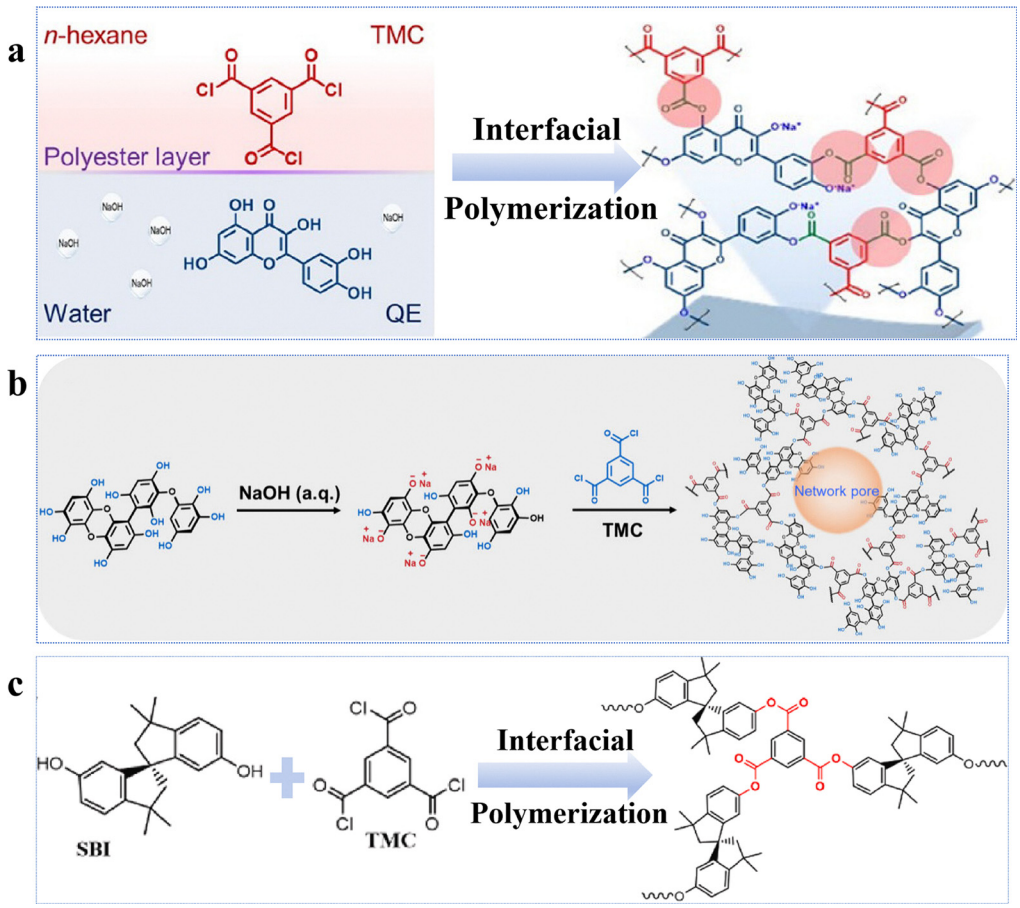

Fig. 4 NF membranes made from phenol-based monomers. (a) Synthesis of the QE-0.2/TMC-0.2 NF membrane. Reproduced with permission from ref. 54. Copyright 2022, American Chemical Society. (b) Synthesis of the Phlorotannins-TMC NF membrane. Reproduced with permission from ref. 57. Copyright 2025, American Chemical Society. (c) Synthesis of the Mem-NaOH-4NF membrane. Reproduced with permission from ref. 84. Copyright 2023, Elsevier.

as cyclodextrin, polyvinyl alcohol, maltitol, and their derivatives. Similar to phenolic monomers, alcohol-based monomers, owing to their low reactivity of –OH groups, can effectively slow down the reaction rate of IP, thereby enabling the fine-tuning of the microstructure of the active layer. Cyclodextrin (CD), a cyclic alcoholic compound, consists of a hydrophobic inner cavity and a hydrophilic outer surface, allowing it to possess unique molecular recognition capabilities and chemical modifiability for surface modifications and structural customization of high-performance NF membranes.[74,86,89–94] For example, the β-CD/Ma_3 membrane fabricated by incorporating β-CD and mannitol into the aqueous phase showed (1) a remarkable permeance of 30.2 L m^{-2} h^{-1} bar^{-1}; (2) impressive anti-fouling capability with a flux recovery rate of 97.2% after three cycles; (3) superior chlorine resistance to withstand 144 000 ppm h NaClO; and (4) a high Na_2SO_4 rejection of 91.7% (Fig. 5a).[86] These enhanced properties arose from the following factors: (1) the large cavity and –OH groups of β-CD imparted the active layer with high porosity and hydrophilicity to augment both permeability and anti-fouling performance; (2) mannitol promoted the densification of the active layer, thereby improving the membrane's retention performance; and (3) the presence of ester groups in the active layer provided effective resistance against chlorine attack.[86] In addition to the cyclic alcohol, linear-chained alcohols have also been explored as aqueous-phase monomers. Polyvinyl alcohol (PVA), a polymeric alcohol characterized by its excellent hydrophilicity, stability, film-forming ability, and environmental friendliness, has been widely employed for NF membranes.[51,87,95–99] For example, the PE-PVA97 loose NF membrane synthesized with NaOH regulation exhibited an outstanding permeance of 44.9 L m^{-2} h^{-1} bar^{-1} and a separation factor of 240 for CR/Na_2SO_4 separation (Fig. 5b).[87] The impressive performance resulted from (1) the smooth and hydrophilic active layer; and (2) its relatively larger pore size and stronger negatively charged surface.[87] Similarly, maltitol (ML), a branched alcohol, has also been utilized to design NF membranes.[53,88] Owing to the smooth, hydrophilic and negatively charged surface, the ML-1.0/TMC membrane had an exceptional permeance of 104.9 L m^{-2} h^{-1} bar^{-1}, a high separation factor of 340 for CR/NaCl separation, and excellent anti-fouling performance with a flux recovery rate of >86% after two cycles (Fig. 5c).[88]

Overall, the alcohol-based NF membrane possesses a smooth, hydrophilic, and negatively charged active layer. These properties

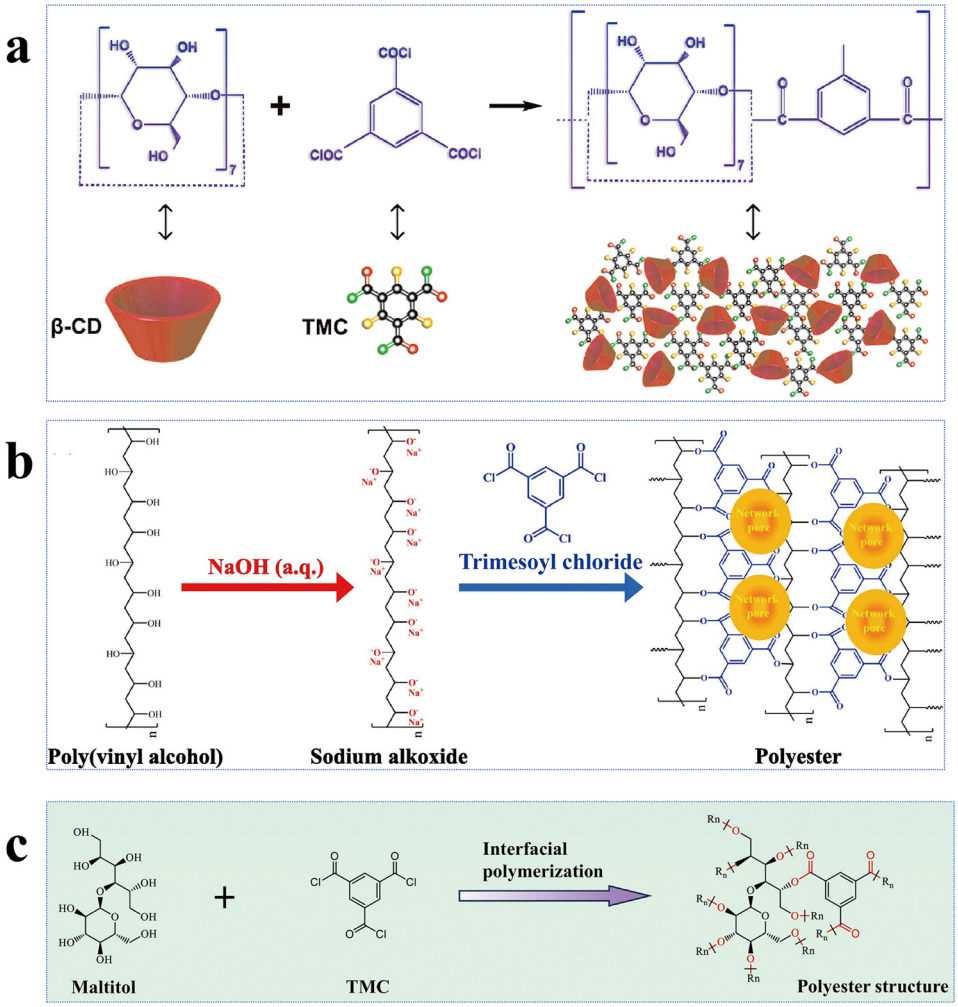

Fig. 5 Alcohol-based monomer NF membranes. (a) The IP process of the β-CD/Ma_3 membrane. Reproduced with permission from ref. 86. Copyright 2023, Elsevier. (b) The IP process of the PE-PVA97 LNF membrane. Reproduced with permission from ref. 87. Copyright 2024, Elsevier. (c) The IP process of the ML-1.0/TMC membrane. Reproduced with permission from ref. 88. Copyright 2024, Elsevier.

synergistically enhance water permeation, minimize adhesion of contaminants, and effectively reject negatively charged solutes with larger molecular weights.

Amine-based monomers

Amino monomers are monomers containing primary and secondary amine, and guanidine groups. Except for the conventional MPD and PIP, diverse amine-based monomers have been explored, including polyethyleneimine (PEI),[103–106] PIP-COOH,[107,108] 1,4-cyclohexanediamine (CHDA),[109] amino acids,[102,105] and triethylenetetramine (TETA).[26] Compared to phenolic and alcoholic monomers, amine monomers induce significantly higher reactivity during IP, enabling the formation of an active layer with a higher degree of crosslinking. However, this also leads to a rapid stacking of disordered polymer chains and forms a thick and dense active layer that causes a trade-off between permeability and selectivity. To address this challenge, non-planar structured amine monomers, characterized by low diffusivity and high steric hindrance, can be utilized to effectively minimize the tightly packed chains and optimize the microstructure of the active layer. 1,4,7,10-Tetraazacyclododecane (Cyclen) is a good example which has a symmetrical macrocyclic structure composed of four secondary amine (–NH–) groups and a 12-membered ring skeleton. As a result of its highly reactive amine groups and inherent structural hindrance, a porous active layer can be created in the resultant NF membranes.[100,110] For instance, the Cyclen-TMC membrane exhibited a remarkable permeance of >39 L m^{-2} h^{-1} bar^{-1} and high selectivities of 22.2 and 955 for the separation of methyl blue/NaCl and tetracycline/NaCl, respectively (Fig. 6a).[100] In addition to Cyclen, adamantane-1,3-diamine (Ad), possessing a rigid polyhedron molecular structure, was used as a monomer to regulate the microstructure of the active layers by reducing the dense packing of the polymer chains through the effect of steric hindrance.[59] Notably, after a NaOH treatment, the pore size was further enlarged due to the hydrolysis of the amide bonds. Consequently, the resulting membrane had an exceptional permeance of 87.7 L m^{-2} h^{-1} bar^{-1}, a high selectivity of 735 for Na_2SO_4/evans blue, and excellent anti-fouling performance with a flux recovery rate of 90.7% after three cleaning cycles (Fig. 6b).[59]

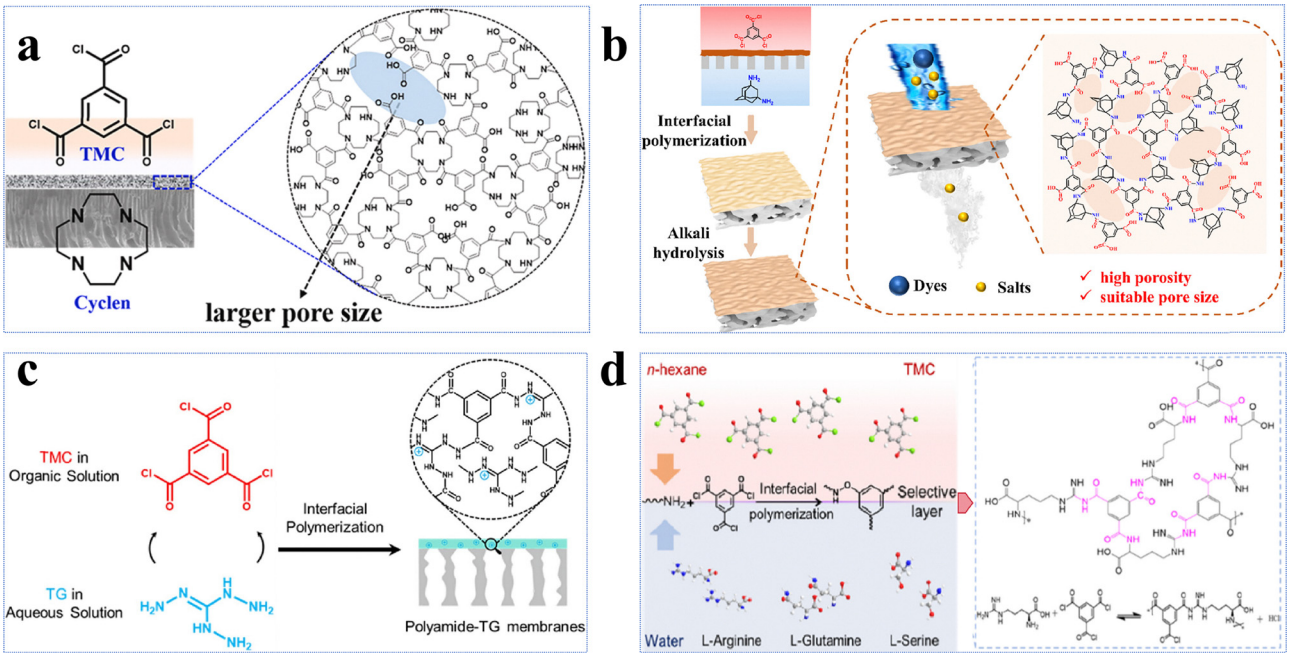

Fig. 6 Amine-based monomer NF membranes. (a) Preparation of the Cyclen-TMC membrane. Reproduced with permission from ref. 100. Copyright 2023, Elsevier. (b) Preparation of the Ad-PA-NaOH membrane. Reproduced with permission from ref. 59. Copyright 2024, Elsevier. (c) Preparation of the polyamide-TG-8 membrane. Reproduced with permission from ref. 101. Copyright 2022, Elsevier. (d) Preparation of the Arg-0.02/TMC-0.2 membrane. Reproduced with permission from ref. 102. Copyright 2023, Elsevier.

Triaminoguanidine (T_g) is another example with a unique structure consisting of three primary amine groups (–NH_2) and one guanidine group (–NH–C(NH)–NH_2). It has been employed in the fabrication of NF membranes for the separation of mono-/divalent salts.[61,101,111,112] Although the polyamide-TG-8 membrane had a relatively low permeance of 1.4 L m^{-2} h^{-1} bar^{-1}, it exhibited an exceptionally high Li^+/Mg^{2+} selectivity of ~83 (Fig. 6c).[101] This arose from the fact that the high polarity of the guanidine groups facilitated the formation of a smooth and hydrophilic active layer with a contact angle of 62.7°, while its relatively thick active layer with an extremely small pore size of 0.35 nm resulted in high resistance for water transport.[101] On the other hand, its positively charged active layer (*i.e.*, +9.5 mV) and unique pore size just between Li^+ (0.34 nm) and Mg^{2+} (0.43 nm) allowed for Li^+ passage while rejecting Mg^{2+} through the combination of the Donnan effect and size exclusion, leading to a high selectivity.[101]

Amino acids, characterized by the presence of both –NH_2 and carboxyl (–COOH) groups, have been effectively employed to design novel NF membranes (Fig. 6d).[102] Among all, the Arg-0.02/TMC-0.2 membrane showed remarkable performance, achieving a high water permeance of 130.4 L m^{-2} h^{-1} bar^{-1}, an exceptionally high selectivity of 227.5 for Na_2SO_4/CR, and outstanding anti-fouling properties with a flux recovery rate of ~90% after three cleaning cycles.[102] This impressive performance resulted from (1) the formation of a loose active layer with a moderate pore size of 1.3 nm by regulating the pH value of L-arginine (Arg) aqueous solutions; and (2) the enhanced hydrophilicity and negative charge (*i.e.*, approximately −30 mV) of the active layer induced by hydrophilic functional groups of Arg.[102]

Overall, the aforementioned diverse amine monomers, each possessing distinct structural advantages, can effectively modulate the surface and physicochemical properties of the active layer to effectively separate the targeted solutes.

Synthetic novel monomers

Given the critical role of novel monomers in determining the structural features and physicochemical properties of the active layer in NF membranes, it is essential to understand their synthetic methods and processes. The novel monomers can be synthesized by means of quaternization and modification of functional groups. Specifically, the former primarily aims to enhance the positive charge density of the monomers, while the latter seeks to improve the reactivity. To effectively separate the targeted solvents/solutes, appropriate strategies should be employed to specifically design the novel monomers with the desired properties to produce NF membranes with superior performance for the recovery of valuable compounds during wastewater reuse.

Quaternization of monomers

Monomer quaternization is a crucial technique to synthesize targeted monomers with specific and superior performance. This process involves converting tertiary amines in precursor monomers into quaternary ammonium groups with a general formula of $R_4N^+X^-$ using alkyl or aryl halides. The resulting quaternized monomers typically carry a positive charge (Table 2). For example, triethanolamine, *N*-methyldiethanolamine, and *N*,*N*-dimethylethanolamine are tertiary amine monomers containing one nitrogen atom and various numbers of hydroxyl

Table 2 Surface and structural properties of novel monomer-based NF membranes

	NF membrane	CA (°)	Roughness (nm)	Zeta potential (mV)	IEP	Thickness (nm)	Pore size (nm)	MWCO (Da)	Permeance (L m^{-2} h^{-1} bar^{-1})	Rejection (%)	Ref.
Monovalent and divalent salts	TET-TMC TFCM	78.3	5.6	+4.0	7.4	60	0.26	389	17.3	$MgCl_2$ 99.5, Na_2SO_4 89.2, and LiCl 27	63
	QSPIP-TMC TFCM	34	4.8	−7.0	6.0	45	0.61	626	22	$MgCl_2$ 93 and LiCl 30	64
	PEI-TMC-DAIB TFCM	39.8	6.4	+13	8.9	95	0.4	672	26.4	$MgCl_2$ 95.8 and LiCl 34.2	66
	PEI-TMC-DHTAB	—	17.5	+58.2	10.2	79	0.23	583	6	$MgCl_2$ 99.2, Na_2SO_4 72, $MgSO_4$ 98, and LiCl 64.2	67
	PEI@DA18C6-PA	45	7.7	+5.1	—	110	0.64	400	10.4	$MgCl_2$ 96.3, $MgSO_4$ 80, Na_2SO_4 40.9, NaCl 51.4, and LiCl 43.4	104
	QEDTP NFM	70	2.5	+28	8.4	100	0.53	508	21.2	$MgCl_2$ 95.8, Na_2SO_4 40.8, and LiCl 55.5	68
	GEM-TMC TFCM	36.6	27.8	+10	8.0	14	0.54	394	19.2	$MgCl_2$ 94.8 and LiCl 40	65
	EDA@PEI-TMC(M-4)	42	16.1	+23	8.2	15.2	0.54	—	5.4	$MgCl_2$ 99.2 and LiCl 36.7	241
	BAIE-TMC(M-0.5)	41.7	33	−12.8	—	57.8	0.39	288	9.7	$MgSO_4$ 94.7, Na_2SO_4 94.0, $MgCl_2$ 88.4, NaCl 21.1, and LiCl 19.3	242
	PEI-TMC-QTHIM	85.6	9	+5	8.1	131	—	—	33	$MgSO_4$ 41, Na_2SO_4 23, $MgCl_2$ 92.2, NaCl 45.5, and LiCl 46.0	70
	BBD-3 TFC	22.1	14.3	−37	3.2	209	0.64	—	31.6	$MgSO_4$ 92.5 and Na_2SO_4 96.1	71
	PIP-TMC-QAEP	38	29.2	−15	5	190	—	—	16.1	$MgSO_4$ 94.2, Na_2SO_4 97.8, $MgCl_2$ 46.9, and NaCl 16.1	69
	LiOH-Am7CD-0.05 TMC	—	—	−35	4.1	29	0.33	—	3.9	$MgSO_4$ 99.3, Na_2SO_4 99.5, $MgCl_2$ 97.6, NaCl 55.2, and LiCl 55	78
	PNIPAM-PA	38.5	37.3	−30	3.6	96.5	—	350	18.2	$MgSO_4$ 96, Na_2SO_4 98, and NaCl 47	184
	DPC@PEI–TMC–1	58.4	35.2	+27.1	9.7	202.5	0.51	516.6	37.3	Na_2SO_4 97.5, $MgCl_2$ 95.8, LiCl 21.3, and NaCl 19.2	243
	PSF-150A-PA	47.3	44.6	−29.7	3.8	31.1	0.11	282	36.1	$MgCl_2$ 96.7 and LiCl 12.7	244
	HPIP NFMs	54	12.9	−9	3	64	0.55	361	14.5	Na_2SO_4 97.5 and NaCl 9.8	245
	Polyarylate (DMAP)	66	7.4	−36	—	87	0.76	920	10.3	Na_2SO_4 93.6	76
	AMTHBA0.25-PAR/PAF/PS	26	17.2	−10	6	208	—	—	25.8	$MgSO_4$ 98.3, Na_2SO_4 98.4, $MgCl_2$ 98.1, and NaCl 18.8	83
	PA-Tg-0.06	25.6	3.8	−68.7	—	55	—	—	12.5	$MgSO_4$ 96.1, Na_2SO_4 99.2, $MgCl_2$ 42.3, and NaCl 42.1	61
	FPA/PES NF	86	3.2	−37	4.8	150	1.31	680	1.1	$MgSO_4$ 71.2, Na_2SO_4 92.6, $MgCl_2$ 39.3, and NaCl 45.9	246
	NF-D	—	—	−92	2	114.3	0.89	1000	10.0	$MgSO_4$ 62, Na_2SO_4 97, $MgCl_2$ 19, and NaCl 65	247
	PA/nylon-M3	35	71.2	−20	5.1	48	0.39	279	33.1	$MgSO_4$ 98, Na_2SO_4 99.2, $MgCl_2$ 62, and NaCl 33	112
	TPT-TMC/PSf TFC	—	—	−28	3.5	35.1	—	—	8.7	$MgSO_4$ 97.0, Na_2SO_4 98.6, and NaCl 40.5	248
Monovalent and divalent salts	QNFM	22.5	53.8	0	7.0	130	0.4	790	51	$MgSO_4$ 81.3, Na_2SO_4 91, $MgCl_2$ 86.7, and NaCl 12.5	162
	$(RCC2_{0.2}\text{-TPC})_5$	60	3.2	−52	3.7	60	0.69	498	9.4	Na_2SO_4 97, $MgCl_2$ 22.8, NaCl 24.9, and LiCl 19.1	249
	$(RCC2_{1.0}\text{-TPC})_5$	62	3.4	−30	4.8	96	0.66	352	3.1	Na_2SO_4 98.6, $MgCl_2$ 93.8, NaCl 42.4, and LiCl 35.1	249
	PANoria(2)/(20)	28.4	30.3	−33.6	—	32	0.62	696	14.5	$MgSO_4$ 92.2, Na_2SO_4 98.6, $MgCl_2$ 36.8, and NaCl 24.8	161
	AEP/TMC = 240	45.2	2.5	+2	7.2	90	0.5	540	7.8	$MgCl_2$ 93.5, Na_2SO_4 65.7, and NaCl 35.2	250
	$M\text{-}E_{1+2}$	—	—	+5.1	—	—	0.54	608	34.3	$MgCl_2$ 97.7 and LiCl 41.2	251
Organic compounds	TFC_{18C6}	60	7.9	—	—	24.1	0.34	194.2	7.2	2,6-Dimethylpyridine 26, 2,5-dimethylphenol 29, 3-methylanisole 36, caffeine 41, 5-bromoisatin 45, 4-iodoanisole 21, tryptamine 89, triptycene 97, octocrylene 99, dipyridamole 100, mometasone furoate 100, rifaximin 100, and rifampicin 100	77
	Cyclen-TBB	57.6	9.1	+18.4	9	150	1.6	5580	77	Doxorubicin hydrochloride 94.0, diammonium glycyrrhizinate 90.9, Congo red 99.9, Victoria blue B 99.9, and acid fuchsin 91.3	60
	MPCM/PAN	90	1	—	—	3.5	0.63	450	21.3	Congo red 91, fuchsine 94, orange G 93, methyl red 75, and methyl orange 73	252
	PA-AdDA TFC	65	18.2	−32.5	3.6	50	0.48	320	20.6	Methyl orange 94.7 and rose bengal 98.5	253
	BAF-PA	—	—	—	—	—	—	585	23.9	Acid fuchsin 90 and Congo red 98	204
	CC3α-PAN	94	—	—	—	80	—	607	43.0	Rose bengal 99.7	254

Table 2 (*continued*)

	NF membrane	CA (°)	Roughness (nm)	Zeta potential (mV)	IEP	Thickness (nm)	Pore size (nm)	MWCO (Da)	Permeance (L m^{-2} h^{-1} bar^{-1})	Rejection (%)	Ref.
Salt/organic compounds	M_{MPA}	38	—	−58	3.8	20.7	0.31	270	12.9	Atenolol 62, sulpiride 67, primidone 72, carbamazepine 64, nalidixic acid 61, indomethacin 82, Na_2SO_4 95, $MgSO_4$ 90, and $MgCl_2$ 44.7	62
	M_{EPA}	2.6	3.75	—	—	17.6	0.28	304	15.6	Atenolol 68, sulpiride 71, primidone 70, carbamazepine 62, nalidixic acid 63, indomethacin 84, Na_2SO_4 93, and $MgSO_4$ 91	62
	8P10-0.5MC30	39.4	2.9	−53.8	2.9	20	0.29	210	15.9	Atenolol 73.4, trimethoprim 66.0, sulpiride 82, primidone 89, carbamazepine 84, sulfamethoxazole 89, nalidixic acid 85, indomethacin 94, xylose 71.1, and MgCl2 41.3	255
Salt/organic compounds	St0.1/TMC0.1-3	62	10.1	−62.5	—	12.5	0.6	4000	81.2	Tetracycline hydrochloride 61, clindamycin phosphate 75, bacitracin 90, Congo red 99.5, MgCl2 10, $MgSO_4$ 15, and NaCl 10	58
	BAIE-TBB(M-0.1)	76.2	15	2.5	6.5	288	1.14	1957	157.1	Victoria blue B 99.6, Congo red 99.6, methyl blue 99.6, Remazol brilliant blue R 99.6, $MgSO_4$ 3.9, Na_2SO_4 3.7, $MgCl_2$ 3.8, and NaCl 3.6	75
	TSM	31.1	13.7	—	—	22	0.6	602	82.6	Fluorescein disodium 62, indigo carmine 85, Congo red 99.9, indocyanine green 99.6, evans blue 99.9, $MgSO_4$ 24, Na_2SO_4 19, $MgCl_2$ 15.1, and NaCl 9.7	256
	PA-QTDEA	53	48.9	−15.4	—	256	0.56	550	32.7	Chlortetracycline hydrochloride 95 and NaCl 11	72
	QE-0.2/TMC-0.2	43	4.96	−70	—	39.3	2.5	5839	198.7	Congo red 99.2 and NaCl 1.6	54
	Ad-PA-NaOH (12.5)	88	5.1	−42	3.5	36.6	1.98	6604	87.2	Evans blue 99.9, eriochrome black T 99.8, Congo red 99.7, $MgSO_4$ 10.9, Na_2SO_4 11.8, $MgCl_2$ 2.6, and NaCl 3.0	59
	TFN-0.2-0.5	30	23.4	−26	—	363	—	—	12.2	Cephalexin 94.7, Na_2SO_4 95.8, and NaCl 20.6	257
	0.3β-CD/APPD/P84	53.4	11.0	−2.5	6.2	2750	0.75	620	209.1	Methyl blue 100, Congo red 99.6, Remanzol brilliant blue R 92.2, Na_2SO_4 8.6, and NaCl 7.7	91
	ZM3	33	16.3	−60	4.9	114	0.27	402	10.7	Methyl blue 99.9 and NaCl 14.3	258
	PIP-COOH/TMC	49.9	3.21	+32.6	3.7	100	2.4	8205	55.8	Reactive red 93.3, methyl blue 93.0, Congo red 94.5, eriochrome black T 93.2, Na_2SO_4 11, and NaCl 5.4	107
	TC-PEA	40.8	13	−42	—	36.0	—	504	11.1	Congo red 98.8 and NaCl 7.4	259
	4AP-TFC_0.05/0.05	61	25.8	−95	3.8	70.2	0.57	492	35.0	Azithromycin 90.4, erythromycin 66.3, roxithromycin 68.5, $MgSO_4$ 96.0, Na_2SO_4 98.5, $MgCl_2$ 50.7, and NaCl 21.5	260
	amino-BIPOL/TMC	70	1.9	−36	3.5	5	0.19	170	17.6	Methyl orange 97.5, neutral dye methyl red 96.3, $MgSO_4$ 96.9, Na_2SO_4 97.5, $MgCl_2$ 33.8, and NaCl 21.9	261
	HHMs	22.9	3.5	−23	4.2	76	0.82	500	104.3	Congo red 99.9, $MgSO_4$ 5.7, Na_2SO_4 6.1, $MgCl_2$ 5.6, and NaCl 5.2	262

Note: NF membrane properties under optimal preparation conditions were recorded. CA refers to the contact angle; the roughness refers to the roughness (Ra) or root mean square roughness (Rq); charge value at pH = 7 or the corresponding monomer concentration was recorded; IEP refers to the isoelectric point; MWCO refers to the molecular weight cut off.

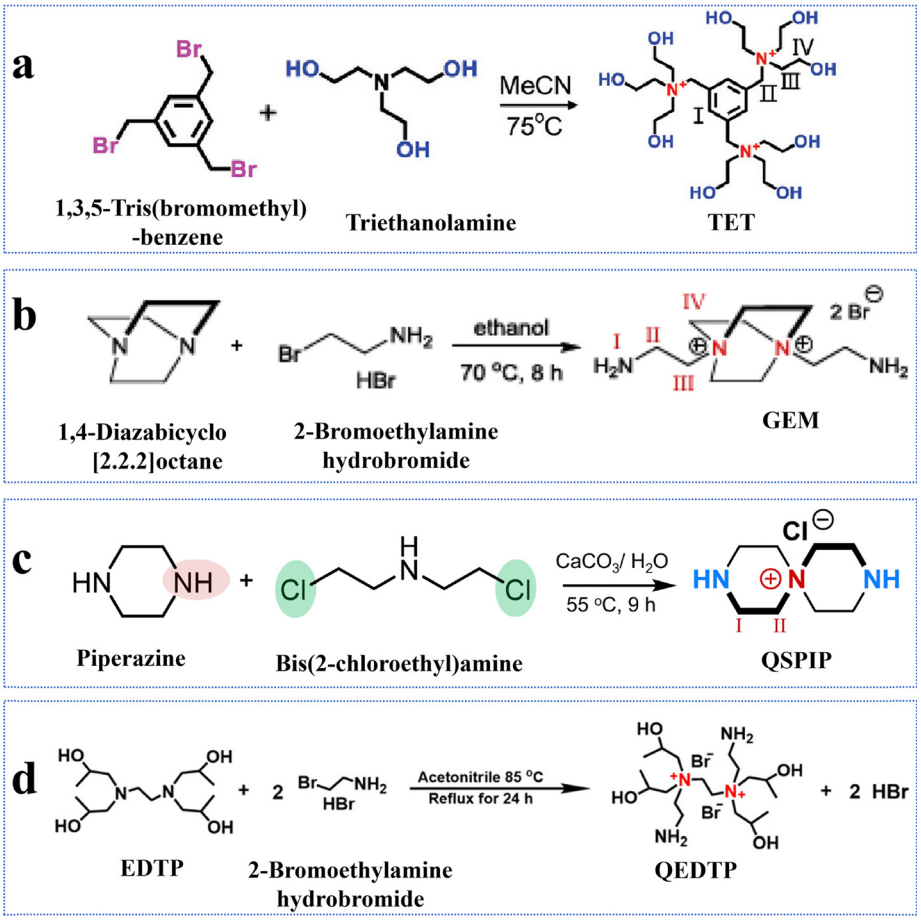

Fig. 7 Quaternary amination reactions of monomers. (a) Synthesis of TET. Reproduced with permission from ref. 63. Copyright 2024, Wiley-VCH. (b) Synthesis of GEM. Reproduced with permission from ref. 65. Copyright 2023, Wiley-VCH. (c) Synthesis of QSPIP. Reproduced with permission from ref. 64. Copyright 2023, Springer Nature. (d) Synthesis of QEDTP. Reproduced with permission from ref. 68. Copyright 2022, Elsevier.

(–OH) groups, which can be quaternized with 1,3,5-tris(bromomethyl)benzene to produce novel monomers; namely, TET, M_2, and M_3 with symmetrical structures. The quaternization reaction for TET is illustrated in Fig. 7a.[63] All three monomers share a benzene ring and three quaternary ammonium groups but differ in the number of hydroxyl (–OH) groups: TET (9) > M_2 (6) > M_3 (3).[63] Despite these differences, polyester-based NF membranes derived from these monomers exhibit similar hydrophilicity, as evidenced by comparable water contact angles, likely due to their analogous structures centered around a benzene ring.[63] In the literature, TET-TMC and M2-TMC membranes have demonstrated superior structural integrity to the M3-TMC membrane, with no apparent surface defects. This could be primarily attributed to the higher crosslinking density between TMC and the monomers with more –OH groups (*i.e.*, TET), resulting in a dense active layer with an optimal pore structure.[63] In addition to amine monomers containing a single nitrogen atom, aza-based monomers with two nitrogen atoms can also be transformed into novel monomers featuring bis-quaternary ammonium groups through quaternization reactions. For instance, 1,4-diazabicyclo[2.2.2]-octane, an amine monomer with a symmetrical cage-like structure, could react with 2-bromoethylamine and 3-bromopropylamine, yielding two novel symmetrical monomers (*i.e.*, GEM and M1, respectively), as illustrated in Fig. 7b.[65] Although GEM possessed a shorter alkyl chain than M1, NF membranes prepared from both monomers exhibited similar permeances of ~20 L m^{-2} h^{-1} bar^{-1} and $MgCl_2$ rejections of ~94%.[65] In particular, the GEM-TMC membrane had a permeance of approximately three times higher and a selectivity of 1.9 times higher than the conventional PIP-TMC membrane. These enhancements arose from three factors: (1) GEM had a significantly lower diffusion rate (*i.e.*, six times lower than PIP) that promoted the formation of a thinner and smoother active layer; (2) the twisted structure of GEM allowed the induction of a highly porous polyamide matrix; and (3) the positively charged GEM enhanced solute rejections due to electrostatic repulsion.[65] Compared to NF membranes synthesized from monomers with a single quaternary ammonium group (*i.e.*, TET-TMC), those derived from bis-quaternary ammonium monomers (*i.e.*, GEM-TMC) exhibited a higher positive charge (*i.e.*, +4 mV *vs.* +10 mV). This elevated charge would enhance the Donnan effect during the selective separation of cations.

Recently, the conventional monomer of PIP, featuring a symmetrical secondary amine (–NH) structure, has been modified to impart NF membranes with superior performance. PIP can undergo a ring-opening reaction with bis(2-chloroethyl)-amine that not only helicalizes PIP but also quaternizes bis(2-chloroethyl)amine. This yields a positively charged monomer (*i.e.*, QSPIP, Fig. 7c) with both -NH and quaternary ammonium ($-N^+$) groups.[64] In the literature, the resultant QSPIP-TMC membrane exhibited a thinner active layer than the control PIP-TMC membrane owing to the lower diffusion rate of QSPIP in hexane. Experimentally, the former (*i.e.*, QSPIP) had a diffusivity approximately 4.8 times lower than the latter (*i.e.*, PIP). Moreover, the twisted QSPIP structure increased the overall porosity of the active layer. Thus, the QSPIP-TMC membrane had a superior permeance of 22 L m^{-2} h^{-1} bar^{-1} and a Li^+/Mg^{2+} selectivity of 8.7.[64]

The quaternized monomers can not only be directly used to prepare high-performance NF membranes but also employed for surface grafting to enhance membrane performance. For example, 2-bromoethylamine hydrobromide could quaternize 1-(trimethylsilyl)imidazole into a novel monomer (*i.e.*, DAIB), which contained both symmetrical primary amine ($-NH_2$) and quaternary ammonium ($-N^+$) groups.[66] The DAIB-grafted PEI-TMC membrane had a smoother and more hydrophilic surface, which could reduce the transport resistance of water molecules across the active layer. Thus, the resultant NF membrane had a permeance approximately 5.6 times higher than that of the pristine membrane.[66] Similarly, QEDTP could be synthesized by quaternizing *N*,*N*,*N*′,*N*′-tetrakis(2-hydroxypropyl)ethylenediamine (EDTP) with 2-bromoethylamine hydrobromide (Fig. 7d).[68] Compared to the control PEI-TMC membranes, the QEDTP-modified membranes displayed significantly higher positive charge of ~14 times, permeance of ~4.4 times, and selectivity of ~2.4 times. These enhancements arose from the secondary grafting reaction between the functional groups ($-NH_2$ and –OH) of QEDTP and the residual acyl chloride groups of TMC. This rearrangement would not only optimize the pore size distribution but also loosen the structure of the modified membrane, thus enhancing its overall performance.[68]

In summary, quaternized monomers have demonstrated their importance in molecularly design high-performance NF membranes. Generally, selecting structurally unique amine monomers and identifying green chemical reagents capable of undergoing quaternization reactions with these monomers are critical steps in designing desirable novel monomers with positive charges. Looking forwards, the development of novel monomers based on specific structural features represents an essential strategy to overcome the permeability-selectivity trade-off relationship for NF membranes.

Modifications of monomers with targeted functional groups

Monomers with desirable functional groups are crucial to design novel NF membranes for specific separation performance. As the –OH groups in raw monomers have a significantly lower reactivity than the $-NH_2$ groups, the disparity in reactivity poses challenges in controlling the reaction rate and crosslinking degree of hydroxyl-rich monomers during IP reactions. This may result in thick active layers with disordered stacking and low porosity.[65] To resolve this issue of low reactivity, modifications of monomers with targeted functional groups provide a promising strategy to form defect-free NF membranes. Currently, the monomer functionalization strategy involving selective introduction of reactive functional groups is primarily employed in novel macrocyclic monomers with well-defined cyclic architectures, such as cyclodextrins and crown ethers.[77,86,113–117] These hydroxyl-rich macromolecular frameworks are expected to enhance monomer reactivity during IP while effectively preserving the inherent porous structure of the active layer of NF membranes, thus enabling a synergistic improvement in both high selectivity and permeability. For example, cyclodextrins with a macrocyclic structure consisting of (1) hydrophilic outer rims full of primary-OH and secondary-OH and (2) hydrophobic inner cavities almost full of C-H groups, are widely utilized in the preparation of NF membranes for environmental applications.[86,113–116] However, if the –OH groups of cyclodextrins can be converted to more reactive $-NH_2$ groups, the resultant NF membrane may have greater adaptability for specific separation requirements.[74,78,115,117] In the literature, with the aid of 1,1′-carbonyldiimidazole and ethylenediamine, the primary-OH groups on the upper (narrow) rims of α-cyclodextrin, β-cyclodextrin, γ-cyclodextrin, and 4-sulfocalix[4]arene have been selectively transformed into highly reactive $-NH_2$ groups. This process yielded four novel monomers—α-CDA, β-CDA, γ-CDA, and SC[4]AA—with average pore diameters of 0.45, 0.61, 0.77, and 0.57 nm, respectively (Fig. 8a).[74] The modified monomers consisting of $-NH_2$ groups at one end showed preferential diffusion in the organic-phase and selectively reacted with terephthaloyl chloride. The resultant active layer had ordered and sub-nanometer open pores of 3.5 nm thick.[74] In addition, the pore size of the active layer increased with an increase in the pore size of the modified monomer. In particular, the α-CDA-TPC-0.1 membrane showed superior performance with a methanol permeance of 5.8 L m^{-2} h^{-1} bar^{-1}.[74] In summary, by selectively enhancing the reactivity of one end of the monomer while maintaining low reactivity at the opposite end, the regional selectivity of IP can be precisely regulated. This enables fine control over the microstructure of the active layer and facilitates the fabrication of high-performance NF membranes featuring well-ordered sub-nanometer channels.

Similarly, β-cyclodextrin was aminated to synthesize heptakis(6-deoxy-6-amino)-β-cyclodextrin (*i.e.*, Am7CD) (Fig. 8b) and employed to fabricate LiOH-Am7CD-0.05 TMC NF membranes with a precisely controlled pore size of 0.34 nm.[78] These membranes had an outstanding Li^+/Mg^{2+} selectivity of 190; however, their permeance was relatively low at 1.9 L m^{-2} h^{-1} bar^{-1}.[78] Although the improved reactivity of aminated cyclodextrins enables precise nanochannel construction for targeted solute separation, the random stacking of macrocyclic monomers leads to irregular nanochannels, limiting the ability of the macrocyclic cavity to confer an optimal permeability to the active layer. This finding further demonstrates that functional

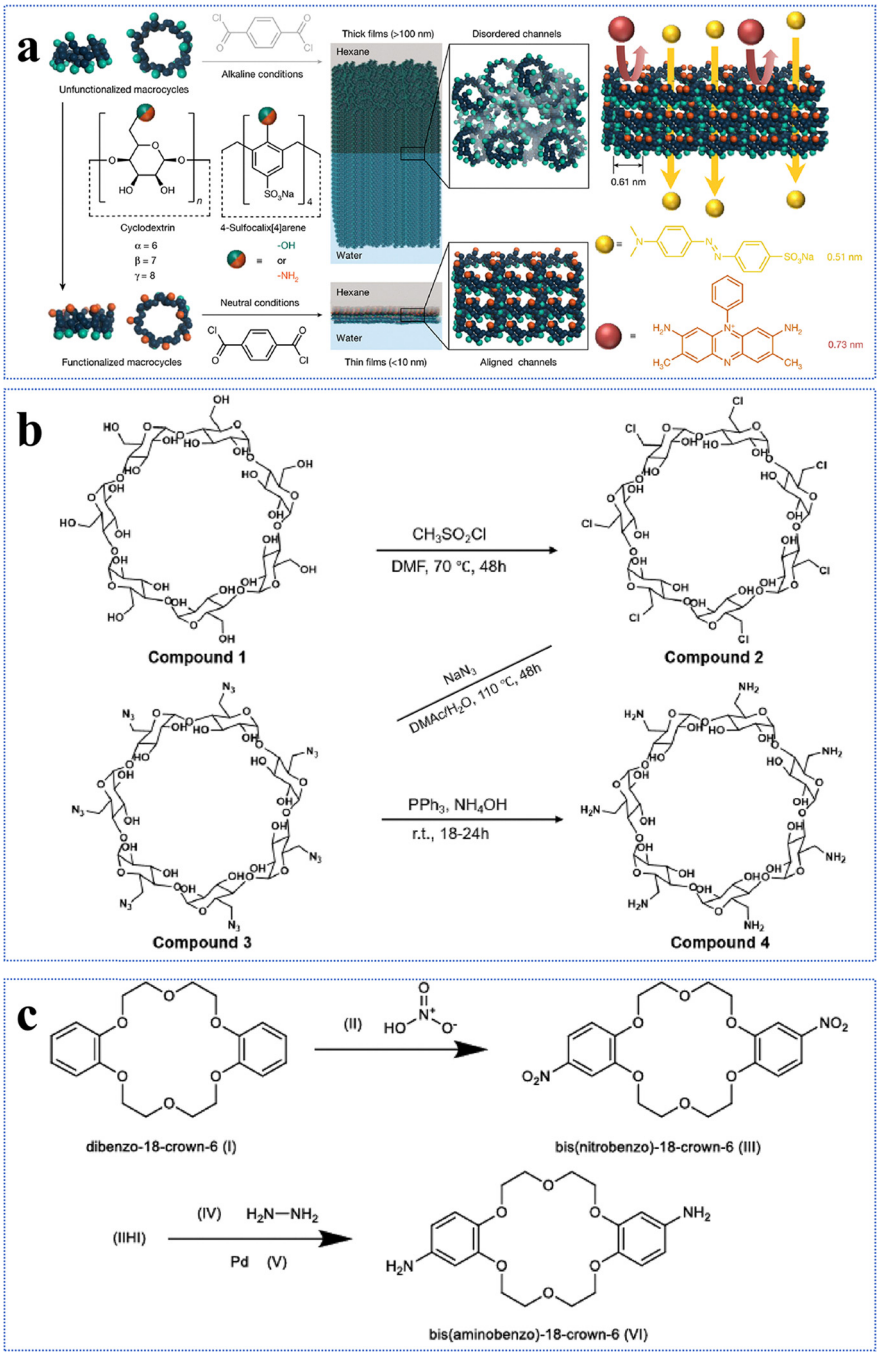

Fig. 8 Modifications of functional groups of monomers. (a) Modifications of α-cyclodextrin, β-cyclodextrin, γ-cyclodextrin, and 4-sulfocalix[4]arene, and IP of the resulting modified monomers. Reproduced with permission from ref. 74. Copyright 2022, American Association for the Advancement of Science. (b) Synthesis of Am7CD. Reproduced with permission from ref. 78. Copyright 2024, Springer Nature. (c) Synthesis of 18C6. Reproduced with permission from ref. 77. Copyright 2024, Springer Nature.

group modification of monomers exacerbates the permeability–selectivity trade-off in NF membranes to some extent. Moreover, coronium, a macrocyclic monomer of significant interest, has been chemically modified to develop sub-nano size membranes with high selectivities toward pharmaceuticals. Specifically, bis(aminobenzo)-18-crown-6 (*i.e.*, 18C6) was obtained by the amino-functionalization of bis(aminobenzo)-18-crown-6 (Fig. 8c).[77] The active layer of the TFC_{18C6} membrane synthesized from the novel macrocyclic monomer of 18C6 had an ideal surface roughness of 7.9 nm, pore size of 0.34 nm, and thickness of 24.1 nm.[77] Meanwhile, it demonstrated a permeance of 7.2 L m^{-2} h^{-1} bar^{-1} for acetonitrile and high separation factors for pharmaceuticals with molecular weights of 100–370 g mol^{-1}.[77] In summary, the targeted modification of monomers with functional groups provides an effective strategy to (1) manipulate the diffusion rates of water-phase monomers into the organic-phase,

(2) regulate the reaction kinetics and (3) control the degree of crosslinking reactions. This approach not only facilitates the construction of defect-free NF membranes with well-connected pores but also enhances solvent permeation rates with precise solute separation.

Overall, the strategy to modify the functional groups of monomers has been primarily applied to macrocyclic monomers with large-ring architectures, achieving significant advancements. Notably, current efforts have largely focused on hydroxyl-rich macrocyclic monomers, where the successful conversion of –OH to $–NH_2$ groups represents a critical milestone in the molecular-level design of tailored NF membranes. Building on this progress, expanding the scope to other types of functional group modifications is essential to systematically elucidate the influence of functional group identity and density on solvent permeation behaviors and solute transport mechanisms within the membrane's active layer. Furthermore, targeted functionalization to enhance monomer reactivity enables precise control over the surface morphology and microstructure of the active layers, leading to a significantly higher solute retention. However, this improvement is frequently accompanied by a decline in solvent permeability. Consequently, whether such strategies can simultaneously enhance selectivity without compromising permeability and thereby overcoming the intrinsic permeability–selectivity trade-off remains to be thoroughly investigated through systematic and in-depth studies.

Synthesis strategies for novel monomer-based NF membranes

In addition to monomer design and selection, the preparation methodology plays a critical role in regulating the permeability, selectivity, and stability of NF membranes. A variety of techniques, including interfacial polymerization (IP), layer-by-layer self-assembly, electrospinning, vacuum deposition, coating, phase inversion, electro-spraying, and surface grafting, have been extensively applied to fabricate NF membranes using conventional monomers (*e.g.* PIP and MPD), demonstrating promising performance in water treatment applications.[4,118] Currently, in the fabrication of NF membranes using novel monomers, IP, layer-by-layer assembly, graft polymerization, and phase inversion assisted post-polymerization have emerged as the predominant and most representative synthetic strategies, owing to their superior material compatibility and precise process controllability (Fig. 9). Specifically, IP has emerged as the dominant approach for fabricating high-performance NF membranes based on novel monomers, owing to its high industrialization applicability, precise parameter control, and operational simplicity. Meanwhile, the layer-by-layer (LbL) self-assembly technique enables precise tuning of the composition and structure of the active layer. Moreover, surface grafting enhances membrane performance through functional modifications of the existing active layer. In contrast, phase inversion assisted post-polymerization can improve

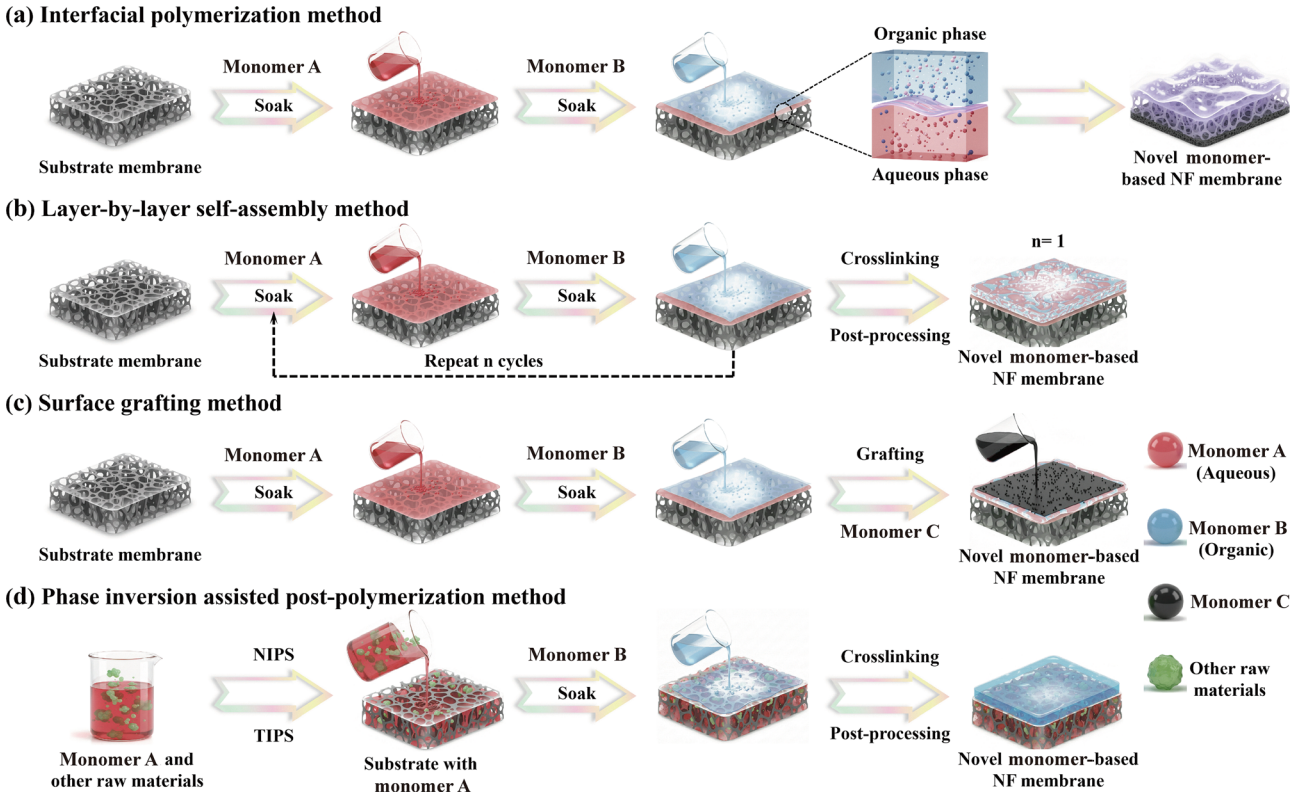

Fig. 9 Preparation methods for novel monomer-based NF membranes. (a) Interfacial polymerization, (b) layer-by-layer self-assembly, (c) graft polymerization, and (d) phase inversion assisted post-polymerization.

the separation performance of the support membrane by optimizing its microstructure and lowering the transport resistance. The following section will provide an in-depth discussion on the synthesis strategies and application advancements of NF membranes incorporated with novel monomers.

Interfacial polymerization

For interfacial polymerization (IP), water-soluble and organic-soluble monomers react vigorously *via* polycondensation at the interface of two immiscible phases, resulting in an ultrathin and dense active layer. Owing to its high compatibility with industrial manufacturing processes and exceptional tunability, IP has emerged as the predominant method for fabricating NF membranes.[4,6,118] In recent years, researchers have developed a range of innovative IP strategies, including anhydrous IP,[43,119] organic-organic IP,[120] gas–liquid IP,[121] low-temperature IP,[122–124] heated IP,[53,125,126] reverse IP,[127–129] photo-assisted IP,[130,131] and additive-assisted IP,[48,132–138] and vapor-phase IP.[121,139–142] These strategies enable precise regulation of the microstructures and separation performance of NF membranes, which is achieved either by modulating the diffusion behavior and interfacial reaction kinetics of aqueous-phase monomers or by tuning the physicochemical state (*e.g.* solubility, concentration) of organic-phase monomers. Specifically, liquid-phase IP (LP-IP) is a well-established strategy, offering rapid reaction kinetics; however, its heavy reliance on volatile organic solvents poses significant environmental and safety risks. Moreover, the vigorous nature of the reaction often results in an excessively thick, highly wrinkled polyamide layer with elevated defect density, thereby compromising both selectivity and permeability, and limiting further gains in separation performance. In contrast, vapor-phase IP (VP-IP) has emerged as a promising alternative to address core limitations of LP-IP by minimizing solvent use, maximizing monomer utilization, enabling precise control over reaction intensity and spatial distribution, and yielding uniform, defect-suppressed polyamide layers, which represents a critical advancement toward sustainable, high-performance NF membrane fabrication. For instance, a VP-IP-derived thin-film composite membrane, prepared by reacting MPD and TMC vapors at the water–air interface, achieved a high water permeance of 3.3 L m^{-2} h^{-1} bar^{-1} and consistently exceeded 94% rejections of various dyes.[139] To further minimize organic solvent consumption, Ingole and his colleagues developed a spray-assisted VP-IP technique by integrating aqueous-phase spraying with controlled TMC vapor delivery.[140] Membranes fabricated *via* this approach achieve a high water flux of 4.7 L m^{-2} h^{-1} bar^{-1} and an exceptional Na_2SO_4 rejection of over 96%, demonstrating robust divalent ion selectivity for divalent ions.[140] Critically, this green synthesis strategy synergistically reduces both aqueous monomer dosage and volatile organic carrier requirements while eliminating toxic solvents entirely, thereby establishing a scalable and environmentally compatible pathway toward sustainable production of high-performance NF membranes.

Fig. 9a presents a step-by-step schematic illustration of the fabrication process for the novel monomer-based NF membranes, clarifying the key synthetic stages and interfacial reactions involved: (1) base membrane pretreatment, (2) water phase impregnation, (3) removal of the excess aqueous solution, (4) organic-phase reaction (IP), (5) post-treatment and curing, and (6) rinsing and storage. Notably, the structures and concentrations of monomers, IP parameters (*e.g.* impregnation duration, crosslinking time, and reaction temperature), and post-treatment conditions, significantly influence the morphologies and separation performance of NF membranes. To date, research efforts have increasingly focused on the development of novel water-soluble monomers and the precise modulation of IP parameters.

Although numerous innovative IP strategies using conventional monomers (*i.e.*, PIP and MPD) have been developed, NF membranes made of novel aqueous-phase monomers, including phenolic-based,[143–149] alcohols-based,[58,85,150–154] amines-based,[119,124,128,155–159] quaternary ammonium salts,[65,160–162] and functional group-modified novel monomers,[74,77,78,115,117] are still predominantly fabricated *via* conventional IP methods. For instance, phloretin (Pt), phlorizin (Pz), and naringenin dihydrochalcone (Ng), three natural polyphenol monomers containing 4, 7, and 9 –OH groups, respectively, were employed to synthesize polyester-based membranes *via* conventional IP process under NaOH activation (namely, Pt-TMC, Pz-TMC, and Ng-TMC).[148] Because Pz and Ng possessed higher molecular weights and more distorted molecular structures than Pt, the former would have slowed down the monomer diffusion into the organic-phase and resulted in an active layer with a lower crosslinking density, higher hydrophilicity, and stronger negative surface charge.[148] However, the latter (*i.e.*, Pt-TMC membrane) exhibited a significantly higher water permeance of 35.2 L m^{-2} h^{-1} bar^{-1}. Additionally, its Na_2SO_4 rejection reached 94.0%, representing 1.1- and 1.5-fold improvements over the Pz-TMC and Ng-TMC membranes.[148] This suggested that the combination of novel monomers in conventional IP processes might yield superior NF membranes.

Layer-by-layer self-assembly

Layer-by-layer (LbL) self-assembly is a versatile technique that deposits oppositely charged polyelectrolytes or functional monomers alternatively onto a substrate surface through intermolecular interactions, leading to the formation of well-defined multilayer active structures. As a ''bottom-up'' fabrication approach, LbL offers precise and tunable control over both the surface properties (*e.g.* surface charge and hydrophilicity) and structural features (*e.g.* thickness and pore size) of the resulting active layer. This high degree of customization can be tailored to meet specific demands on active-layer design and surface functionalization with the aid of diverse materials for applications requiring efficient solute separation. The typical LbL procedures involve (Fig. 9b): (1) substrate pretreatment, (2) deposition of the first polyelectrolyte, (3) intermediate rinsing to remove unbound species, (4) deposition of the second polyelectrolyte with opposite charge or complementary functionality, (5) subsequent rinsing, (6) repetition of steps (2)–(5) for *n* cycles to build up the desired number of bilayers,

(7) post-treatment processes such as crosslinking or drying, and (8) final cleaning and storage. Notably, key parameters, including the choice of polyelectrolytes (*e.g.* phenolic or amine-based), the number of deposition cycles, and the deposition method (*e.g.* dip coating, spray coating, or spin coating), exert significant influences on the morphology and overall performance of the resulting membranes.

In recent years, advanced functional materials such as metal–organic frameworks (MOFs), covalent organic frameworks (COFs), graphene oxide, titanium dioxide, and carbon nanotubes have been successfully integrated into the LbL self-assembly process to fabricate membranes.[163–166] Moreover, this strategy has been extended to high-performance NF membranes using phenol-based monomers[167–169] and amine-based monomers.[24,170–181] In addition, tannic acid (TA), a representative plant-derived polyphenol featuring abundant benzene rings and multiple –OH groups, has been adopted for NF membrane fabrication *via* the LbL technique. Historically, TA was first deposited *via* dip-coating on a polyethersulfone (PES) support membrane as an intermediate layer for subsequent covalent anchoring of a positively charged PEI.[168] Later, negatively charged MXene nanosheets were assembled through electrostatic interactions to construct NF membranes with a well-defined layered architecture ($(PEI/MXene)_4$/TA/PES).[168] The membrane had an outstanding water permeance of 204.0 L m^{-2} h^{-1} bar^{-1} and an exceptionally high selectivity of 758.1 for NaCl/evans blue.[168] This superior performance arose from its gradient-structured active layer. The dense bottom layer formed by TA and PEI effectively rejected large-molecule dyes, whereas the more porous top layer assembled from PEI and MXene facilitated rapid water transport by providing low-resistance pathways.[168]

In addition, poly(allylamine hydrochloride) (PAH), a cationic amine monomer abundant in primary amine groups ($-NH_2$), has been extensively employed in the LbL process for NF membranes owing to its capacity for both electrostatic interactions and covalent bonding.[174] Specifically, PAH was first deposited by dip-coating onto the surface of a PES support membrane, followed by a polydopamine (PDA) coating *via* Michael addition reaction. Polyanion poly(sodium 4-styrenesulfonate) (PSS) was sequentially assembled onto the PAH-PDA interface through electrostatic attraction, ultimately yielding a well-defined multilayer NF membrane ($(PAH/PDA/PSS)_4$).[174] Compared to the control membrane without a PDA intermediate layer, the as-prepared membrane had a water permeance increased by 8.4 L m^{-2} h^{-1} bar^{-1} (*i.e.*, an increment from 13.5 to 21.9 L m^{-2} h^{-1} bar^{-1}) without deterioration in the $MgCl_2$ rejection.[174] This improvement was primarily attributed to the specific reaction between PDA and PAH, which enabled the formation of a dense interfacial spacer layer. This layer effectively reduced excessive adsorption and infiltration of PSS chains, thereby resulting in a thinner and more uniform active layer.[174] Similarly, a novel cationic polyelectrolyte (*i.e.*, TPAH), prepared by grafting PAH with trimethylamine *N*-oxide (TMAO), was used for NF membranes (*i.e.*, (PSS/TPAH)*n*) instead of PAH-PDA, yielding a higher $MgCl_2$ rejection (96.1% *vs.* 94.8%),[24] which was attributed to the improved hydrophilicity and more uniform spatial distribution of positive charges imparted by the TPAH monomer.

Graft polymerization

Graft polymerization is a highly effective surface modification technique that enables precise regulation and functionalization of surface chemistry on membranes through the covalent attachment of functional monomers. The process typically involves four key steps (Fig. 9c): (1) pretreatment of the base membrane, (2) initiation of the graft polymerization reaction, (3) post-treatment to stabilize the grafted layer, and (4) thorough cleaning and proper storage. Generally, the length and density of the grafted polymer chains are governed by multiple interdependent factors including (1) physicochemical properties of the pristine membrane, (2) molecular structures and concentrations of the monomers, and (3) reaction conditions. Each of them plays an important role in determining the microstructure and separation performance of the resulting membrane in terms of selectivity and stability.[28]

To enhance the selective separation of cationic solutes, positively charged monomers, such as quaternary ammonium salts or amine-based monomers (*e.g.* PEI), are preferred to be grafted onto the membrane surface. They can not only enhance the positive charge density but also precisely modulate the pore size distribution of the active layer to strengthen the Donnan effect and improve the rejection of target cations.[26,27,67,68,111,182,183] For instance, 3,5-dimethylhydrazide-benzyl trimethyl ammonium bromide (DHTAB), synthesized *via* a two-step quaternization reaction using 5-bromomethyl-isophthalate, trimethylamine, and hydrazine hydrate,[67] could increase the surface charge density of the pristine PEI-TMC membrane by approximately two-fold, thereby significantly raising the $MgCl_2$ rejection from 95.4% to 99.2% and achieving a high separation factor of 60.1 for Li^+/Mg^{2+}.[67] Clearly, the joint effects from the protonated $-NH_2$ and the intrinsic quaternary ammonium groups in DHTAB synergistically enhanced the positive charge density on the membrane surface that strengthened the Donnan exclusion.[67]

To improve the anti-fouling performance of NF membranes, monomers containing abundant hydrophilic functional groups like amine, hydroxyl, carboxyl, and sulfonic acid groups are often grafted onto the membrane surface. These monomers not only improve the surface hydrophilicity of the resultant membranes but also induce a stable hydration layer to effectively prevent the adsorption and deposition of foulants.[68,71–73,83,105,182,184,185] For instance, the grafting of poly(*n*-isopropylacrylamide) (PNIPAM) onto the surface of a brominated PIP-TMC membrane *via* atom transfer radical polymerization (ATRP) substantially improved the membrane's anti-fouling capability. It achieved a flux recovery rate (FRR) of 90.4% during bovine serum albumin (BSA) fouling-cleaning cycles.[184] This performance enhancement arose from the significant reduction in adhesion force between the modified membrane and BSA. It dropped from −1.68 to −0.62 mN m^{-1}, thereby BSA would not be adsorbed and deposited on the membrane surface.

Monomers with intrinsic bactericidal activity, such as quaternized ammonium, imidazole derivatives, capsaicin, or antibiotics have been grafted to endow the membranes with antibacterial properties. These membranes show effectiveness to disrupt the integrity of bacterial cells or interfere with their essential metabolic processes.[29,69,71,83,105,185,186] For instance, the IM-P membrane, fabricated by grafting 1-(3-aminopropyl)imidazole (IM-N) onto the PIP-TMC membrane, had a higher inhibitory activity against *Escherichia coli* (*E. coli*) due to its higher surface hydrophilicity and formation of a robust hydration layer against bacterial adsorption.[29] Similarly, a pH-responsive antibacterial NF membrane (APBA-TMC) was developed by grafting the antibiotic streptomycin (ST) onto a membrane synthesized using 3-aminophenylboronic acid (APBA) as the aqueous-phase monomer. It exhibited an inactivation efficiency of $\geq$97% against both *E. coli* and *Staphylococcus aureus* (*S. aureus*).[186]

Phase inversion-assisted post-polymerization

Phase inversion assisted post-polymerization is used to transform a homogeneous polymer solution into a solid porous membrane with well-defined microstructures by means of phase separation under controllable thermodynamic conditions. This process primarily encompasses two approaches: non-solvent induced phase separation (NIPS) and thermal induced phase separation (TIPS).[30–36] Today, NIPS has become the most established and widely implemented technology to produce industrial-scale support membranes due to its advantages of operational simplicity, high process efficiency, excellent controllability, and superior membrane performance. A typical NIPS process comprises five key stages (Fig. 9d): (1) preparation of casting solutions, (2) solution casting and shaping, (3) liquid–liquid phase separation (*i.e.*, coagulation), (4) post-treatment, and (5) rinsing and storage. Beyond fabricating substrate membranes, the phase inversion method has been used to fabricate mixed matrix membranes by blending nanomaterials (*e.g.* MOFs, MXenes, and carbon-based materials) into the casting solution, which has been extensively utilized in applications such as water purification and gas separation.[187–196]

Recent studies have demonstrated the incorporation of functional monomers into the casting solution for the fabrication of NF membranes by integrating NIPS and IP techniques. For example, APBA was introduced into a polysulfone (PSf) casting solution to prepare the support membrane, followed by immersion in a coagulation bath containing TA to *in situ* form a pH-responsive boronate ester network *via* reaction between boronic acid groups and –OH groups.[197] A loose NF membrane (BC/LNF) was therefore constructed after crosslinking with TMC.[197] Because the boronate ester network would dissociate and release boronic acid groups under acidic conditions, it created grafting sites for the antibiotic kanamycin (KM). Thus, the resultant membrane had efficient immobilization and impressive antibacterial properties.[197] It not only had a high water permeance of 134.9 L m^{-2} h^{-1} bar^{-1} and a CR rejection of 95.4% but also exhibited over 93% inactivation efficiency against both *E. coli* and *S. aureus*. Likewise, an acid-resistant NF membrane (NFDATB-TMC) was prepared by reacting the 3,3′-diamine-Tröger's base (DATB)-contained polyethersulfone (PES) substrate with TMC.[198] In addition, to have a Na_2SO_4 rejection of 98.1% under neutral conditions, the resulting membrane had rejections of over 96% to heavy metal ions (Fe^{3+}, Ni^{2+}, Cr^{3+}) and dyes (Crystal Violet, Rhodamine B, Black Curcumin, and CR) under extreme acidic conditions (pH = 1), albeit with a relatively low water permeance (5.3 L m^{-2} h^{-1} bar^{-1}).[198] The exceptional acid resistance was primarily attributed to the unique V-shaped rigid structure of the DATB monomer, which greatly enhanced the chemical stability of the membrane matrix by restricting chain mobility and minimizing hydrolytic degradation under harsh acidic conditions.

Interface regulation strategies for novel monomer-based NF membranes

Given that IP has emerged as the dominant technique for the development of novel monomer-based NF membranes, this chapter aims to provide a comprehensive review of recent advances in optimizing the IP process through various regulation strategies to fabricate high-performance NF membranes. Developing advanced strategies to precisely regulate the structure of the active layer is crucial for achieving efficient separation of solvents/solutes or solute/solute mixtures, thereby overcoming the trade-off relationship between permeability and selectivity in NF membranes. The reactivity of aqueous-phase monomers and their diffusion kinetics into the organic-phase are the two primary rate-controlling factors in the IP process. Moreover, they not only govern the surface morphology and hydrophilicity of the active layer, but also critically dictate its crosslinking density, pore size distribution, and nanoscale network architecture. Therefore, with the aid of appropriate alkalis, surfactants, ionic liquids, co-solvents, or co-reactants can modulate the diffusion processes and reaction kinetics of aqueous-phase and organic-phase monomers at the water/solvent interface for the subsequent IP reaction and form an active layer with desirable pore structures (*i.e.*, high porosity, small pore size, and controlled thickness) and surface characteristics (*i.e.*, enhanced hydrophilicity and charge density) (Fig. 10). As a result, this approach enhances both the permeation and separation performance of NF membranes.[108,199–202] However, one must understand the underlying mechanisms and analyze which additives influence the performance of novel monomer-based NF membranes in order to provide valuable insights for optimizing the next-generation NF membranes.

The influence of alkali addition

The molecular structure and intrinsic physicochemical properties of monomers, including functional group identity and stoichiometry, molecular weight, steric bulk, and acid dissociation constant (pK_a), directly govern their interfacial diffusion behavior and reaction kinetics during the IP process. Consequently, rational monomer design and structure-guided regulation constitute the fundamental scientific basis for engineering the active layer of high-performance NF membranes. Among conventional aqueous-phase monomers, nucleophilic reactivity

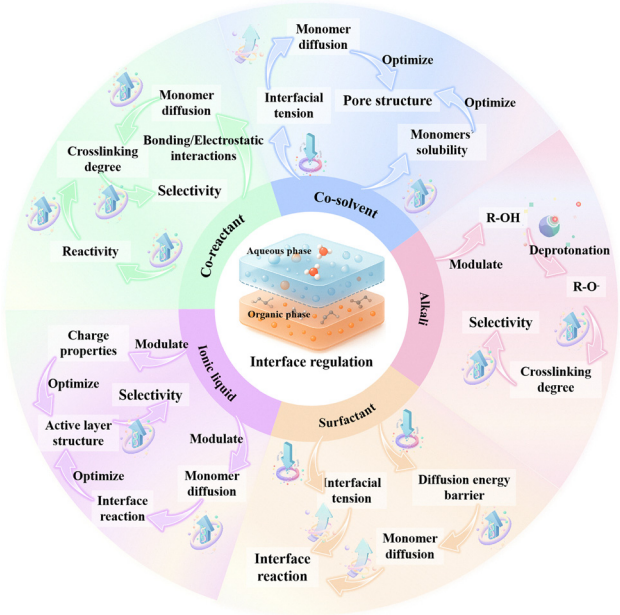

Fig. 10 Interface regulation strategies for novel monomer-based NF membranes.

follows a well-established hierarchy: primary amine-based > phenol-based > alcohol-based (R–OH). Given the inherently low nucleophilicity of phenolic and alcoholic monomers, alkaline additives are routinely employed in the aqueous phase to facilitate deprotonation, thereby generating more reactive anionic species and accelerating both interfacial condensation and crosslinking network formation. Critically, the pK_a values of phenolic hydroxyls (9.0–10.0) are substantially lower than those of aliphatic alcoholic hydroxyls (15.5–18.0), enabling efficient and selective deprotonation of phenols under typical IP conditions. This yields highly nucleophilic phenoxide anions ($-O^-$), which readily undergo acyl substitution with TMC to form densely crosslinked, thin-film polyester networks (Fig. 10). In contrast, aliphatic alcohols remain largely protonated and kinetically inert under these conditions, resulting in negligible covalent incorporation and poor network integrity. Hence, alkaline modulation is mechanistically justified and practically effective for phenol-based IP systems. While for alcohol-based systems, alternative strategies, including phase-transfer catalysis, or pre-activation *via* acylation, are essential to achieve viable crosslinking density and membrane performance. Therefore, alkali agents are strategically employed to enhance the IP reactivity of phenolic monomers, primarily by promoting their deprotonation under mild alkaline conditions to generate highly nucleophilic phenoxide anions ($-O^-$). This enhanced nucleophilicity accelerates covalent cross-linking between phenolic and acyl chloride monomers, enabling the formation of an ultrathin, defect-controlled active layer that simultaneously achieves a high solvent permeance and a sharp solute selectivity. In the literature, stevioside (St), a bio-based monomer consisting of a non-planar twisted structure and abundant –OH groups was employed to enhance the reactivity of IP because its –OH groups could be deprotonated to alcoholate ions ($-O^-$) upon the addition of NaOH. This led to the formation of a dense and thin active layer.[58] Specifically, an optimized NaOH addition of 0.05 M not only deprotonated the –OH groups of the aqueous monomer to accelerate the IP reaction but also neutralized the acidic chloride (HCl) generated during the IP process, thus forming an ideal active layer. The resulting $St_{0.1}/TMC_{0.1}$-3 membrane had the best permeance of 81.2 L m^{-2} h^{-1} bar^{-1} and selectivity of ~11.4 for NaCl/tetracycline hydrochloride mixtures (Fig. 11a).[58] However, a relatively higher NaOH concentration of 0.125 M would hydrolyze the ester bonds in the active layer, resulting in decreases in both crosslinking degree and retention performance (*i.e.*, a Na_2SO_4 rejection of ~58%).[58] Therefore, one must carefully tune the base concentration or the pH value of the IP process to form an active layer with an appropriate crosslinking degree for the optimal balance between permeability and selectivity. In summary, the use of alkali in IP reactions of NF membranes improves the reaction activity because the deprotonation of –OH groups offers a novel approach to controllably design high-performance NF membranes. However, the precise control of alkali concentration and reaction time remains challenging, as excessive hydrolysis can lead to an overly porous active layer and weak mechanical strength. Future research should focus on (1) coordinated regulation of these multi-factors (*i.e.*, acid + alkali, alkali + temperature), (2) development of green alkali reagents (*i.e.*, bio-derived alkalis); and (3) optimization of these parameters to precisely control the alkali treatment with the aid of *in situ* characterizations and computational simulation.

The influence of surfactant addition

Unlike the alkali-based regulation strategy, which primarily modulates monomer reactivity *via* deprotonation, surfactants exert precise control over interfacial mass transfer kinetics by simultaneously lowering both the interfacial tension and the diffusion energy barrier for water-phase monomers approaching the water/solvent interface (Fig. 10). Specifically, since the water-phase monomers generally have a slower diffusion rate than the IP reaction rate, a concentration gradient could arise at the water/solvent interface and affect the crosslinking degree of the active layer. To address this issue, surfactants, characterized by their unique amphiphilic structure featuring both hydrophilic and hydrophobic groups, are used to reduce the interfacial tension between the aqueous and organic-phases. This leads to a faster and more uniform diffusion of aqueous-phase monomers to the water/solvent interface and forms a denser and more wrinkled active layer structure.[205,206] According to the charge characteristics of hydrophilic groups, surfactants can be categorized into four main types: (1) anionic (*e.g.* sodium dodecyl sulfate (SDS),[207–209] sodium dodecylbenzene sulfonate (SDBS),[210] sodium *n*-decyl sulfate (SDES)[132]); (2) cationic (*e.g.* hexadecyltrimethylammonium chloride (CTAC),[211,212] hexadecyltrimethylammonium toluene-*p*-sulphonate (CTAT),[211] benzalkonium chloride (BAC)[205]); (3) nonionic (*e.g.* tween 80,[211,213] nonylphenol polyoxyethylene ether (NP-10)[214]); and (4) zwitterionic types (*e.g.* sulfobetaine vinylimidazole (SBVI),[215]

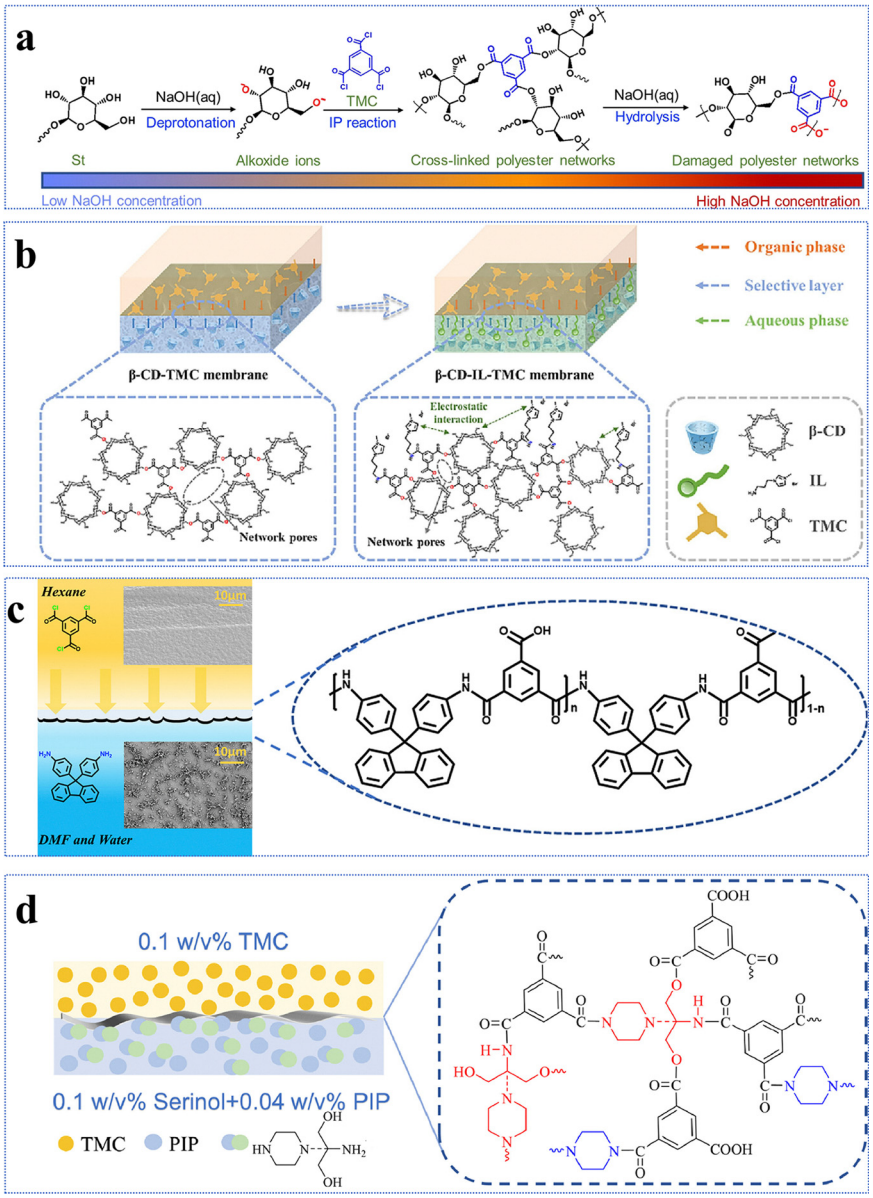

Fig. 11 Interface regulation strategies for novel monomer-based NF membranes. (a) Preparation of the $St_{0.1}/TMC_{0.1}$-3 membrane *via* NaOH-mediated regulation. Reproduced with permission from ref. 58. Copyright 2023, American Association for the Advancement of Science. (b) Preparation of the β-CD-IL-TMC-0.3 membrane *via* ionic-liquid-mediated regulation. Reproduced with permission from ref. 203. Copyright 2023, Elsevier. (c) Preparation of the BAF-PA membrane *via* co-solvent-mediated regulation. Reproduced with permission from ref. 204. Copyright 2023, Elsevier. (d) Preparation of the NF-0.1S + 0.04P membrane *via* co-reactant-mediated regulation. Reproduced with permission from ref. 47. Copyright 2024, Elsevier.

3-((2-aminoethyl) dimethylammonio) propane-1-sulfonate (sulfobetaine) (ADSS)[216]). Among them, anionic and cationic surfactants are the most used surfactants for regulating the properties of NF membranes. For example, early studies introduced anionic surfactants, such as SDS and dodecyl phosphate, to minimize the diffusion energy barrier of aqueous monomers to the oil phase. This facilitated more uniform and rapid diffusion, and optimized the pore size distribution and effective thickness of the selective layer.[206,209,217] Furthermore, anionic surfactants were also used to help stabilize the microbubbles generated during the IP reaction, which helped form an active layer with abundant interconnected pores.[218] For instance, adding 0.06 wt% SDS to a positively charged amine monomer (*i.e.*, TET) solution induced a water microphase on the substrate surface. It not only created an unstable water/solvent interface but also resulted in a ''ridge-valley'' wrinkled morphology on the polyester NF membrane.[63] The ''ridge-valley'' structure has been proven to significantly increase the contact surface area between the solvent/solute and the membrane, effectively mitigating the trade-off relationship between permeability and selectivity. Additionally, cationic surfactants also play a role in controlling the hydrolysis of critical functional groups in novel monomers. In the literature, dodecyl trimethyl ammonia bromide (DTAB) was employed to

inhibit the hydrolysis of ester groups in aqueous-phase monomers (*i.e.*, MPIP or EPIP), thereby reducing the mass transport resistance and decreasing the negative charge density of the active layer.[62] Subsequently, NaOH was added to hydrolyze ester groups in the free fragments within the active layer.[62] This sequential approach, adding a surfactant initially and then followed by an alkali treatment, not only reduced the thickness and pore size of the active layer but also enhanced its internal pore connectivity for solvent/solute transport. However, the mechanisms underlying the regulation of the IP process for novel monomer-based NF membranes by nonionic or zwitterionic surfactants, as well as their feasibility, remain underexplored.

Overall, surfactants have emerged as crucial additives to tune the separation performance of the active layer by reducing interfacial tension, inducing wrinkled structures, and protecting functional groups. However, the residual surfactants may induce undesired effects, such as loose pores and membrane fouling. Future research should focus on (1) developing bio-based surfactants; (2) integrating multi-parameter regulation (*e.g.* temperature and pH control); and (3) employing *in situ* monitoring and computational simulations to achieve precise control over the IP process.

The influence of ionic liquid addition

Ionic liquids (ILs) represent a unique class of liquid salts composed of organic cations and inorganic anions, exhibiting properties such as low volatility, high viscosity, scalability, and controllability.[219] These intrinsic properties confer exceptional interfacial compatibility on ionic liquids and empower them at the molecular scale to precisely regulate: (1) the aggregation behavior of aqueous-phase monomers in the bulk phase, (2) their migration kinetics across the water/solvent interface, and (3) the dispersion uniformity and local concentration distribution of acyl chloride monomers in the organic phase (Fig. 10).[220–223] Therefore, ILs enable controllable regulation of the active layer's crosslinking density and structural architecture by precisely modulating the polarity of the interfacial microenvironment, thereby enhancing monomer mass transfer efficiency and interfacial contact probability. In recent years, ILs have been employed to modulate the interfacial diffusion of both PIP and TMC so that the key properties of the active layer, including charge density, thickness, and hydrophilicity can be precisely manipulated.[224–228] More importantly, the application of ILs has been extended to novel aqueous-phase monomer systems (*e.g.* PEI and cyclodextrin derivatives), which commonly possess large molecular weights, high hydrophilicity, and pronounced steric hindrance. These characteristics collectively impede interfacial mass transfer kinetics, hinder complete crosslinking, and consequently induce defect formation and structural heterogeneity within the active layer. In contrast, ionic liquids modulate the interfacial microenvironment through synergistic mechanisms, including electrostatic screening, hydrogen-bond complexation, and ion-pair stabilization, to selectively destabilize the thermodynamic stability of the monomer hydration shell, thereby enabling directional monomer migration and controlled interfacial enrichment. For instance, the AEMIC-PEI-CC NF membrane synthesized with the aid of 1-aminopropyl-3-methylimidazolium chloride ([AEMIm][Cl]) showed outstanding separation of rare earth elements.[223] The resulting membrane had a permeance 1.4 times higher than that of the pristine membrane, while maintaining a comparable selectivity of 39.0 for HCl/YCl_3. It could also withstand strong acid environments over 30 days at pH = 1.[223] This remarkable performance arose from the fact that the IL-induced water/organic interface channels allowed PEI to diffuse across the interface and react with cyanuric chloride (CC).[223] Clearly, the IL-IP strategy could increase porosity and small pores abundantly and augment positive charge density *via* IL's tertiary amine groups, leading to a faster solvent permeation and higher Y^{3+} retention.[223] Similarly, the β-CD-IL-TMC-0.3 membrane synthesized from an IL of 1-aminopropyl-3-methylimidazolium bromide and β-CD in the water phase had an ethanol permeance of 5.7 L m^{-2} h^{-1} bar^{-1} and a nearly 100% retention of naphthol green B (Fig. 11b).[203] It was found that the IL increased the crosslinking degree and integrity of the active layer for a high dye rejection, while the β-CD's large cavity boosted the solvent permeation.[203] In addition, an IL with a high viscosity may impede monomer diffusion across the reaction interface and result in a thinner active layer for a higher solvent permeation. For example, the APAN-F-0.5 membrane prepared from 1-butyl-3-methylimidazolium tetrafluoroborate ([Bmim][BF4]) had a high methanol permeance of 124.1 L m^{-2} h^{-1} bar^{-1} and an excellent retention of large dyes (*i.e.*, >98.8% for dyes of >647 Da).[222] Overall, ILs endowed the active layer of NF membranes with structural tunability, interfacial activity, and chemical compatibility, and have emerged as versatile regulators for tailoring the membrane structure and performance. Generally, they function dually as "interface architecture directors" and "reaction microenvironment modulators" during IP. Their multi-scale, multi-mechanism collaborative regulation enables precise engineering of critical physicochemical properties of the NF active layer, including morphology, crosslinking network density, pore size distribution, and charge identity and spatial distribution, offering a green and efficient strategy for next-generation high-performance membranes.

The influence of co-solvent addition

Co-solvents are auxiliary components that play a pivotal regulatory role in the IP process. Fundamentally, they constitute a third-phase medium with trace amounts in either the aqueous or organic phase, which rarely participates in the main-chain polycondensation reaction yet systematically modulates interfacial transport kinetics and thermodynamic parameters. Specifically, co-solvents exert dual synergistic functions: (1) by differentially tuning the molecular dispersion state and local polarity environment of acyl chloride monomers in the aqueous-phase and organic-phase monomers, and (2) reducing the water/solvent interfacial tension, thereby precisely governing their effective interfacial concentration gradients and trans-interfacial diffusion fluxes (Fig. 10). Critically, the co-solvent functions exclusively through physical microenvironment

engineering, introducing no additional reactive functional groups and preserving the fundamental chemical architecture of the polyamide active layer. Consequently, co-solvents enable directional, quantitative, and reproducible control over key microstructural parameters of the active layer; namely, thickness, pore connectivity, surface roughness, crosslinking density gradient across the thickness direction, and degree of nanoscale phase separation, without altering its intrinsic chemical composition. In the literature, low-polarity, medium-dielectric-constant co-solvents (*e.g.* acetone and ethyl acetate) have demonstrated the above characteristics by reducing interfacial tension and diffusion barrier, thus forming dense NF membranes with high separation performance.[201,229] On the contrary, high-polarity co-solvent systems (*e.g.* choline chloride-ethylene glycol, phytic acid dodecasodium salt) effectively reduce water/solvent interfacial tension; however, their strong hydrogen-bond donor/acceptor capability promotes extensive hydrogen-bonding networks with aqueous-phase monomers (*e.g.* PIP), thereby impeding bulk-phase diffusion and interfacial availability.[230,231] Additionally, their elevated dynamic viscosity hinders both the mobility of organic-phase monomers in bulk-phase and their adsorption kinetics at the interface. This facilitates the rational design and scalable fabrication of an ultrathin selective layer with a high permeability. Therefore, the practical implementation of co-solvents requires a systematic evaluation of polarity, hydrogen-bond donor/acceptor strength, dynamic viscosity, and ternary phase behaviour, followed by synergistic optimization to align with both the chemical identity of the monomer system and the structural targets of the membrane.

The co-solvent regulation strategy has been strategically extended to diverse functional monomers to modulate interfacial polymerization kinetics, thereby enhancing performance. For example, 9,9-bis(4-aminophenyl)fluorene (BAF), featuring a rigid structure, was used in a co-solvent system of DMF/water–hexane to synthesize BAF-PA membranes with a high methanol permeance of 23.9 L m^{-2} h^{-1} bar^{-1} and an excellent dye separation of $>90\%$ (Fig. 11c).[204] Here, DMF was used as the main solvent while water was utilized as the co-solvent. Their combination solved the solubility issue of BAF and promoted the reverse diffusion of TMC into the DMF/water phase. The resultant membrane had a smoother and more porous active layer for superior OSN performance.[204] In conclusion, the co-solvent-mediated reverse regulation strategy offers a novel approach to handle poorly soluble amine monomers for IP processes.

Overall, co-solvents transcend their conventional role as dissolution aids and instead act as molecular regulators to orchestrate IP kinetics, directing active-layer nanostructure evolution, and enabling quantitative coupling among monomer chemistry, interfacial transport dynamics, and morphological outcome. Future research should prioritize establishing quantitative structure–performance relationships that link co-solvent molecular descriptors (*e.g.* polarity, H-bonding capacity) with interfacial parameters and membrane performance. This necessitates a rational, multi-parameter screening framework to identify green and renewable co-solvents compatible with scalable interfacial polymerization processes.

The influence of co-reactant addition

Co-reactants are compounds participating in the IP process between aqueous and organic-phase monomers. Slightly different from the previous additions, this approach not only influences the microstructure but also alters the composition of the active layer. Generally, it shows effectiveness to (1) modulate the diffusion behavior of amine monomers (*i.e.*, PIP) during IP *via* hydrogen bonding or electrostatic interactions; and (2) optimize the microstructure and performance of the active layer (Fig. 10).[92,231] In recent years, novel monomers such as capsaicin derivatives (*i.e.*, AMTHBA), glycerol, mannitol, boric acid, 4-hydroxypiperidine, lignin, cyclen, and crown ether have been employed as co-reactants to regulate the syntheses of novel monomer-based NF membranes.[47,83,86,90,97,112,128,149,232–239] Basically, they functioned as ''activators'' for those low-reactivity aqueous-phase monomers to enhance their reactivity. As a result, the NF-0.1S + 0.04P NF membrane prepared using both PIP and serinol had a high permeance of 18.5 L m^{-2} h^{-1} bar^{-1} and a $MgSO_4$ rejection rate of 95.5% (Fig. 11d).[47] Experimental results confirmed that a traced amount of PIP would work as a co-reactant to activate the inert serinol *via* the ''bridge effect''. It effectively resolved the critical issue of serinol's inertness to crosslink with TMC and overcame the reliance on traditional and highly reactive monomers.[47] Additionally, co-reactants can function as ''fillers'' in the active layer to tackle issues such as broad pore size distribution and insufficient crosslinking. For example, the TIHP-0.15 membrane prepared with tannic acid (TA) as a co-reactant for HP-β-CD showed an exceptional permeance of 82.9 L m^{-2} h^{-1} bar^{-1} and a NaCl/tetracycline selectivity of 17.6.[90] The addition of TA not only reduced pore sizes through its macromolecular steric hindrance effect but also enhanced hydrophilicity and charge density because of its abundant hydroxyl groups. Thus, the newly developed NF membrane had superior performance to the pristine one in terms of permeability, selectivity, antifouling performance, and chlorine resistance.[90] Similarly, the TFC-NA + TAEA-0.03 membrane made from the macrocyclic monomer of Noria with the aid of tris(2-aminoethyl)amine (TAEA) as a co-reactant exhibited a Na_2SO_4 rejection 68.7% higher than the pristine one without TAEA (*i.e.*, TFC-NA + TAEA-0.03 *vs.* TFC-NA) while maintaining a comparably high permeance of 15.3 L m^{-2} h^{-1} bar^{-1}.[232] This improvement resulted from (1) the filling of TAEA to the large pore defects induced by Noria; and (2) the preservation of a high degree of crosslinking to enhance both selectivity and permeability.[232] It is also noteworthy that crown ethers, characterized by a cyclic architecture composed of ether oxygen atoms and featuring multiple cavity sizes, can selectively coordinate with alkali metal ions, enabling their application in the tailored design of nanofiltration membranes for LiCl/$MgCl_2$ separation.[235,237,240] The unique molecular structure of crown ethers allows them to function as aqueous-phase monomers that effectively modulate the IP process, thereby refining the microstructure of the

polyamide active layer. For example, the NF-0.6 membrane fabricated using 18-crown-6 ether as a co-reactant with PIP achieved an excellent water permeance of 26.1 L m^{-2} h^{-1} bar^{-1} and a high Na_2SO_4 rejection rate of 97.6%.[237] This superior performance could be attributed to two key mechanisms: (1) hydrogen bonding between 18C6 and PIP suppressed the diffusion of PIP toward the organic-phase interface, resulting in a significantly thinner polyamide layer that facilitated a rapid water transport; and (2) the intrinsic macrocyclic cavity of 18C6 moderately increased the free volume and porosity within the active layer, enhancing permeability even though this might slightly compromise solute retention for small molecules.[237] Overall, strategically leveraging the structural features of functional monomers to achieve a synergistic balance between permeability and selectivity represents a crucial approach to overcoming the performance limitations of NF membranes.

In summary, the structure and performance of the active layer can be effectively optimized by introducing co-reactants that would (1) enhance the reactivity of inert monomers, (2) compensate for the low crosslinking degree, or (3) mitigate large pores caused by macrocyclic monomers.

Structure-performance relationships and underlying synergistic mechanisms of novel monomer-based NF membranes

Despite the widespread application of conventional NF membranes in water treatment due to their well-established manufacturing processes and cost-effectiveness, there are unsolved challenges. Customers want (1) higher permeability and higher selectivity; (2) greater adaptability to the complicated compounds in modern wastewater; and (3) superior chemical and performance stability for broader applications. To meet these urgent demands, novel monomers have been developed for advanced NF membranes. Table 2 comprehensively summarizes their chemical properties and analyzes their underlying synergistic mechanisms to improve the permeability, selectivity, and stability for the development of high-performance NF membranes.

Permeability and mechanisms

The permeability of NF membranes is a key indicator of their separation performance, typically measured by water flux per unit pressure, time, and effective membrane area (L m^{-2} h^{-1} bar^{-1}). In practical applications, NF membranes with a high permeability are essential to facilitate water transport, increase separation efficiency and reduce treatment costs. Therefore, most recently developed NF membranes using novel monomers have shown significant improvements in permeability. Their permeances range from 1.1 to 209.1 L m^{-2} h^{-1} bar^{-1} with an average value of 35.3 L m^{-2} h^{-1} bar^{-1} (Fig. S1a and Table 2), which is much higher than those of traditional membranes such as NF90 (2.9 L m^{-2} h^{-1} bar^{-1}) and NF270 (7.7 L m^{-2} h^{-1} bar^{-1}).[263,264] This significant advancement in permeance arises from the improved understanding of (1) the role of novel monomers to modulate the microstructure of the active layer; and (2) the synergistic effects of surface properties and structural features when designing high-permeability NF membranes. More importantly, to achieve a higher permeability without compromising the selectivity, future research should focus on the key factors that influence permeability. Accordingly, four core optimization strategies are proposed: tailoring monomer chemical structures, optimizing IP reaction parameters, refining the IP process, and employing advanced post-treatment techniques (Fig. 12).

Generally, novel monomers influence permeability by modulating surface properties including contact angle, roughness, and surface charge. Because the water contact angle is a direct indicator of the membrane's hydrophilicity, a smaller water contact angle indicates greater membrane wettability, beneficial

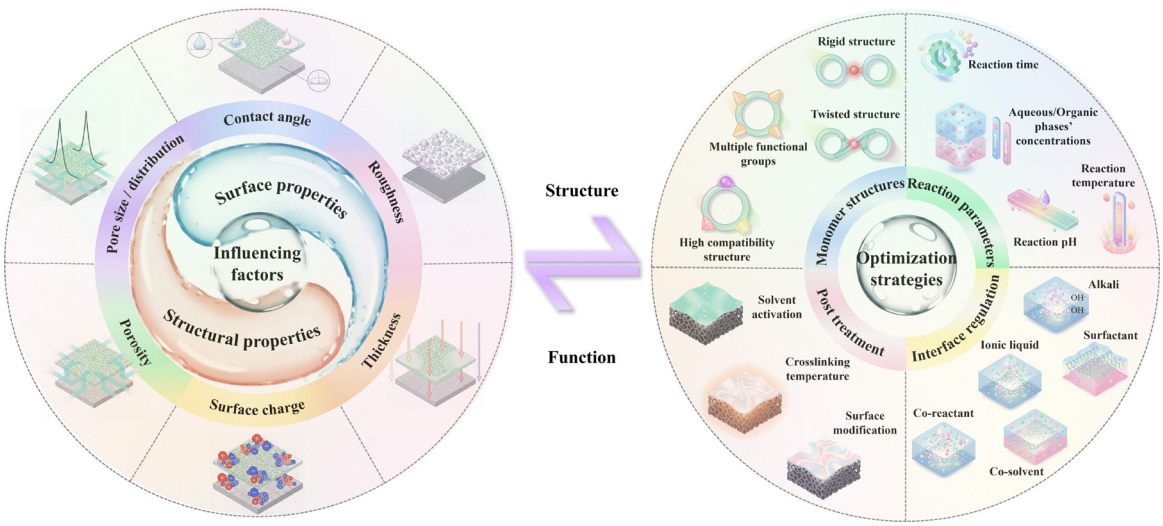

Fig. 12 Key factors influencing permeability and optimization strategies for novel monomer-based NF membranes.

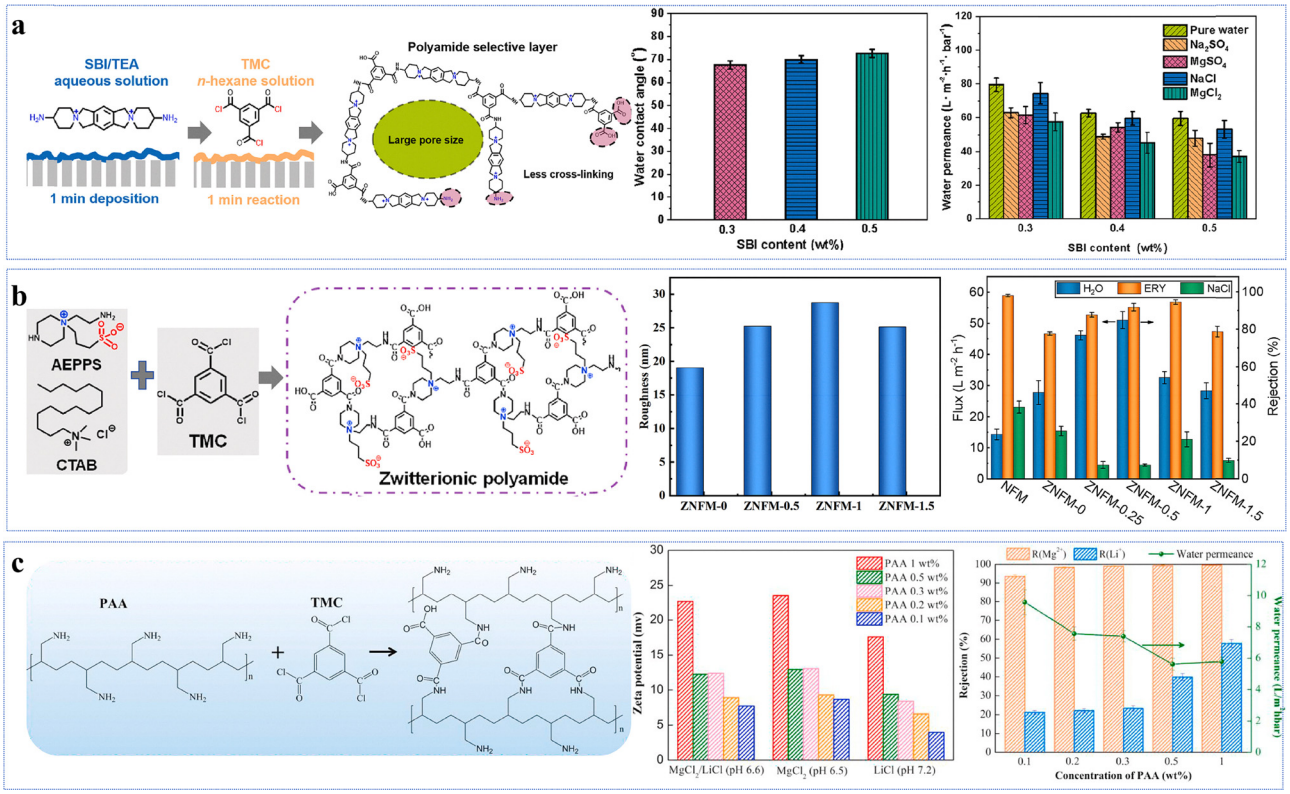

Fig. 13 The influence of surface properties on permeability. (a) The influence of contact angle on the SBI-TMC membrane. Reproduced with permission from ref. 234. Copyright 2025, Elsevier. (b) The influence of surface roughness on the ZNFM membrane. Reproduced with permission from ref. 134. Copyright 2022, Elsevier. (c) The influence of surface charge on the PAA/TMC membrane. Reproduced with permission from ref. 155. Copyright 2023, Elsevier.

for a higher permeability. For example, the permeance of the SBI-TMC membranes made from a high SBI concentration decreased from 79.6 to 59.6 L m^{-2} h^{-1} bar^{-1} as the contact angle increased from 67.6° to 72.6° (Fig. 13a).[234]

Additionally, surface roughness is another critical factor. Normally, a rougher surface provides a larger effective area for liquid transport across the membrane. For example, the water permeance of the ZNFM membranes increased from 5.8 to 10.6 L m^{-2} h^{-1} bar^{-1} and then decreased to 5.8 L m^{-2} h^{-1} bar^{-1} as roughness varied from 19.0 to 25.2 and to 25.1 nm and the thickness changed from 131 to 78 and to 120 nm (Fig. 13b).[134] These variations in permeance, roughness and thickness resulted from different effects of phase transfer catalysts on interfacial polymerization.[134] Apart from surface hydrophilicity and roughness, surface charge also plays an important role in determining the permeability.

The difference in dielectric constant between water molecules and the NF membrane's surface creates electrostatic interactions affecting water molecule orientation and transport at pore entrances.[266–270] For instance, when increasing the polyallylamine (PAA) concentration, the resulting membrane exhibited a higher positive charge density, owing to the incorporation of more protonated $-NH_2$ groups in the active layer. However, it also resulted in a denser active and reduced permeability. Thus, the water permeance dropped from 9.6 to 5.8 L m^{-2} h^{-1} bar^{-1} when increasing the surface potential from approximately 7 to +23 mV (Fig. 13c).[155] In summary, the type and structure of functional groups in the novel monomers influence membrane permeability by modulating surface properties.

In addition, novel monomers influence permeability by modulating structural properties, including active layer thickness, pore size (*i.e.*, pore diameter) and porosity. Among these, the active layer thickness plays a critical role in governing the mass transport distance and resistance of water molecules *via* (1) lateral surface diffusion; and (2) vertical penetration across pores.[62,255,271,272] An ultrathin active layer can significantly reduce the mass transport distance but may compromise mechanical strength and selectivity. For instance, the water permeance of the LNF membrane decreased from 23.0 to 8.6 L m^{-2} h^{-1} bar^{-1} as the active layer thickness increased from 83.2 to 123.2 nm because a higher bis-tris propane concentration was employed in IP in the latter case that formed a thicker active layer and reduced the permeability (Fig. 14a).[265] In addition to thickness, pore size plays an important role in determining membrane permeability. Depending on the unwanted solutes, a sharp or a narrow pore size distribution is preferred to balance water transport and solute rejection. Ideally, this involves the combination of (1) large pores with low desolvation energy barriers to enhance the water permeance;

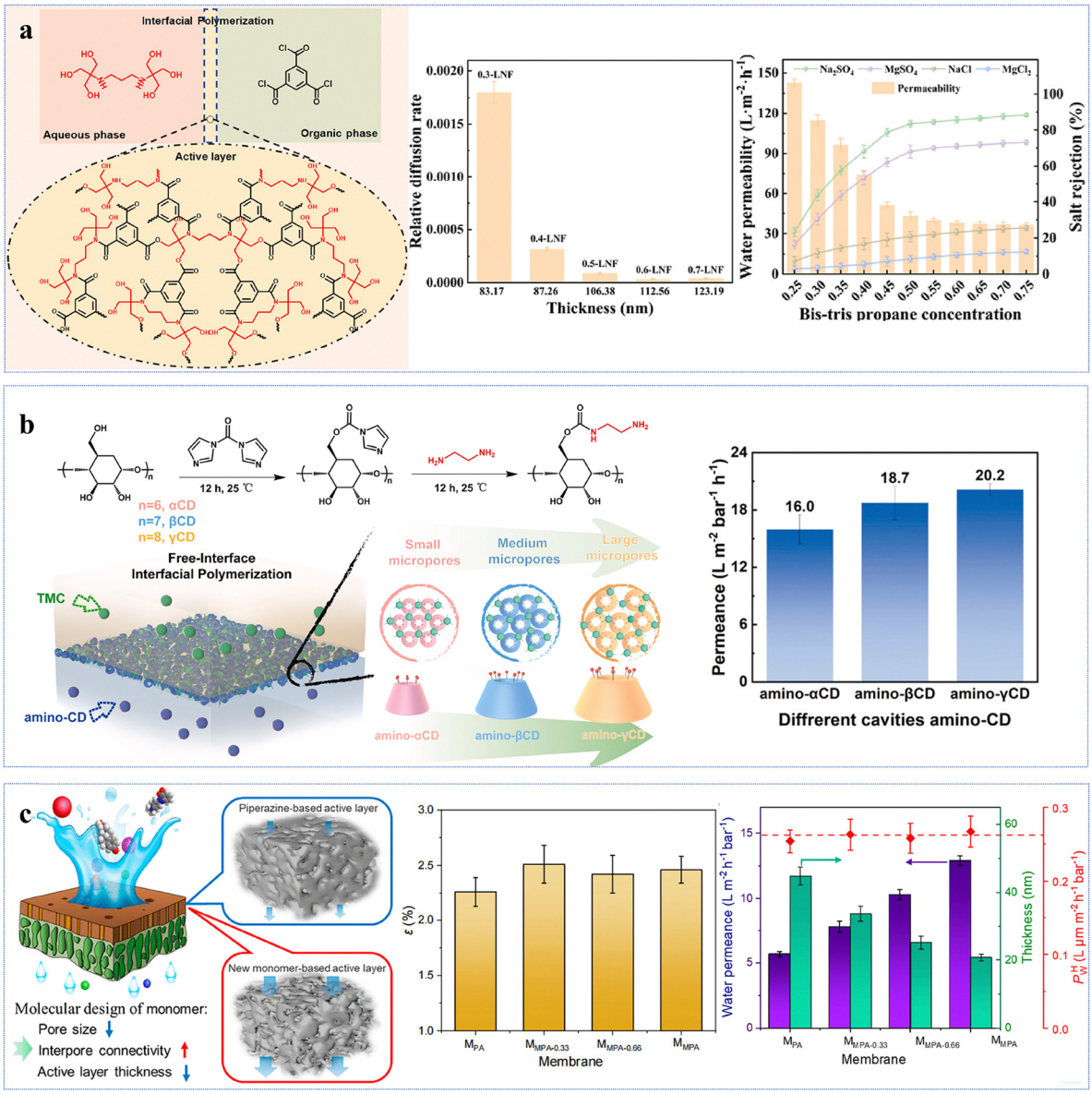

Fig. 14 The influence of structural properties on permeability. (a) The influence of active layer thickness on the LNF membrane. Reproduced with permission from ref. 265. Copyright 2022, Elsevier. (b) The influence of pore size on the amino-CD-based membrane. Reproduced with permission from ref. 115. Copyright 2025, Elsevier. (c) The influence of porosity on the M_{MPA} and M_{EPA} membranes. Reproduced with permission from ref. 62. Copyright 2022, American Chemical Society.

and (2) small pores with a high selectivity to effectively reject the unwanted solutes. Macrocyclic molecules, such as cyclodextrin and cucurbit[6]uril, featuring a unique ''hydrophilic rim-hydrophobic cavity'' structure, allow precise control over pore sizes.[74,91,115,117,273–275] For instance, with the increase in pore sizes of amino-αCD (0.29 nm), amino-βCD (0.33 nm), and amino-γCD (0.35 nm), the permeances of the corresponding membranes increased progressively from 16.0 to 18.7 to 20.2 L m^{-2} h^{-1} bar^{-1} (Fig. 14b).[115] So far, the pore sizes of the existing novel monomer-based NF membranes range from 0.11 to 2.5 nm (Fig. S1f).

Furthermore, porosity is another key parameter affecting membrane permeability.[276,277] A higher porosity provides additional channels for water permeation, thereby enhancing the membrane permeability. For instance, NF membranes (*i.e.*, MMPA and MEPA) prepared using ester-based amine monomers followed by alkaline hydrolyses had water permeances of 12.9 and 15.6 L m^{-2} h^{-1} bar^{-1}, respectively. These values were much higher than that (*i.e.*, about 5.7 L m^{-2} h^{-1} bar^{-1}) of the control membrane without using the novel monomers and alkaline hydrolysis.[62] The substantial improvements arose from the formation of numerous sub-nanometer pores triggered by the NaOH-induced hydrolyses of ester groups in M_{PA} and E_{PA} (Fig. 14b). They not only enhanced pore connectivity but also boosted the average porosity of the MMPA and MEPA active layers by 0.21% and 0.54%, respectively.[62] Here, the hydrolyzable

ester groups in the active layer functioned as a chemical switch to regulate pore sizes and customize the molecular structure of active layers. In summary, employing novel monomers and controllable IP with the aid of process optimization provides a valuable strategy to develop high-permeability NF membranes with greater channel connectivity and lower mass transport resistance. However, challenges related to long-term stability and cost-effectiveness remain to limit their large-scale industrial applications. Future research could focus on multi-parameter collaborative design to establish a quantitative model including contact angle, roughness, surface charge, thickness, pore size, and porosity. Moreover, research should prioritize green preparation methods to advance large-scale applications for complex wastewater treatment and resource recovery.

Selectivity and mechanisms

The selectivity of NF membranes is another critical parameter for assessing their separation efficiency. High-selectivity NF membranes are essential to improve the quality of effluents and maximize the recovery of valuable compounds from wastewater resources. However, this requires precise solute separation through the synergistic control of pore size and its distribution while maintaining a high permeance. Herein, we systematically investigate the mechanisms that enhance the selectivity of novel monomer-based NF membranes to separate (1) monovalent/divalent ions; (2) water/organic compounds; and (3) salt/organic compounds. As the separation factor (S) is defined as the rejection ratio of solute A to solute B, a higher S value generally indicates superior separation performance. The selective separation mechanisms of an NF membrane not only depends on its pore size and pore-size distribution, molecular weights, geometric shapes and hydration sizes of unwanted solutes, but also the membrane-solute–solvent interactions due to (1) their differences in solubility parameters; (2) the Donnan effect and (3) dielectric effects (Fig. 15). When the size of a solute exceeds the pore size of a membrane, the size exclusion would dominate the rejection mechanism (Fig. 15). Additionally, the charged surface of a membrane would selectively repel ions of the same charge by means of electrostatic repulsion (Fig. 15). Meanwhile, interface polarization, induced by differences in dielectric constants between the membrane material and the solvent (water), would hinder the membrane transport of low-dielectric solutes, such as hydrophobic organic compounds, *via* dielectric repulsion (Fig. 15).[62,269]

However, a quantitative analysis of these interactions remains lacking. One must conduct a systematic analysis to examine the correlation between the structural features and solute rejection. The following sections give comprehensive assessments of how structural characteristics of novel monomers influence the selectivity of NF membranes for these three applications. To enhance the selectivity of NF membranes, two fundamental strategies are proposed: optimize the pore structure of the active layer and regulate the chemical properties on the membrane surface (Fig. 15).

Specifically, the development of highly reactive aqueous-phase monomers and their well-matched organic-phase counterparts, precise regulation of interfacial cross-linking temperature, and incorporation of functional additives to modulate the

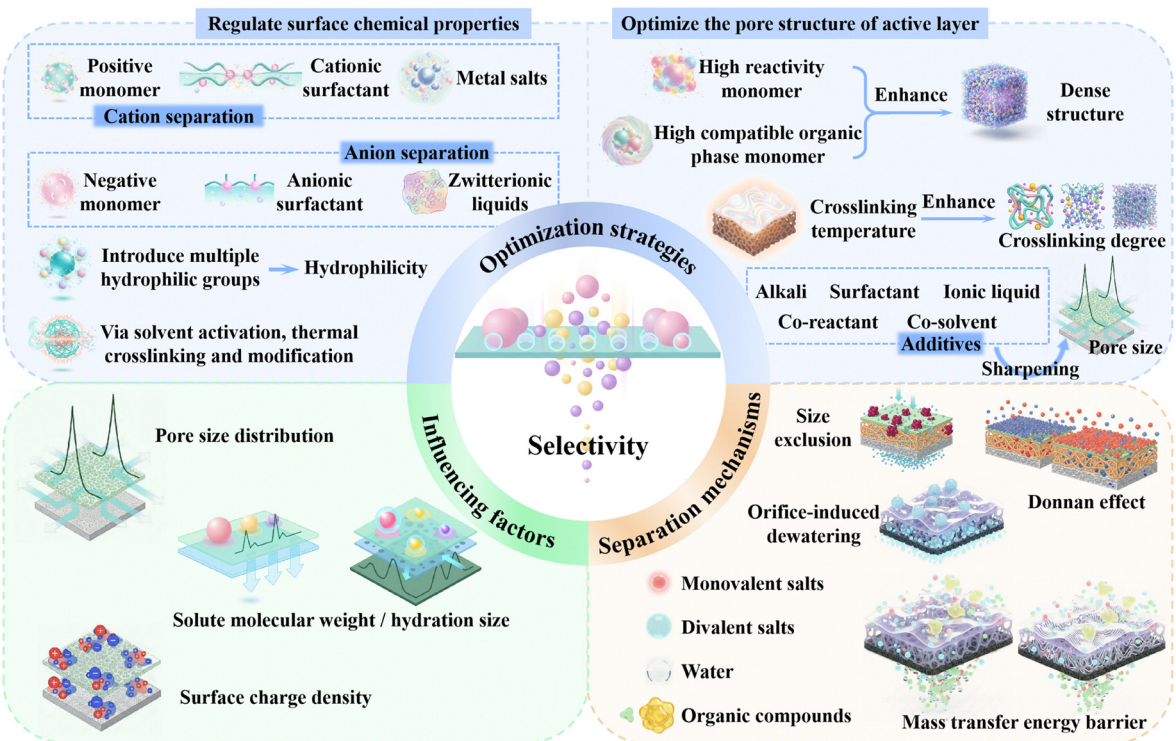

Fig. 15 Key factors influencing selectivity and optimization strategies for novel monomer-based NF membranes.

IP process represent key strategies for controlling the pore structure of the active layer of NF membranes (Fig. 15). Furthermore, by rationally designing monomer characteristics, such as charge properties, functional group types, and quantities according to the charge features of target solutes, the surface chemical properties of NF membranes can be precisely tailored, thereby improving the solute selectivity and separation efficiency (Fig. 15).

Mechanisms to separate monovalent/divalent salts

Although NF membranes have been widely utilized for water reuse and resource recovery from brine and high-salinity wastewater.[278–285] The recent demands from lithium-ion batteries as power storage have escalated the need to have an efficient Li^+ extraction from brine solutions where a higher mass ratio of magnesium over lithium exists.[286] In addition, environmental regulations urgently request the textile industry to recycle both dyes and organic/inorganic chemicals (*i.e.*, NaCl and Na_2SO_4) used in textile processes for human health protection and resource sustainability. However, the traditional NF membranes face difficulties in these applications due to their limited adaptability and insufficient selectivity. So far, some novel monomer-based NF membranes have been developed to selectively separate monovalent and divalent salts, such as $LiCl/MgCl_2$ (*i.e.*, Li^+/Mg^{2+}) and $NaCl/Na_2SO_4$ (*i.e.*, Cl^-/SO_4^{2-}).[61,104,111,149,183,224,239,241,245,251,287–291] Here, we evaluate their separation performance. As shown in Fig. S3. The rejections of NaCl and LiCl vary from 3.0% to 92.1% and 12.7% to 64.2%, respectively, while those for $MgSO_4$, Na_2SO_4, and $MgCl_2$ range from 3.9% to 99.3%, 3.7% to 99.5%, and 2.6% to 99.5%, respectively (Fig. S3a). Generally, 86.2% of the membranes exhibit a rejection rate below 50% for NaCl, while 81.3% show similar performance for LiCl. In contrast, 50.0%, 67.6%, and 50.0% of the membranes achieve rejection rates above 90% for $MgSO_4$, Na_2SO_4, and $MgCl_2$, respectively (Fig. S3a). However, challenges remain in enhancing selectivity, particularly for NaCl, where performance is constrained by the nonlinear interplay of structural parameters.

Fig. S4 systematically evaluates their selective separation performance and elucidates the solute/solute separation mechanisms based on the correlation between separation factors and structural parameters. Interestingly, 83.8% of the membranes exhibit a monovalent salt rejection rate below 50%, while 60.0% show a divalent salt rejection rate exceeding 90% (Fig. S4a). Additionally, the separation factors for monovalent to divalent salts vary from 0.4 to 146, with an average value of 19.4 (Fig. S4b). Figs. S4d–f correlates the separation factor of Li^+/Mg^{2+} as a function of permeance, pore size, and surface potential. The permeability of the novel monomer-based NF membranes for Li^+/Mg^{2+} separation ranges from 3.1 to 37.3 L m^{-2} h^{-1} bar^{-1} with an average value of 18.4 L m^{-2} h^{-1} bar^{-1}, while the separation factor varies from 1.1 to 146.0 with an average value of 28.0 (Fig. S4d). Although the hydrated radii of Li^+ and Mg^{2+} are close to each other (*i.e.*, 0.38 *vs.* 0.43 nm), the NF membranes with a well-defined pore size distribution can separate them through size exclusion.[249] Analyses reveal that only 27% of the membranes have pores with a radius of $\leq$0.38 nm (*i.e.*, the hydrated radius of Li^+) (Fig. S4e), suggesting limited sieving efficiency for Li^+. One must further refine the pore size distribution with an average pore radius of $<$0.35 nm to enhance the size-based separation.

Additionally, given that both Li^+ and Mg^{2+} carry positive charges, positively charged membranes should facilitate a higher Li^+/Mg^{2+} selectivity through the Donnan effect. In the literature, approximately 60% of the novel monomer-based NF membranes had positively charged surfaces. The surface potentials could reach as high as +58.2 mV with the incorporation of two positively charged monomers, namely, PEI and DHTAB (Fig. S4f).[67] Overall, these findings imply the great potential of novel monomer-based NF membranes for Li^+/Mg^{2+} separation by combining the synergistic effects of size exclusion and the Donnan effect. However, one must overcome the issues such as broad pore size distribution and uneven charge density as illustrated in the following examples.

For instance, the GEM-TMC membrane prepared from a novel distorted monomer (GEM) containing symmetrical primary amine ($-NH_2$) and quaternary ammonium ($-N^+$) groups had a separation factor of 11.5 for Li^+/Mg^{2+} separation, which was 13 times higher than that of the control PIP-TMC membrane of 0.88 (Fig. 16a).[65] This significant improvement arose from the fact that GEM had a lower diffusion rate and a higher reactivity than PIP in the organic-phase, resulting in a thinner and more porous active layer suitable for solute transport.[65] In addition, the resultant membrane had a highly positive surface charge of +10 mV that could effectively repel Mg^{2+} by means of the Donnan effect.[65] In contrast, although the PIP-TMC membrane had a smaller pore size of 0.3 nm, it failed to achieve selective separation due to its negatively charged surface, which attracted both Li^+ and Mg^{2+}, and allowed them to pass through.[65] Therefore, to achieve precise separation of Li^+/Mg^{2+}, it is more effective to enhance the surface positive charge or charge density rather than relying on size exclusion in negatively charged NF membranes.

In another example, the incorporation of LiOH enabled the construction of ordered self-assembled channels derived from amine-functionalized cyclodextrin (Am7CD) consisting of 7 $-NH_2$ and 14 $-OH$ groups. The resulting LiOH-Am7CD-0.05 TMC membrane had vertically aligned sub-nanometer channels with a pore size of 0.34 nm and a sieving threshold of 0.66 nm, achieving a high Li^+/Mg^{2+} selectivity of 190 (Fig. 16b).[78] Because Li^+ had a lower hydration energy than Mg^{2+}, the former could diffuse through the nanochannels across the membrane easier than the latter. Additionally, the easier dehydration of Li^+ enhanced its electrostatic interaction with the membrane surface, facilitating its transport and further improving the selectivity. Clearly, the high Li^+/Mg^{2+} selectivity of this membrane resulted from both steric hindrance and dehydration mechanisms rather than by the Donnan effect.[78]

The development of the TET-TMC membrane was another notable advancement. It was a positively charged polyester NF membrane containing three quaternary ammonium groups. Because it had an ultra-narrow pore size of 0.26 nm, Mg^{2+} with

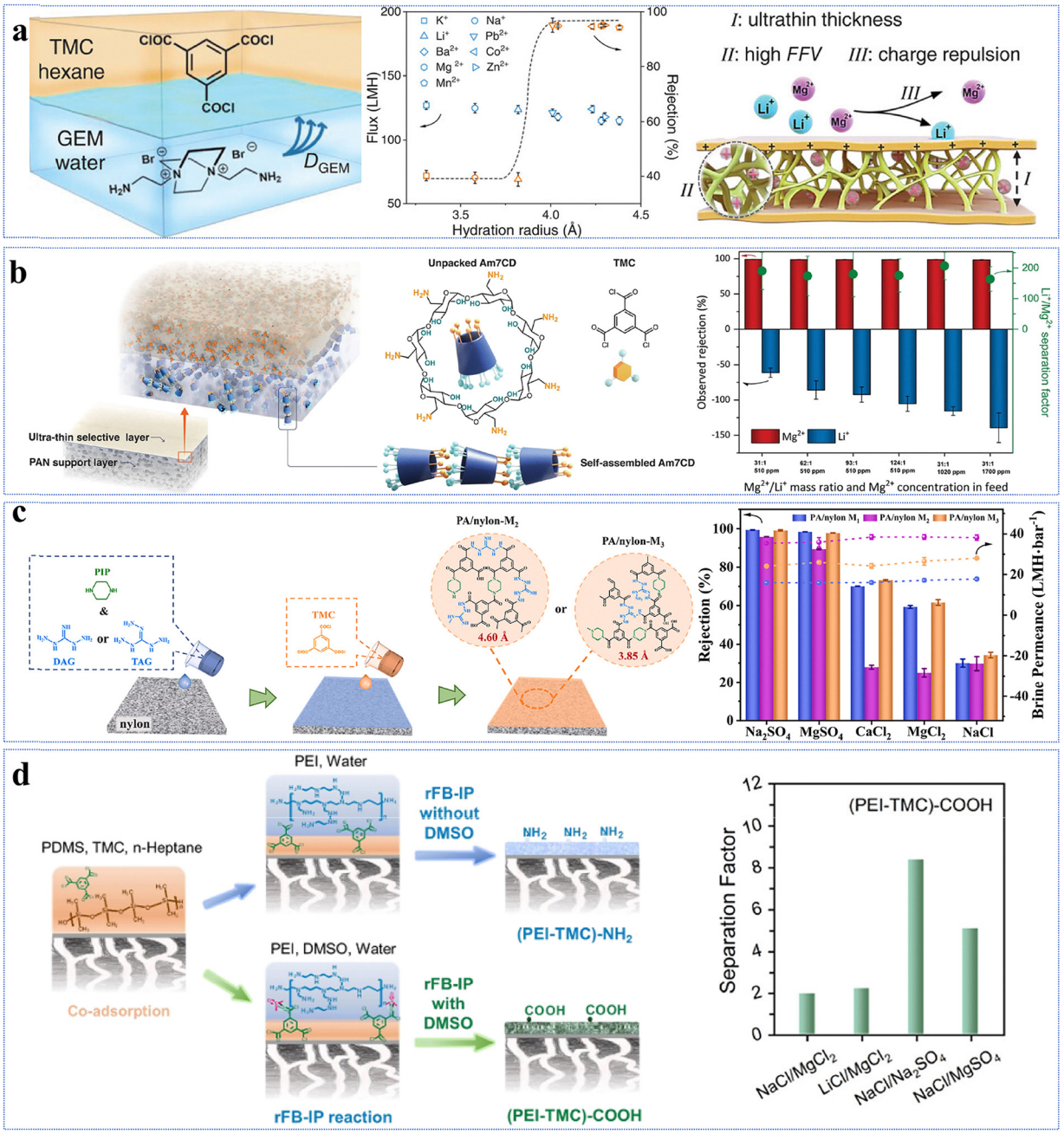

Fig. 16 Novel monomer-based NF membranes for Li^+/Mg^{2+} and Cl^-/SO_4^{2-} separations. (a) Separation performance of the GEM-TMC membrane. Reproduced with permission from ref. 65. Copyright 2023, Wiley-VCH. (b) Separation performance of the LiOH-Am7CD-0.05 TMC membrane. Reproduced with permission from ref. 78. Copyright 2024, Springer Nature. (c) Separation performance of the PA/nylon-M3 membrane. Reproduced with permission from ref. 112. Copyright 2023, Elsevier. (d) Separation performance of the (PEI-TMC)-COOH membrane. Reproduced with permission from ref. 292. Copyright 2024, American Chemical Society.

a hydrated radius of 0.43 nm could be almost rejected by size exclusion.[63] As a result, it exhibited an exceptionally high Li^+/Mg^{2+} separation factor of 146. Additionally, (1) the novel monomer imparted a positive charge to the membrane surface; and (2) the hydrolysis of ester groups reduced the negative charge, the combination of both factors led to strengthening of the Donnan effect.[63] In comparison, the QSPIP-TMC cationic membrane, characterized by its loose and porous structure, only had a Li^+/Mg^{2+} separation factor of 10.[64] Although the Donnan effect still worked, its effectiveness reduced significantly because the membrane had an average pore size larger than the hydrated radius of Mg^{2+} (*i.e.*, 0.61 *vs.* 0.43 nm) and there was not much size exclusion to retain Mg^{2+}. In short, grafting quaternary ammonium salt monomers onto the membrane surface can enhance its positive charge to improve Li^+/Mg^{2+} selectivity by the Donnan effect, but one must control the pore size.[66–70]

In addition to the aforementioned strategy of synthesizing positively charged monomers *via* quaternization reactions for

constructing novel monomer-based NF membranes for Li^+/Mg^{2+} separation, the design of NF membranes leveraging the unique chemical structures and molecular recognition capabilities of non-synthetic monomers offers an equally effective approach to achieving high-efficiency Li^+/Mg^{2+} separation. For example, crown ethers, characterized by their well-defined cyclic cavities of specific dimensions and multiple ether oxygen atoms, are capable of forming stable coordination complexes with specific metal cations such as Li^+, K^+, and Ca^{2+} through ion–dipole interactions, thereby enabling selective ion recognition and facilitated transport. Moreover, crown ethers are widely regarded as ideal candidate monomers for developing advanced membrane materials that integrate molecular recognition functionality with selective ion transport pathways.[236,240,293] Specifically, by employing PEI and hydrophilic Girard reagent T (GRT) as aqueous-phase monomers and grafting dibenzo-14-crown-4 diamine (DAB14C4) to construct well-defined ion transport channels, the DAB14C4@PEI/GRT@PSF membrane was successfully fabricated.[293] This membrane exhibited an excellent permeance of 13.7 L m^{-2} h^{-1} bar^{-1}, and a high separation factor of 63.6 for Li^+/Mg^{2+} separation. The superior performance arose from two synergistic mechanisms: (1) the incorporation of GRT enhanced the hydrophilicity of the aqueous phase, effectively mitigating the disordered stacking of polymer chains in the active layer and thereby facilitating a faster water molecule transport; (2) DAB14C4 exhibited significantly stronger binding affinity toward Li^+ than Mg^{2+}, enabling preferential recognition of Li^+ within the membrane pores. Moreover, due to its lower dehydration energy barrier, Li^+ undergoes more facile desolvation and penetrates the selective layer more readily, thus promoting a highly efficient Li^+ transport.[293]

Similarly, (1) the introduction of a second organic-phase monomer (isophthaloyl chloride, IPC); and (2) the adjustment of the IPC-to-TMC ratio in IP reactions would help control the acyl chloride group density. Both modifications can increase the positive charge of the active layer and strengthen the electrostatic repulsion against Mg^{2+} to improve the Li^{2+}/Mg^{2+} selectivity.[294] In summary, the NF membranes developed from novel monomers have achieved a high selectivity for Li^+/Mg^{2+} separation by leveraging both size exclusion and the Donnan effect. Future research should focus on (1) refining pore size distribution to precisely enhance the size exclusion effect, (2) minimizing the Li^+ rejection, and (3) optimizing the charge density by using highly positively charged monomers to improve Mg^{2+} rejection. However, excessive positive charge densities should be avoided to prevent additional resistance to water transport.

Fig. S4g–h correlates the Cl^-/SO_4^{2-} selectivity of the novel monomer-based NF membrane as a function of permeance, pore size, and surface potential. Generally, the permeance of these membranes ranges from 1.1 to 209.1 L m^{-2} h^{-1} bar^{-1} with an average of 38.6 L m^{-2} h^{-1} bar^{-1} (Fig. S4g). The corresponding separation factors vary from 0.71 to 89.6 with an average value of 25.2. Given that the hydrated radii of Cl^- (0.33 nm) and SO_4^{2-} (0.38 nm) are relatively close, NF membranes must have a narrow pore size distribution to achieve a high selectivity through size exclusion, a mechanism similar to the Li^+/Mg^{2+} separation. Fig. S4h shows that the pore size distribution of these novel monomer-based NF membranes typically ranges from 0.19 to 2.4 nm, with an average pore size of 0.72 nm. Notably, 9.52% of the pores are smaller than or equal to the hydrated radius of Cl^- (0.33 nm). Because both Cl^- and SO_4^{2-} are negatively charged, membranes with a negative surface charge are more effective for Cl^-/SO_4^{2-} separation due to the Donnan effect. Fig. S4i confirms this trend where 74.1% of these novel NF membranes exhibit a negative surface charge. Theoretically, NF membranes made of negatively charged novel monomers with pore sizes ranging from 0.34 to 0.38 nm are preferred for Cl^-/SO_4^{2-} separation because they can achieve efficient separation by means of the Donnan effect. In the literature, the PA/nylon-M3 membrane has shown a significantly high separation factor of 83.8 for $NaCl/Na_2SO_4$ since it had a high negatively charged surface of −20 mV and a pore size of 0.39 nm (Fig. 16c).[112] In comparison, the BAIE-TMC (M-0.5) membrane only exhibited a separation factor of 13.2 for $NaCl/Na_2SO_4$.[242] Although the protonation of the tertiary amino groups in BAIE endowed the membrane with a negatively charged surface of −12.8 mV, the value was not high enough for effective electrostatic repulsion of SO_4^{2-}.[242] Since both PA/nylon-M3 and BAIE-TMC membranes had almost the same pore size of 0.39 nm, they should have almost the same size exclusion towards SO_4^{2-}. Therefore, the above two examples strongly suggest that increasing the surface charge density is the key to enhancing membrane efficiency for the separation of multivalent co-ions.

In another example, the (PEI-TMC)-COOH membrane was prepared *via* reverse flexible-chain binding IP (rFB-IP), where a highly polar dipolar aprotic solvent of dimethyl sulfoxide (DMSO) was employed as the charge regulator. The resultant membrane exhibited a separation factor of 8.4 for $NaCl/Na_2SO_4$ (Fig. 16d).[292] Because DMSO could interact with the carbonyl oxygen of TMC *via* dipole–dipole interactions, this would not only protect the acyl chloride groups of TMC but also form –COOH.[292] Thus, the membrane was transformed from positively charged to negatively charged for separating Cl^- and SO_4^{2-} ions by the Donnan effect (Fig. 16d).[292]

Moreover, 18-crown-6 and 15-crown-5, cyclic macrocyclic compounds, were incorporated as aqueous co-monomers into the PIP solution, where they formed host–guest complexes with PIP *via* hydrogen bonding interactions.[239] This interaction effectively suppressed the interfacial diffusion of PIP, enabling the fabrication of advanced NF membranes with a thinner, rougher selective layer and higher negative charge density. Experimental results demonstrated that, compared to the conventional PIP-TMC membrane with a permeance of 12.5 L m^{-2} h^{-1} bar^{-1}, the permeances of the TFC-CE18 and TFC-CE15 membranes increased by approximately 10 and 8 L m^{-2} h^{-1} bar^{-1}, respectively. Simultaneously, their NaCl/Na_2SO_4 selectivity was significantly enhanced to 224 and 240, respectively, representing a marked improvement over the control membrane (70).[239] This superior selectivity was primarily attributed to the distinctive molecular architecture of the

crown ethers: (1) The ether-rich cyclic cavities not only enhanced membrane hydrophilicity, facilitating water transport, but also introduced additional negatively charged sites, thereby intensifying electrostatic repulsion against multivalent anions such as SO_4^{2-}. (2) By retarding PIP diffusion at the interface, the crown ethers moderated the IP kinetics, leading to a polyamide active layer with a reduced crosslinking density, larger effective pore size, and a more open structure. These features collectively enhanced permeability. Furthermore, the larger hydrated radius and higher charge density of SO_4^{2-} resulted in a significantly higher diffusion energy barrier compared to Cl^- when traversing the membrane matrix, thus amplifying ion sieving performance.[239] Consequently, the strategic incorporation of crown ether co-monomers with well-defined cavity dimensions and tailored functionality enables synergistic regulation of both the membrane's microstructure and surface properties, concurrently enhancing size exclusion and Donnan effects, and ultimately achieving highly efficient separation of NaCl and Na_2SO_4.

In summary, the novel monomer-based NF membranes have achieved notable advancements for Cl^-/SO_4^{2-} separation primarily through the Donnan effect. Future research should focus on membranes with precisely controlled pore sizes and negative surface charges to accurately separate monovalent and divalent anion salts.

Mechanisms to separate organic compounds

Global warming resulting from industrial emission of CO_2 and other greenhouse gases has changed the R&D direction of NF membranes. For example, most pharmaceutical companies in the old days would discharge or burn their effluents depending on their concentrations of organic compounds (*i.e.*, organic solvents and residual drugs) in on-site incinerators. Now, these practices are no longer allowed and have been mostly discontinued. Instead, they must recycle these effluents to lower the greenhouse gases in the air. Thus, developing NF membranes for water/organic compound separations has become important[38,295–303] to recover or remove organic compounds, such as dyes,[204,252,254,273,274,304,305] pharmaceuticals,[89,257,306–308] and organic micropollutants.[309–311] Usually, the conventional NF membranes aim to separate water, salts and impurity compounds with low molecular weights (MWs) below 100 Da.[312] In contrast, the novel monomer-based NF membranes aim to selectively separate organic compounds within a MW range of 100–300 Da.[77] Fig. S5 summarizes the performance of these NF membranes for the separation of water/organic compounds as a function of key parameters. They have water permeances ranging from 2.9 to 209.1 L m^{-2} h^{-1} bar^{-1} with an average value of 48.4 L m^{-2} h^{-1} bar^{-1} (Fig. S5a), which is significantly higher than those of commercial NF membranes (*i.e.*, NF90). Additionally, 57.8% of the membranes have achieved a rejection rate of $\geq$90% (Fig. S5a). Given the hydrophobic nature of most organic compounds, hydrophilic membranes (contact angle $<60^\circ$) are more favorable for water permeation and organic matter retention.

For instance, the hydrophilic membrane TFC_{18C6} synthesized using bis(aminobenzo)-18-crown-6 (18C6) as the monomer had separation factors of 26.3 for 4-iodoanisole (234 Da) and 79.0 for triptycene (254 Da) and octocrylene (361 Da) (Fig. 17a).[77] The high separation factors arose from the macrocyclic structure of 18C6, which reduced the IP reaction rate and formed a dense active layer with a smaller pore size of 0.34 nm and a MWCO of $\sim$194 Da. This enabled the membrane to perform size exclusion of organic compounds with a MWCO ranging from 200 to 370 Da.[77] Similarly, the hydrophilic membrane Cyclen-TBB achieved over 90% rejections of antibiotics (*i.e.*, doxorubicin hydrochloride (580 Da, positively charged), diammonium glycyrrhizinate (857 Da, negatively charged)) (Fig. 17b) and dyes (*i.e.*, CR (697 Da, negatively charged), Victoria blue B (506 Da, positively charged), acid fuchsin (586 Da, negatively charged)) (Table 2).[60] The high rejections resulted from two factors: (1) both TBB and cyclen imparted the active layer with an absence of oxygen-containing groups and a high density of positively charged groups (–NH and $-N^+$), enabling the membrane to exhibit a positive surface charge of +18.4 mV; and (2) the macrocyclic structure of Cyclen provided the membrane with a relatively large pore size of 1.6 nm, allowing it to effectively retain organic substances with MWCO values greater than 500 Da.[60] Clearly, the synergistic combination of the Donnan effect and size exclusion is the driving cause for effective separation.

Likewise, the PA-AdDA TFC membrane had rejection rates of 94.7% for methyl orange (327.3 Da, negatively charged) and 98.5% for rose bengal (1017.6 Da, negatively charged) (Fig. 17c).[253] The high rejections came from aforementioned similar factors: (1) the rigid and bulky AdDA structure restricted excessive chain packing and formed loose micropores that are able to retain solutes with a MWCO below 320 Da; and (2) the residual –COOH groups in the active layer imparted the membrane with a high negative surface charge of -32.5 mV that repulsed the negatively charged solutes by the Donnan effect.[253]

In another example, the BAHPF/TMC membrane was fabricated *via* the IP method using 9,9-bis(3-amino-4-hydroxyphenyl)fluorene (BAHPF), a novel aqueous-phase monomer containing two amino groups ($-NH_2$) and two phenolic hydroxyl groups (–OH).[145] This membrane achieved a high methanol permeance of 17.9 L m^{-2} h^{-1} bar^{-1} while exhibiting excellent rejection rates of 98.0% for tetracycline (TC, 444 Da) and 95.9% for orange G (OG, 452 Da), both of which exceeded the membrane's molecular weight cut-off of 298 Da.[145] The superior separation performance could be attributed to three key structural advantages: (1) the rigid and twisted conformation of the BAHPF monomer restricted dense packing of the polymer chains, thereby enhancing the microporosity and interconnectivity of free volume elements within the polyamide selective layer, facilitating rapid solvent transport; (2) the retained phenolic –OH groups contributed to a higher negative surface charge density, strengthening electrostatic repulsion against anionic solutes through the Donnan effect; (3) the compact molecular architecture combined with highly reactive amino groups promotes extensive cross-linking during polymerization, resulting in a dense network with a small effective pore size that corresponded to a low MWCO of 298 Da. Consequently, the

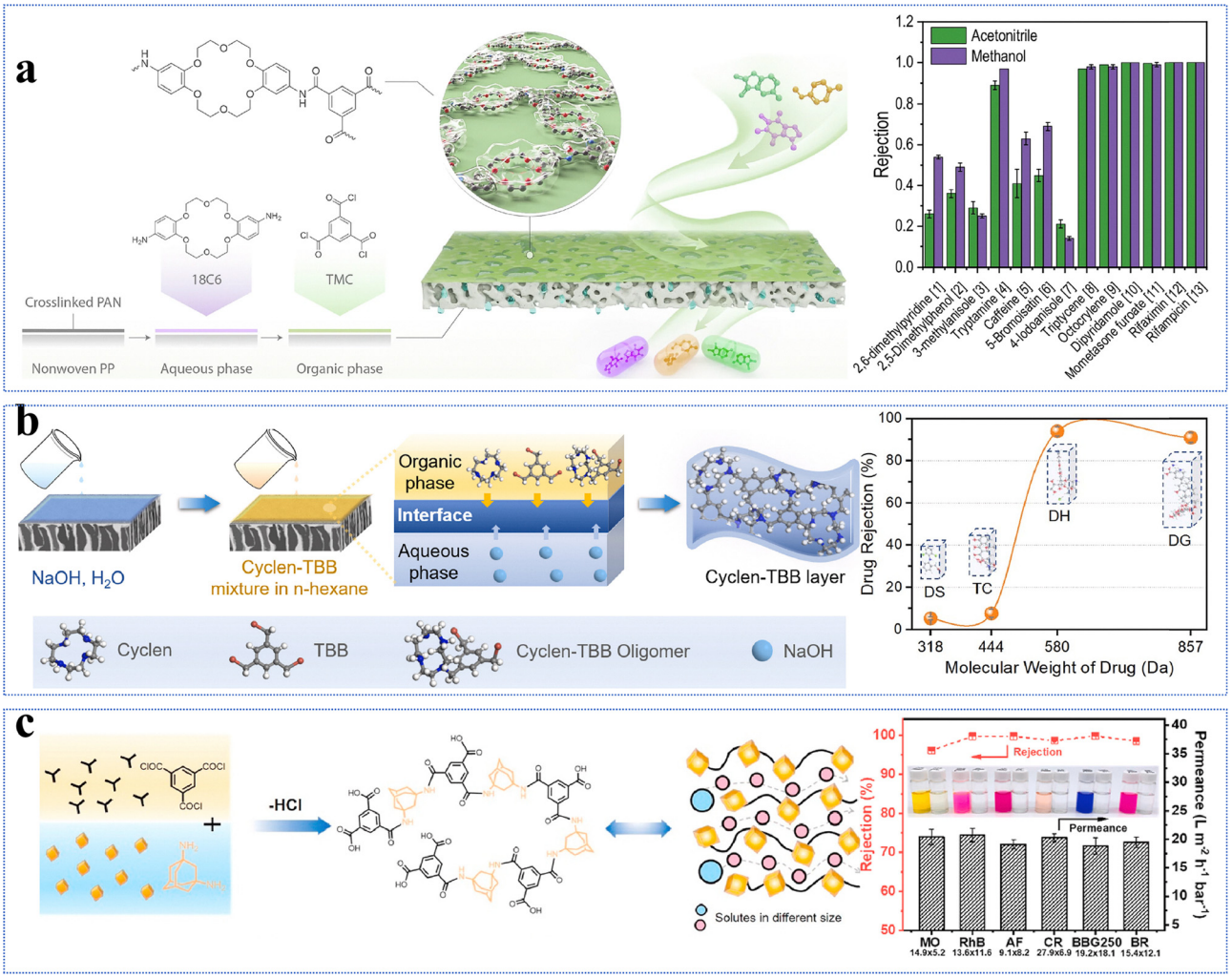

Fig. 17 Novel monomer-based NF membranes for the separation of organic compounds. (a) Separation performance of the TFC18C6 membrane. Reproduced with permission from ref. 77. Copyright 2024, Springer Nature. (b) Separation performance of the Cyclen-TBB membrane for antibiotics. Reproduced with permission from ref. 60. Copyright 2023, Elsevier. (c) Separation performance of the PA-AdDA TFC membrane for dye molecules. Reproduced with permission from ref. 253. Copyright 2023, Elsevier.

membrane enabled efficient solute retention by synergistically leveraging size exclusion and Donnan effect mechanisms, demonstrating great potential for high-performance OSN applications.

In summary, the novel monomer-based NF membranes have exhibited great potential for the separation of water/organic compounds by leveraging the combined effects of size exclusion and the Donnan effect. Future research should focus on developing multifunctional monomers and chemically resistant NF membranes consisting of asymmetrically charged active layers to precisely separate organic compounds for industrial applications in the fields of drug purification and wastewater reuse.

Mechanisms to separate salt/organic compounds

Novel monomer-based NF membranes have also been explored for applications such as salt/dye[82,147,150,160,234,256,259,262,265,313–316] and salt/antibiotic separations[100,115,135,185,317,318] because salts are often used in the dye and antibiotic industries. Fig. S6 summarizes the correlation between their permeances and rejection rates along with the influencing factors. As shown in Fig. S6a, the rejection rates of organic compounds, monovalent salts, and divalent salts range from 41% to 100%, 1.6% to 92.1%, and 2.6% to 98.5%, respectively. Notably, 58.0% of the membranes achieve rejection rates of organic compounds over 90%, while 100% and 65.1% of the membranes exhibit rejection rates of monovalent and divalent salts below 50%, respectively (Fig. S6a). To further investigate the relationship between membrane characteristics and separation performance, Fig. S7 plots their separation factors for monovalent salts/organic compounds and divalent salts/organic compounds as a function of influencing factors. Generally, the rejection rates for monovalent salts, divalent salts, and organic compounds are 1.6 to 92.1%, 2.6 to 98.5%, and 41 to 100%, respectively (Fig. S7a). Additionally, the separation factors for monovalent salts/organic compounds and divalent salts/organic compounds range from 0.5 to 9230 and 0.04 to 9140,

with average values of 475.0 and 239.8, respectively (Fig. S7b). Furthermore, 54.0% and 35.0% of the separation factors exceed 20 for monovalent salts/organic compounds and divalent salts/organic compounds, respectively (Fig. S7b). Clearly, it is more conducive to separate the former than the latter due to the greater size and charge differences between monovalent salts and organic compounds.

Additionally, Fig. S7c depicts their upper limits of permeability and selectivity. Fig. S7d shows that only 33.8% of the membrane pores are smaller than the hydrated radii of both Cl^- (0.33 nm) and SO_4^{2-} (0.38 nm), indicating that the separation of salt/organic compounds cannot be solely counted on size exclusion. Analyses confirm that 77.3% of the membranes exhibit negative surface charges to reject negatively charged organic compounds, while 22.7% of the membranes have positive surface charges to reject cationic salts (*e.g.*, Na^+ rejection rate $<30\%$) (Fig. S7e). Similar to the previous cases, both size exclusion and the Donnan effect are the driving mechanisms to separate these salts and organic compounds. However, their performance is constrained by the broad pore size distribution and inadequate charge matching. Future efforts should focus on multi-parameter collaborative design (*i.e.*, refining pore size distribution and dynamic charge regulation) and cross-disciplinary technology integration (*i.e.*, intelligent responsive materials and biomimetic recognition mechanisms). The following gives valuable examples.

The NF-TPEI membrane fabricated from TMAO-modified PEI (TPEI) and TMC exhibited a separation factor of 469.5 for CR/NaCl (Fig. 18a).[79] This performance stems from the pivotal role of TMAO in the TPEI monomer design. The strong hydrogen bonding between TMAO and water molecules along with the steric hindrance introduced by the long TPEI chains slowed the IP reaction rate. This led to the formation of a thin, hydrophilic, and microporous active layer with a MWCO of 17 kDa and an average pore size of 1.34 nm. In addition, TMAO enriched the active layer with zwitterionic functional groups ($-N^+-O^-$), while the membrane surface retained a net negative charge of -9 mV. Thus, the negatively charged CR was rejected

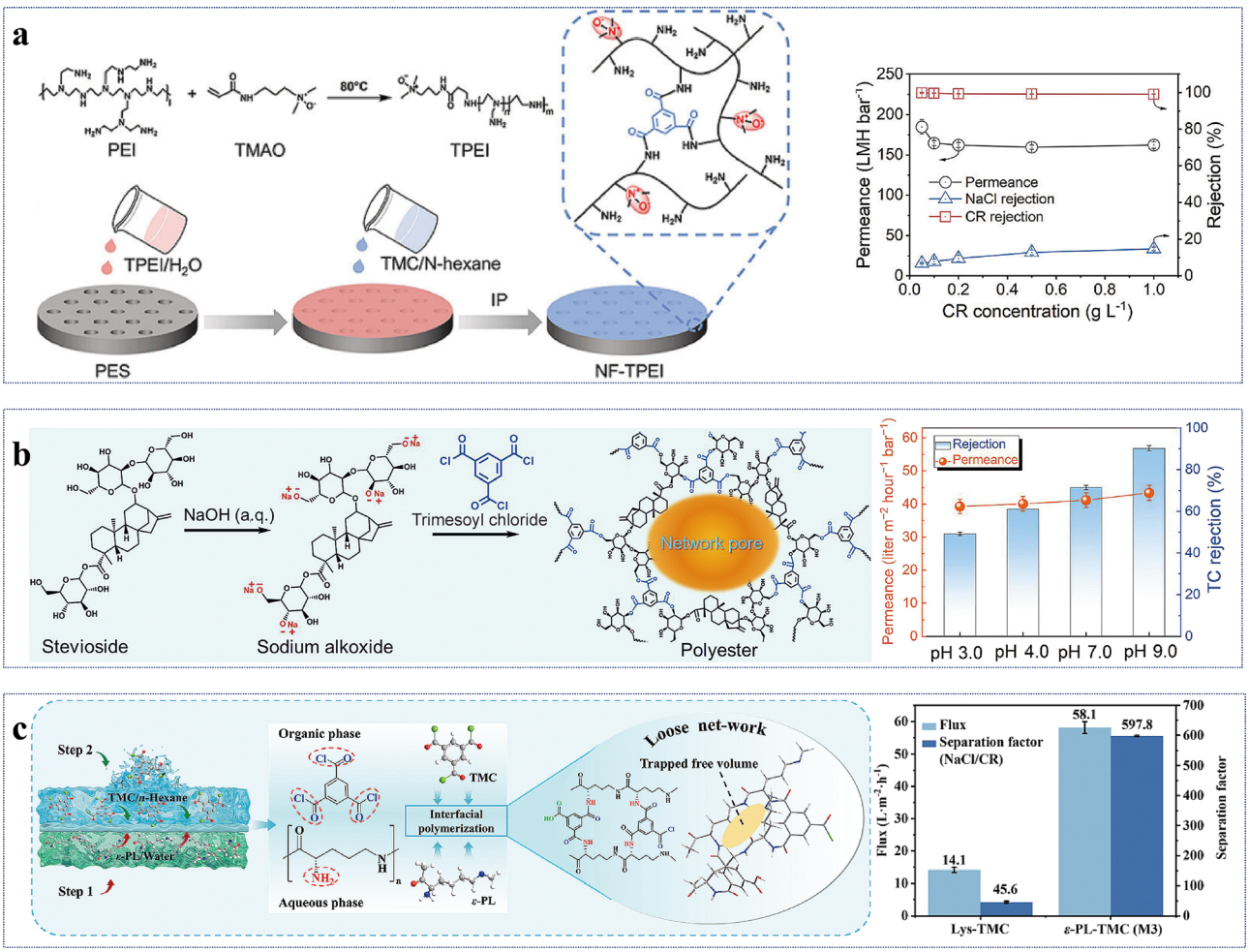

Fig. 18 Novel monomer-based NF membranes for the separation of salt/organic compounds. (a) Separation performance of the NF-TPEI membrane. Reproduced with permission from ref. 79. Copyright 2023, American Chemical Society. (b) Separation performance of the $St_{0.1}/TMC_{0.1}$-3 membrane. Reproduced with permission from ref. 58. Copyright 2023, American Association for the Advancement of Science. (c) Separation performance of the ε-PL-TMC(M3) membrane. Reproduced with permission from ref. 315. Copyright 2025, Elsevier.

by the Donnan effect.[79] In addition, CR tends to form aggregates. Thus, even though the membrane had a MWCO significantly larger than CR (*i.e.*, 697 Da), it rejected CR clusters *via* size-exclusion mechanisms.

Similarly, the $St_{0.1}/TMC_{0.1}$-3 membrane synthesized by regulating stevioside (St) with NaOH had separation factors of 2.3 and 11.3 for NaCl/tetracycline at pH values of 4.0 and 9.0, respectively (Fig. 18b).[58] The separation arose from the synergistic effects of the following factors: (1) the bulky and distorted St monomer with rich –OH groups would slow down its diffusion during IP and form a defect-free active layer with a relatively large pore size of 0.6 nm; (2) the abundant remaining –COOH groups would impart a strong negative surface charge of −62.5 mV to repulse tetracycline *via* the Donnan effect while allowing NaCl to permeate through; and (3) more importantly, as an amphoteric compound, tetracycline had pH-dependent electrical properties. It would transit from a neutral to a negatively charged state as the pH increased and alter its interactions with the membrane.[58]

Likewise, the ε-PL-TMC (M3) membrane, prepared using ε-polylysine (ε-PL) as the aqueous phase monomer, had a separation factor of 597.8 for NaCl/CR (Fig. 18c).[315] The high selectivity was driven by two factors: (1) the high reactivity of $–NH_2$ groups in ε-PL and its long-chain structure with significant steric hindrance helped to form a loose yet well-defined porous network with a moderate pore size of 0.34 nm and a MWCO of 665 Da; and (2) the resulting structure allowed efficient NaCl permeation while effectively retaining CR through size exclusion.[315]

In addition, the BAIE-TBB (M-0.1) membrane displayed exceptional separation factors of (1) 241 for NaCl and four dyes (*i.e.*, methyl blue, CR, Victoria blue B, and Remazol brilliant blue R); and (2) ∼ 240 for divalent salts (*i.e.*, $MgSO_4$, $MgCl_2$, Na_2SO_4) and the same dyes.[75] This remarkable performance resulted from two factors: (1) strong size sieving, as the membrane has an average pore size of 1.14 nm that was much smaller than the dye molecules; and (2) a weakly positive surface charge of +2.5 mV, which minimized electrostatic interactions with salt ions (*i.e.*, Na^+ and Mg^{2+}) and allowed their permeation.

In summary, the charge regulation strategy is crucial in balancing retention and permeation by maintaining a moderate surface charge and preventing strong electrostatic interference.[75] When membranes have pore sizes smaller than the targeted organic molecules, size sieving becomes the dominant mechanism. However, charge or hydrophobic interactions must complement each other for efficient separation.

Mechanisms to enhance membrane stability

The chemical and mechanical stability, and long-term operational reliability of NF membranes are important for their applicability in industrial wastewater treatment. Usually, membrane stability is primarily assessed by measuring permeability and selectivity after a prolonged exposure to model pollutants, oxidants, acidic or alkaline environments, or bacteria (Fig. 19). Insufficient membrane stability including (1) pore fouling caused by organic compounds, colloids, and microorganisms; (2) structural degradation from exposure to strong acids, bases, and oxidants; and (3) mechanical damage due to high pressure and frequent cleaning cycles can not only shorten the membrane's lifespan but also adversely impact treatment efficiency, operational costs, and effluent quality. Overall, membrane stability is influenced not only by fabrication methods and intrinsic structural properties, but also by water quality characteristics, operating conditions, and cleaning protocols (Fig. 19). To overcome these issues, Table 3 shows that researchers have developed novel monomer-based

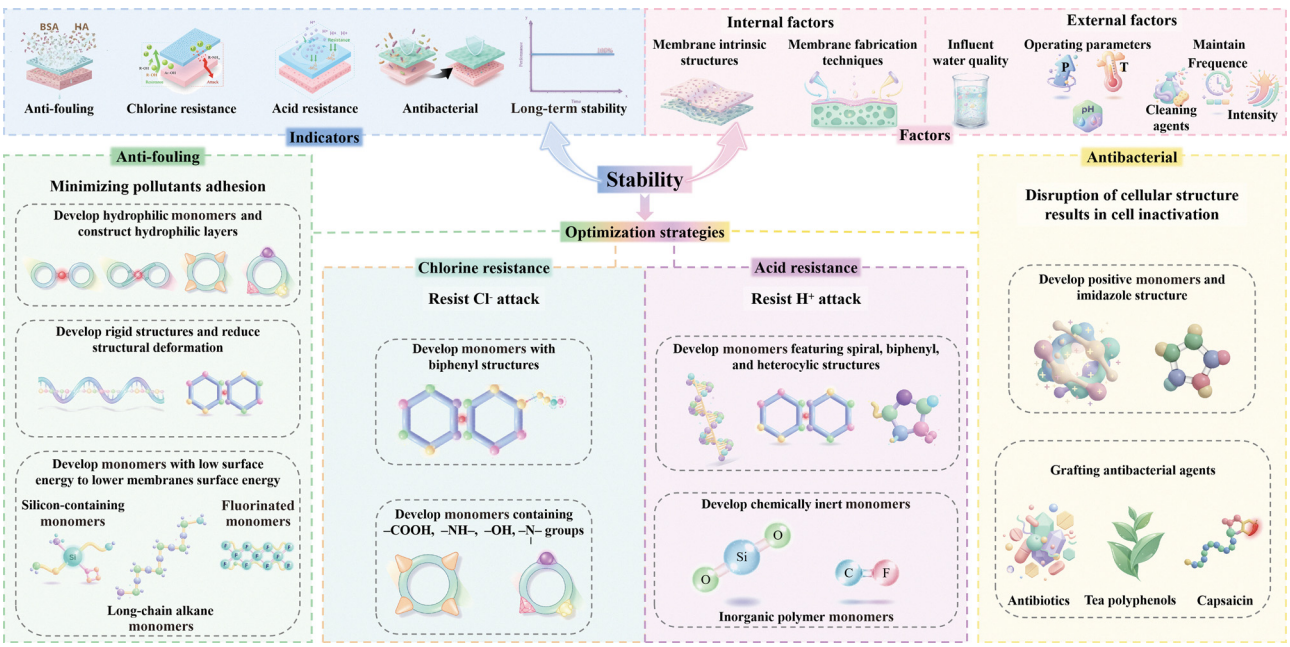

Fig. 19 Key factors influencing stability and optimization strategies for novel monomer-based NF membranes.

Table 3 Stability of novel monomer-based NF membranes

NF membrane	Stability	Type	Ref.
TET-TMC TFCM	200 000 ppm h NaClO, pH = 7, water permeance = 17.3 L m^{-2} h^{-1} bar^{-1}, R_{MgCl_2} = 83%	Chlorine resistant	63
QSPIP-TMC TFCM	80 000 ppm h NaClO, pH = 6, water permeance = 30 L m^{-2} h^{-1} bar^{-1}, R_{MgCl_2} = 85%	Chlorine resistant	64
QEDTP NFM	100 ppm BSA, pH = 6.4, FRR_3 = 53.9%	Anti-fouling	68
BAIE-TMC(M-0.5)	100 ppm BSA, FRR_3 = 99.8%; 100 ppm HA, FRR_3 = 99.6%	Anti-fouling	242
BBD-3 TFC	1000 ppm BSA, FRR_2 = 94.6%; *Escherichia coli* and *Bacillus subtilis*	Anti-fouling and anti-bacterial	71
PIP-TMC-QAEP	100 ppm BSA, FRR_2 = 95.7%; *Escherichia coli*; Water permeance = 16.7 L m^{-2} h^{-1} bar^{-1}, $R_{Na_2SO_4}$ = 97.5% in a 12 days' continuous operation	Anti-fouling, anti-bacterial and long-term	69
PNIPAM-PA	100 ppm BSA, FRR_2 = 90.4%	Anti-fouling	184
Polyarylate (DMAP)	200 000 ppm h NaClO, water permeance = 10.4 L m^{-2} h^{-1} bar^{-1}, $R_{Na_2SO_4}$ = 93.4%; water permeance = 8.4 L m^{-2} h^{-1} bar^{-1}, $R_{Na_2SO_4}$ = 95.0% in a 60 days' continuous operation; water permeance = 23.7 L m^{-2} h^{-1} bar^{-1} and $R_{Na_2SO_4}$ = 92.7% in 10 h consecutive cross-flow operation for 95 °$C_{Na_2SO_4}$ solution	Chlorine resistant, long-term and heat resistance	76
PA-*g*-TETA (3 wt%)	Water permeance = 48 L m^{-2} h^{-1}, R_{MgCl_2} = 99%, R_{LiCl} = -38% in a 3 days' continuous operation	Long-term	26
AMTHBA0.25-PAR/PAF/PS	500 ppm BSA, FRR_2 = 93.6%; 500 ppm HA, FRR_2 = 100%; 500 ppm SA, FRR_2 = 98%; antibacterial ratio of *Staphylococcus aureus* = 90.8%	Anti-fouling and anti-bacterial	83
PA-Tg-0.06	1000 ppm BSA, FRR_2 = 89%	Anti-fouling	61
FPA/PES NF	500 ppm BSA, FRR_2 = 99.1%; 500 ppm HA, FRR_2 = 98.0%	Anti-fouling	246
PA/nylon-M3	$R_{tetracycline}$ = 100% in 24 h continuous operation	Long-term	112
TPT-TMC/PSf TFC	Water permeance = 8.7 L m^{-2} h^{-1} bar^{-1} and R_{MgSO4} = 94.2% at 0.05 M H_2SO_4 for 720 h	Acid resistant	248
QNFM	Antibacterial ratios of *Escherichia coli* and *Staphylococcus aureus* = 95% and 99%	Anti-bacterial	162
PANoria(2)/(20)	100 ppm BSA, pH = 7.4, FRR_5 = 95.2%; 100 ppm BSA FRR_5 = 96.8%; antibacterial ratio of *Escherichia coli* = 92.8%	Anti-fouling and anti-bacterial	161
AEP/TMC = 240	500 ppm BSA, FRR_1 = 51%; R_{MgCl_2} = 94%, $R_{Na_2SO_4}$ = 65%, $R_{acid\ fuchsin}$ = 94%, $R_{methyl\ orange}$ = 84% in 30 h continuous operation	Anti-fouling and long-term	250
$St_{0.1}/TMC_{0.1}$-3	10 000 ppm NaClO, pH = 5 and 7, water permeance = 80 L m^{-2} h^{-1} bar^{-1}, $R_{Na_2SO_4}$ = 78%; 100 ppm BSA, pH = 7, FRR_2 = 73.2%; 100 ppm HA, pH = 7, FRR_2 = 85.6%	Chlorine resistant and anti-fouling	58
TSM	1000 ppm BSA, FRR_5 = 98%; water permeance = 82.4 L m^{-2} h^{-1} bar^{-1} and $R_{congo\ red}$ = 99% in 500 h continuous operation for 90 °C Congo red solution	Anti-fouling and heat resistance	256
PA-QTDEA	1000 ppm BSA, FRR_2 = 84%	Anti-fouling	72
Ad-PA-NaOH (12.5)	Water permeance = 40 L m^{-2} h^{-1} bar^{-1}, $R_{evans\ blue}$ = 99.7%, R_{NaCl} = 3.6%, FRR = 90.7% in a 11 days' continuous operation	Long-term	59
TFN-0.2-0.5	Water permeance = 4 L m^{-2} h^{-1} bar^{-1}, $R_{cephalexin}$ = 92.4% in 25 h continuous operation	Long-term	257
ZM3	100 ppm methyl blue, FRR_2 = 94.8%; 100 ppm BSA, $FRR_{20\,h}$ = 95.7%; 100 ppm NaAlg, $FRR_{20\,h}$ = 96%	Anti-fouling	258
PIP-COOH/TMC	100 ppm reactive red 195, $FRR_{25\,h}$ = 84%; $R_{reactive\ red\ 195}$ = 99%, $R_{Na_2SO_4}$ = 10% in 40 h continuous operation	Anti-fouling and long-term	107
4AP-TFC_0.05/0.05	14 400 ppm h NaClO, water permeance = 44 L m^{-2} h^{-1} bar^{-1}, $R_{Na_2SO_4}$ = 95%; pH = 3, 72 h, $R_{Na_2SO_4}$ = 98%; Water permeance = 35 L m^{-2} h^{-1} bar^{-1}, $R_{Na_2SO_4}$ = 98% in 70 h continuous operation	Chlorine resistant, acid resistant and long-term	260
HHMs	1000 ppm BSA, FRR_5 = 96%; water permeance = 103.8 L m^{-2} h bar in 50 h continuous operation	Anti-fouling and long-term	262
TAD-TBB TFCM	96 000 ppm h NaClO, pH = 7, water permeance = ~14 L m^{-2} h^{-1} bar^{-1}, R_{MgCl_2} = 90%; water permeance = 13.9 L m^{-2} h^{-1} bar^{-1} and R_{MgCl_2} = 90.4% at 2 M HCl for 21-day	Chlorine resistant and acid resistant	341

Note: FRR = the flux recovery rate, where X in FRRX = the number of cycles. BSA = bovine serum albumin; HA = humic acid; SA = sodium alginate.

NF membranes with enhanced chemical stabilities by integrating innovative monomers with optimized membrane structures for complex wastewater environments. To develop NF membranes with enhanced stability, it is crucial to prioritize the development of targeted novel monomers and optimize membrane fabrication processes (Fig. 19). Specifically, the anti-fouling performance of NF membranes has been systematically improved through strategies including the development of hydrophilic monomers and construction of hydrophilic layers, the design of rigid structures to suppress deformation, and the synthesis of low surface energy monomers to reduce membrane surface energy. Additionally, the chlorine resistance of NF membranes can be effectively enhanced through the development of monomers featuring biphenyl structures and functional groups. Moreover, the acid resistance of NF membranes is synergistically enhanced through the development of monomers featuring helical, biphenyl, and heterocyclic architectures, the construction of chemically inert monomer systems, and the incorporation of inorganic polymer monomers. Furthermore, the antibacterial performance of nanofiltration membranes can be effectively enhanced by designing cationic monomers, incorporating imidazole structures, and grafting antibacterial agents. The following subsections provide a comprehensive analysis of the relevant content with illustrative examples for further clarification.

Mechanisms to enhance anti-fouling performance

It is known that continuous NF operations under pressure may cause organic, inorganic, or biological fouling that reduces separation efficiency, energy consumption, and membrane lifespan.[319–323] Fundamentally, the fouling tendency of a membrane is determined by its chemical properties (such as hydrophilicity, roughness, pore size, and surface charge) and operating conditions (such as pH, temperature, concentration, and pressure).[322–327] While physical and chemical cleaning are commonly employed to mitigate fouling, frequent cleaning can compromise membrane integrity and performance. Researchers have explored innovative strategies such as (1) adopting surface modifications (*i.e.*, grafting hydrophilic monomers,[71,83,328] applying renewable coatings[182,329]); and (2) developing smart membranes (*i.e.*, stimulus-responsive membranes,[9,184,330–332] patterned membranes,[333–336] novel monomer-based membranes[246,256,337,338]) to optimize membrane characteristics by (1) enhancing hydrophilicity; (2) adjusting roughness; (3) controlling surface charge density; and (4) refining pore size. Additionally, optimizing fluid dynamics helps to minimize the adhesion and deposition of foulants.[339,340] Typically, the anti-fouling propensity of novel monomer-based NF membranes is evaluated using bovine serum albumin (BSA), humic acid (HA), and sodium alginate (SA) as model contaminants (Table 3). The flux recovery ratio (FRR) has been used as a key metric after multiple pollution-cleaning cycles. Herein, some progress on anti-fouling membranes is elaborated.

For instance, compared to the control membrane of PA-PIP which had an FRR of 72%, the PA-Tg-0.06 NF membrane showed a significantly higher FRR of 89% after two consecutive contamination-cleaning cycles using 1000 ppm BSA as the foulant (Fig. 20a).[61] The improvement came from two key characteristics of the PA-Tg-0.06 NF membrane. It had a highly hydrophilic surface with a contact angle of 25.6°. Thus, it would

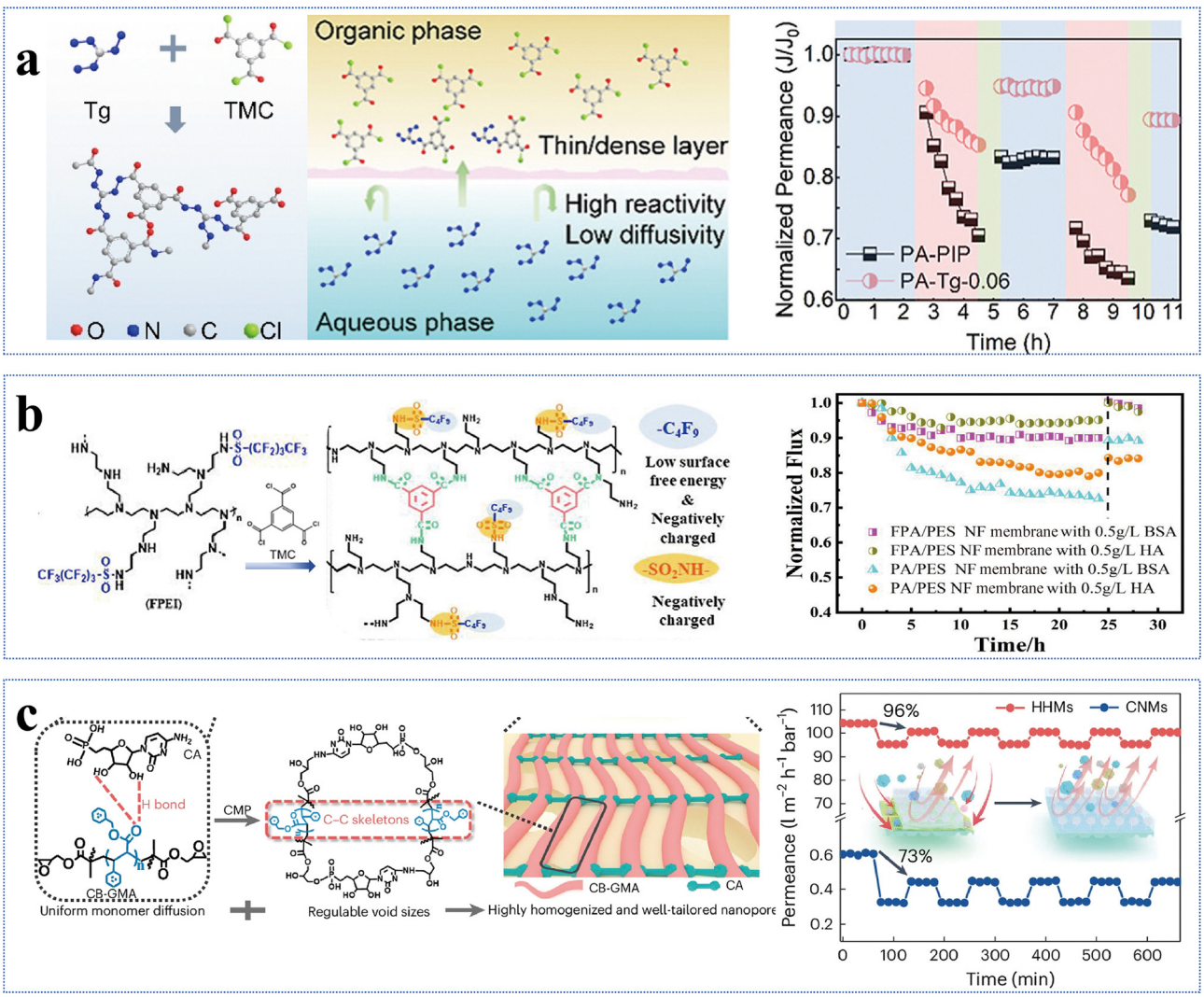

Fig. 20 Anti-fouling resistance of novel monomer NF membranes. (a) Preparation of the PA-Tg-0.06 NF membrane and its normalized permeance during the anti-fouling evaluation. Reproduced with permission from ref. 61. Copyright 2023, Elsevier. (b) Preparation of the FPA/PES NF membrane and its anti-fouling performance. Reproduced with permission from ref. 246. Copyright 2020, Elsevier. (c) Preparation of the HHMs NF membrane and its anti-fouling performance. Reproduced with permission from ref. 262. Copyright 2024, Springer Nature.

form a stable hydration layer and minimize direct contact between BSA and the active layer surface. In addition, it had a strong negative charge of −68.7 mV, which would effectively repel negatively charged BSA molecules and keep them from adhesion and accumulation on the active layer surface.[61] Similarly, the FPA/PES NF membrane, prepared with an omniphobic perfluoro-functionalized polyethyleneimine (FPEI) monomer, also maintained a high FRR after two contamination-cleaning cycles using 500 ppm BSA and HA as foulants.[246] In particular, its permeance remained relatively stable over 5 h, whereas that of the control membrane gradually decreased (Fig. 20b).[246] The superior anti-fouling behave arose from two similar factors: (1) the perfluoro-functionalized polyethyleneimine (FPEI) monomer effectively reduced the surface free energy of the active layer from 39.9 to 31.1 mJ m^{-2}, thereby minimizing BSA or HA adhesion on the active layer; and (2) the sulfonyl groups and fluorinated groups imparted a strong electronegativity of −37 mV to the active layer, thus repulsing negatively charged BSA or HA molecules and reducing their adhesion and accumulation on the surface (Fig. 20b).[246] Furthermore, the HHM membrane maintained an FRR of 96% even after five cycles of contamination-cleaning using 1000 ppm BSA as the foulant (Fig. 20c).[262] This remarkable anti-fouling propensity resulted from the hydrophilic groups of –OH, $–NH_2$, and phosphate groups in the novel organic-phase monomer of cytidine 5′-monophosphate. They would not only induce a hydrophilic and smooth surface but also help form a hydration layer to effectively reduce foulant deposition (Fig. 20c).[262] In short, some novel monomer-based NF membranes have demonstrated excellent anti-fouling propensity. However, current evaluations rely on a limited set of model contaminants and limited cycle times. Future research should prolong the testing duration and investigate the anti-fouling mechanisms in practical industrial applications.

Mechanisms to enhance chlorine resistance

Due to its strong oxidizing properties, chlorine is commonly used in cleaning processes to degrade foulants and recover membrane performance.[342,343] However, polyamide-based NF membranes are highly susceptible to oxidation in chlorine-containing environments. Specifically, chlorine can attack the hydrogen atoms in the amide bonds (–CO–NH–), leading to *N*-chlorination and subsequent Orton rearrangement. Both degrade membrane performance and shorten the membrane life.[344–347] To improve chlorine resistance, novel monomer-based NF membranes have been strategically designed to minimize or eliminate chloride-induced damage to the active layer. Table 3 summarizes these NF membranes with superior chlorine resistance.[49,58,63,64,76,260,348] For instance, the QSPIP-TMC membrane, after being immersed in 200 ppm NaClO (pH = 6) for 400 hours, maintained a stable $MgCl_2$ rejection of ∼92% and a water permeance of ∼22 L m^{-2} h^{-1} bar^{-1}. In contrast, the control membranes (PEI-TMC and BAPP-TMC) showed drastic declines in $MgCl_2$ rejections to 14% and 4%, respectively.[64] The enhanced chlorine resistance arose from the absence of active hydrogen in the amide bonds. As illustrated in Fig. 21a, the active layer features a secondary amine (–NH–) structure rather than the primary amine ($–NH_2$) structure.[64]

Additionally, polyester-based NF membranes exhibit superior chlorine resistance due to the inactivity of ester bonds (–CO–O–) to chlorine. For example, the TET-TMC membrane exhibited remarkable chlorine resistance when being exposed to 500 ppm NaClO (pH = 7) for 400 hours. It maintained a stable permeance of ∼17 L m^{-2} h^{-1} bar^{-1} and a $MgCl_2$ rejection of ∼95% (Fig. 21b).[63] In contrast, under the same conditions, the control membrane (PEI-TMC) experienced an 86% reduction in $MgCl_2$ rejection and a sharply increased permeance of >90 L m^{-2} h^{-1} bar^{-1}.[63] Similarly, the polyarylate (DMAP) membrane also displayed excellent chlorine resistance when being exposed to 200 000 ppm h NaClO. It maintained a stable water permeance of 10.4 L m^{-2} h^{-1} bar^{-1} and a Na_2SO_4 rejection of ∼93%.[76] The superior chlorine resistance resulted from the utilization of bisphenol monomers (*i.e.*, 2,4-(4-hydroxyphenyl)-2,3-phthalazin-1-one, BPPZ) and TMC (Fig. 21c).[76] In other words, the incorporation of –OH containing monomers in the above NF membranes was the key to reducing chlorine attacks. In summary, to endow NF membranes with enhanced chlorine resistance, the active layer must lack the active hydrogen. Therefore, designing innovative monomers and refining membrane preparation techniques are important to prevent active hydrogen from being present in the amide bonds (–CO–NH–). Alternatively, one may incorporate nanoparticles with functional NH_2 groups in the active layer to shift the sites of chlorine attack, as illustrated in ref. 349.

Mechanisms to enhance acid resistance

Acidic wastewater is a prevalent type of industrial effluent. Under extremely low pH conditions (*i.e.*, pH value <2), the conventional polyamide layer is susceptible to hydrolysis induced by H^+ *via* nucleophilic substitution reactions. This results in structural degradation such as enlarged pore size and reduced thickness, which subsequently leads to performance decline.[350–352] To address this issue, researchers have explored the use of novel monomers to design NF membranes with enhanced acid resistance and stability.[81,129,244,247,248,348,353–357] For instance, Fig. 22a shows the wTB-PA NF membranes prepared by incorporating acid-resistant monomers (*i.e.*, 2,8-diamino-4,10-dimethyl-6*H*,12*H*-5,11-methanodibenzo[1,5]-diazocine, TBDA) into the substrate membrane through a three-step process.[353] After immersion in a H_2SO_4 solution for 7 and 14 days, the control membrane ($M_{PIP\text{-}TMC}$) decreased its Na_2SO_4 rejection by 57.5% and 93.7%, respectively, from its initial value of 95.6%, while its permeability increased sharply.[353] In contrast, the novel monomer-based NF membranes exhibited excellent acid resistance. Specifically, the M1 membrane maintained a high Na_2SO_4 rejection of 85.6% after 63 days of immersion, showing only an 8.2% decline from the initial value of 93.8%, with a relatively stable permeability (Fig. 22a).[353] The superior acid resistance was caused by the rigidity and V-shaped dihedral angle structure of the TBDA monomers.[353]

Additionally, the bisAPAF-TMC/PES NF membrane using 2,2-bis(3-amino-4-hydroxyphenyl)-hexafluoro-propane (bisAPAF) as

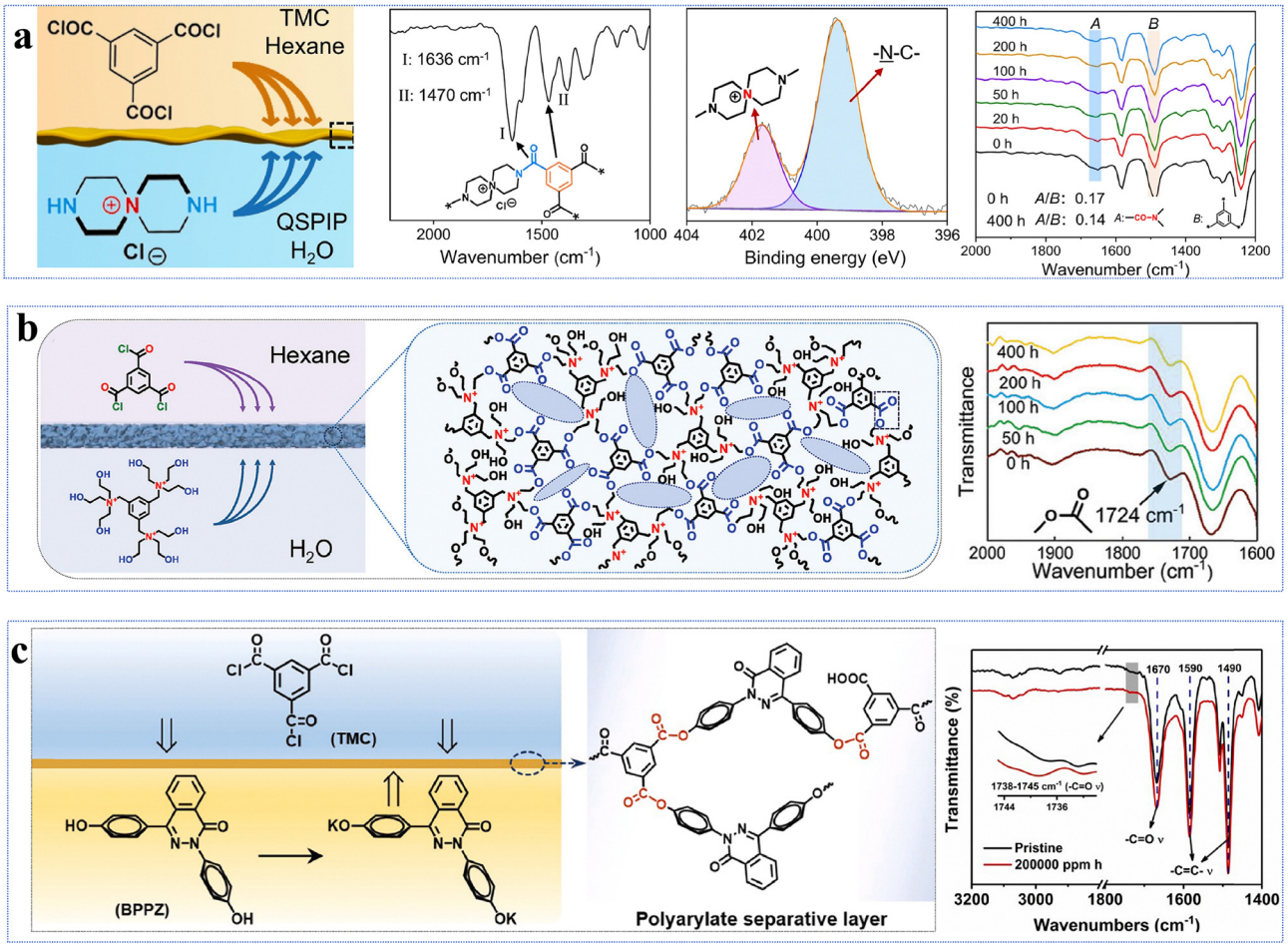

Fig. 21 Chlorine resistance mechanisms of novel monomer NF membranes. (a) Interfacial polymerization, ATR-FTIR and XPS spectra of the QSPIP-TMC membrane. Reproduced with permission from ref. 64. Copyright 2023, Springer Nature. (b) The network structure and FT-IR spectrum of the TET-TMC membrane immersed in a NaClO solution. Reproduced with permission from ref. 63. Copyright 2023, Wiley-VCH. (c) The network structure and FT-IR spectrum of the polyarylate (DMAP) membrane immersed in NaClO solution. Reproduced with permission from ref. 76. Copyright 2024, Elsevier.

the aqueous-phase monomer had minimal changes in membrane permeance of 12.7 L m^{-2} h^{-1} bar^{-1} and Na_2SO_4 rejection of 86.5% after acid treatment for 720 h, while those of the control membrane (PIP-TMC/PES) deteriorated markedly (Fig. 22b).[354] The outstanding acid resistance arose from two factors: (1) the formation of a fully aromatic structure increased the energy barrier to acid hydrolysis of the polyamide network; and (2) the strong steric hindrance effect of the –C(CF$_3$)$_2$ groups strengthened the structural stability (Fig. 22b).[354] Similarly, the TAD-TBB NF membrane synthesized from two novel monomers, 1,4,7,10-tetraazacyclododecane (TAD) and 1,2,4,5-tetrakis-(bromomethyl)benzene (TBB), also exhibited negligible changes in water permeance of 13.9 L m^{-2} h^{-1} bar^{-1} and $MgCl_2$ rejection of 90.4% after being exposed to 2 M HCl for 21 days (Fig. 22c).[341] This excellent stability was owing to the low polarization degree of the C–N–C bonds formed through the interaction between TAD and TBB, which effectively resisted the hydrolysis of the active layer induced by H^+ (Fig. 22c).[341] Furthermore, the PE-PSA$_{10000}$ membrane, synthesized using PEI and naphthalene-1,3,6-trisulfonyl chloride (NTSC), displayed excellent acid resistance due to the stable sulfonic acid groups of –SO_3H (Fig. 22d).[81] After immersion in 20 wt% H_2SO_4 at 80 °C for 24 h and 30 days, the resultant membrane maintained a stable permeance of ~7.2 L m^{-2} h^{-1} bar^{-1} and high rejections of >90% for $MgCl_2$, NaCl, and $MgSO_4$.[81] In summary, the current acid-resistant NF membranes derived from novel monomers primarily depend on 2 strategies; namely, (1) the incorporation of sulfonic acid groups; and (2) the use of rigid-twisted benzene-ring-containing monomers. Both impart the active layer with a stable network structure to resist nucleophilic substitution attacks. However, R&D on acid-resistant NF membranes remains limited, while the existing manufacturing processes are relatively complex. Future work should focus on developing novel acid-resistant monomers and simplifying the overall fabrication process for easy scalability.

Mechanisms to enhance antibacterial performance

Biological contamination is one of the primary issues when applying NF membranes for wastewater treatment. The microbial growth and biofilm formation on membranes will not only diminish separation performance and service life but also increase energy consumption and operational costs.[358,359] In

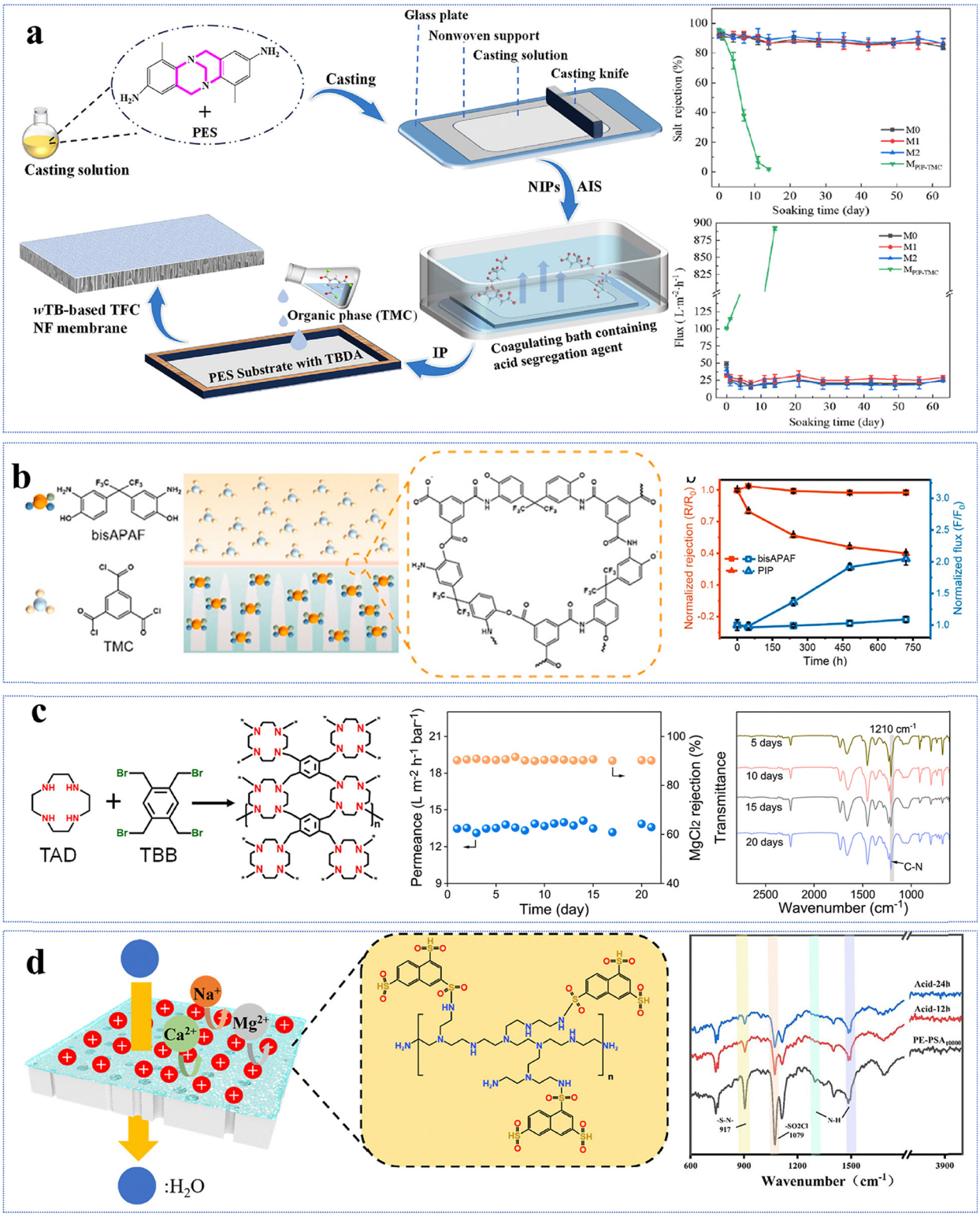

Fig. 22 Acid resistance of the novel monomer NF membranes. (a) Preparation processes of the wTB-PA NF membrane and the impact of 20 wt% H_2SO_4 on its separation performance using Na_2SO_4 of 2000 ppm. Reproduced with permission from ref. 353. Copyright 2024, Elsevier. (b) Preparation processes of the bisAPAF-TMC/PES membrane and the impact of 20 w/v% H_2SO_4 on its separation performance. Reproduced with permission from ref. 354. Copyright 2022, Elsevier. (c) Preparation and performance of the TAD-TBB membrane, and its ATR-FTIR spectra after 21-day immersion in a 2 M HCl solution. Reproduced with permission from ref. 341. Copyright 2024, Elsevier. (d) ATR-FTIR spectra of the PE-PSA_{10000} membrane soaked in 20 wt% H_2SO_4 for 12 h and 24 h. Reproduced with permission from ref. 81. Copyright 2024, Elsevier.

recent years, researchers have investigated and developed novel monomer-based NF membranes with antibacterial properties against both Gram-negative and Gram-positive bacteria (Table 3).[64,69,71,75,83,161,162,186,242] For instance, the BBD-3 TFC membrane could effectively inhibit both *Escherichia coli* (*E. coli*) and *Bacillus subtilis* (*B. subtilis*).[71] The outstanding antibacterial performance resulted from two key mechanisms: (1) the positively charged quaternary ammonium pyridine groups in the novel monomer of bis(2-hydroxyethyl)-bipyridine-diium derivatives electrostatically interacted with the negatively charged polysaccharides and phospholipids in the bacterial membrane, leading to cell rupture and disintegration; and (2) the long hydrophobic chains attached to these groups could penetrate the bacteria membrane, disrupting its physicochemical properties (Fig. 23a).[71] Similarly, the QNFM membrane had remarkable antibacterial efficiencies, achieving 95% against *E. coli* and 99% against *Staphylococcus aureus* (*S. aureus*).[162] The high efficacy was attributed to the electrostatic interactions between the positively charged quaternary ammonium groups in cellulose nanocrystals (Q-CNC) and the negatively charged phospholipids and proteins on the bacterial surface (Fig. 23b).[162] These interactions compromised the cytoplasmic membrane's permeability, causing leakage of cytoplasmic components and ultimately leading to microbial death.[162]

In addition, both the BAIE-TMC (Fig. 23c) and BAIE-TBB (Fig. 23d) membranes had impressive antibacterial efficiencies of approximately 98% against *E. coli* and *S. aureus*.[75,242] The superior performance stemmed from two primary factors: (1) the membranes had high hydrophilicity and low roughness that would significantly reduce bacterial adhesion to the functional layer; and (2) the imidazole moiety of BAIE could disrupt the bacterial membrane and inactivate its activity.[75,242] Notably, these two membranes exhibited a slightly stronger antibacterial effect against *S. aureus* than *E. coli* because the latter had a

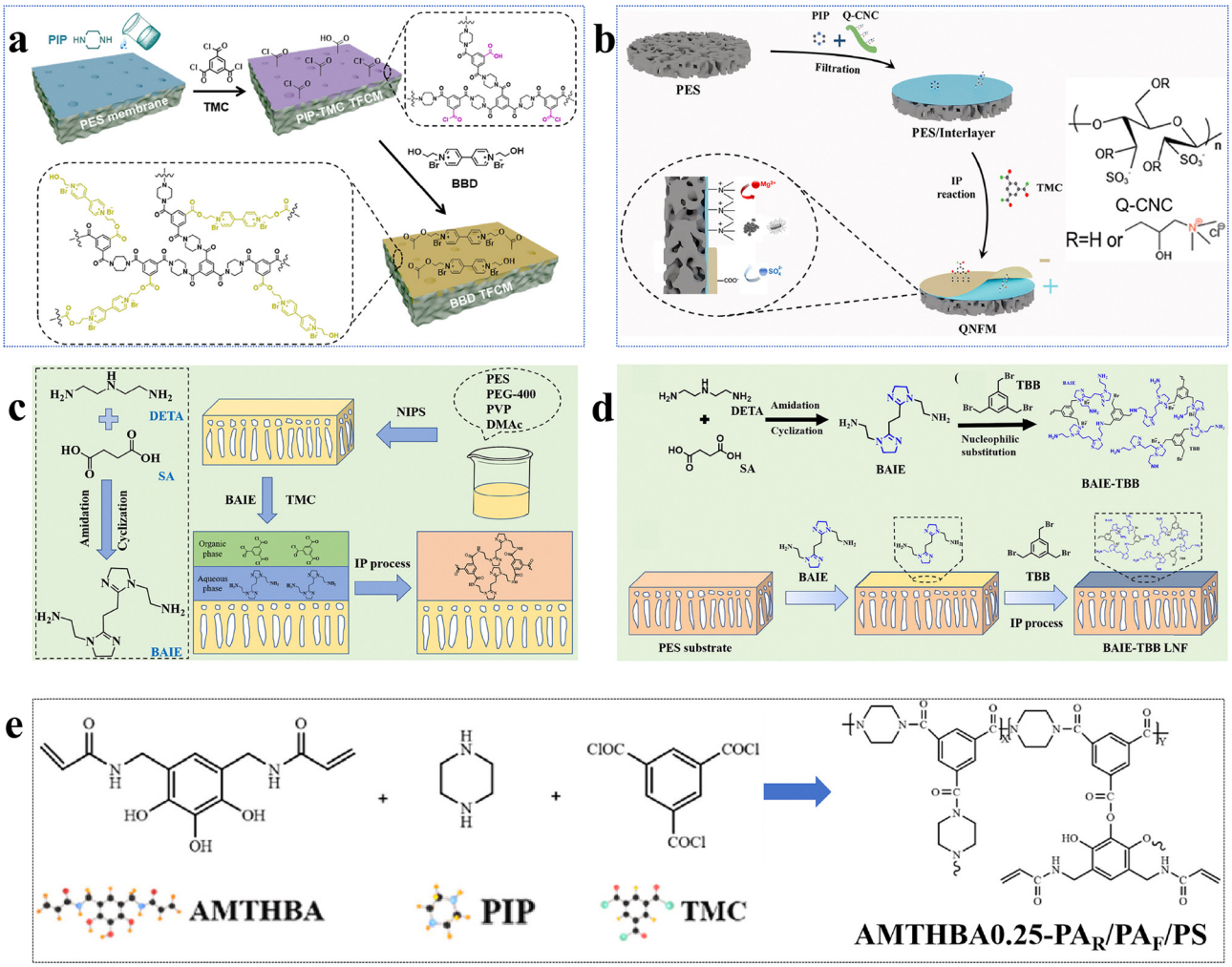

Fig. 23 Antibacterial resistance mechanisms of the novel monomer-based NF membranes. (a) Preparation diagram of the BBD-3 TFC membrane. Reproduced with permission from ref. 71. Copyright 2022, Elsevier. (b) Preparation diagram of the NF membrane with Q-CNC intermediate layers. Reproduced with permission from ref. 162. Copyright 2024, Elsevier. (c) Preparation diagram of the BAIE monomer and BAIE-TMC NF membrane. Reproduced with permission from ref. 242. Copyright 2024, Elsevier. (d) Preparation diagram of the BAIE monomer and BAIE-TBB LNF membrane. Reproduced with permission from ref. 75. Copyright 2024, Elsevier. (e) Preparation diagram of the AMTHBA0.25-PA$_R$/PA$_F$/PS membrane. Reproduced with permission from ref. 83. Copyright 2023, Elsevier.

double-layered cell wall with an outer membrane to impede the penetration of antibacterial groups such as long-chain quaternary amines.[162] Additionally, the AMTHBA0.25-PA_R/PA_F/PS membrane showed excellent antibacterial performance by achieving 90.8% inhibition against *S. aureus*. Its capsaicin derivatives (*i.e.*, AMTHBA) could gradually induce contraction and deform the bacterial cell wall so that the cell membrane would be ruptured and deactivated (Fig. 23e).[83] Overall, some novel monomer-based NF membranes have displayed strong antibacterial effects against both Gram-negative and Gram-positive bacteria by means of (1) reducing bacterial adhesion and inhibiting biofilm formation due to high membrane hydrophilicity and low roughness; and/or (2) disrupting bacterial cells through electrostatic interactions between positively charged groups (*i.e.*, quaternary ammonium groups, imidazole groups) and the negatively charged bacterial components. Future research should identify cost-effective functional monomers or nanoparticles such as MXene.[360,361] By incorporating them into the active layer, one may either further enhance these electrostatic interactions or deform bacteria to deactivate the bacteria during wastewater treatment.

Summary and outlook

In this review, we systematically examine the influence of diverse novel monomer structures on the structural features and surface properties of NF membranes, and provide an in-depth analysis of how monomer molecular architectures and functional group types govern membrane permeability, selectivity, and stability. While NF membranes derived from advanced monomers have demonstrated notable progress in overcoming the intrinsic permeability-selectivity trade-off, critical challenges remain, including high costs, limited long-term stability, and poor adaptability in complex wastewater matrices. By establishing structure–property–performance correlations, this review offers mechanistic insights and a rational design framework for next-generation NF membranes, advancing their sustainable deployment in water reuse and the recovery of high-value compounds.

In terms of outlook, novel monomer-based NF membranes have demonstrated superior separation performance primarily due to the unique structural advantages of their active layers. This provides a clear direction for future breakthroughs in innovative material design, theoretical analyses, and commercial applications. To bridge the gap between "high performance in laboratories" and "reliable industrial applications", it is essential to evaluate technical and economic feasibility through a synthesis-performance-cost paradigm. This will help transition water treatment from a traditional "high-energy consumption" separation to a new paradigm centered on "resource recycling". Based on the current major challenges, specific recommendations for the development of next-generation NF membranes are as follows (Fig. 24):

(1) Development of multi-functional novel monomers. Although novel monomers consisting of single functional groups have endowed the membranes with specific properties, there is a lack of exploration of their contributions. In addition, the underlying mechanisms of multifunctional monomers on membrane structures and performance remain poorly understood. Future research should prioritize the design and development of multi-functional monomers at a molecular structural level (*e.g.* planar *vs.* twisted configurations), and systematically investigate the critical roles of functional groups on membrane permeability, selectivity, and overall stability.

(2) Analysis of microscopic IP mechanisms. Parameters, such as monomer concentration, reaction time, and temperature, play key roles in governing the diffusion rates of monomers and their crosslinking processes. Due to the lack of real-time *in situ* monitoring technology, the current molecular-level dynamic analysis remains inadequate to accurately regulate the network structure in the active layer. Therefore, it is necessary

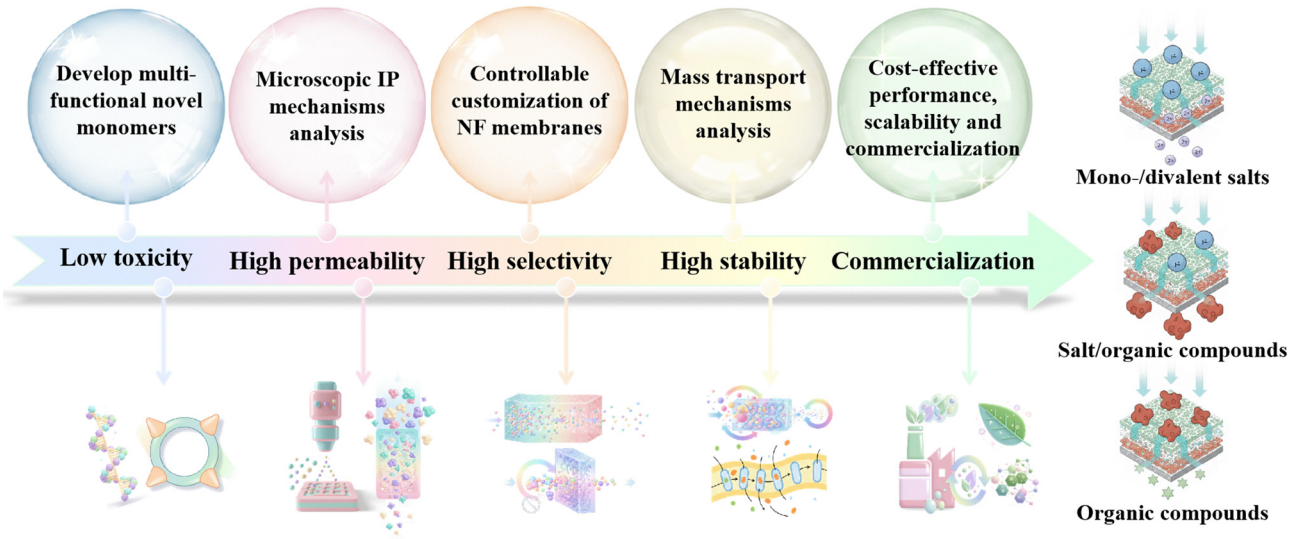

Fig. 24 Development potential of the next-generation NF membranes.

to develop high-resolution co-application technologies like ultrafast Fourier transform infrared spectroscopy (FTIR) and microfluidic chips, combined with simulation methods such as molecular dynamics (MD) and dissipative particle dynamics (DPD), to reveal the dynamic correlation between monomer diffusion and network formation at a molecular level.

(3) Controllable customization of advanced NF membranes. Although most novel monomer-based NF membranes have partially overcome the trade-off relationship between permeability and selectivity. The comprehensive performance of membranes is governed by a synergistic interplay of multiple factors, including monomer characteristics (*e.g.* chemical reactivity, molecular weight, and the types and numbers of functional groups), IP parameters (*e.g.* monomer concentration, reaction time, crosslinking temperature, and additive usage), post-treatment processes (*e.g.* heat treatment and surface modification), and operating conditions (*e.g.* operating pressure, pH, and temperature). These factors are intricately interconnected and collectively dictate membrane structure and performance, forming the fundamental basis for the rational design of tailored membrane materials and their efficient deployment in targeted applications. Therefore, future research should focus on the systematic control of these key parameters and deepen the understanding and regulation of their coupled effects to advance both the performance and long-term stability of NF membranes. Meanwhile, how to balance their mechanical strength, operation flexibility and long-term stability remains challenging. Specifically, the development of facile, cost-effective, and scalable membrane preparation methods should be prioritized to enable efficient batch production and large-scale manufacturing. Interdisciplinary collaborative innovation and artificial intelligence should be leveraged to establish a standardized ''design-structure-performance'' database and to predict the optimal reaction conditions and performance limitations for desired parameters.

(4) Analysis of mass transport mechanisms. Current research on mass transport mechanisms across a NF membrane is constrained by oversimplified models, inadequate characterization resolutions, and insufficient multi-scale simulations. Advanced characterizations and simulation modeling are essential to understanding the dynamic processes of mass transport and guiding the precise design of functional channels. Future efforts should integrate (1) high-resolution techniques such as *in situ* liquid-phase transmission electron microscopy (TEM), ultrafast spectroscopy; (2) sub-nanometer chemical imaging methods like atomic force infrared spectroscopy (AFM-IR) and scanning electrochemical microscopy (SECM); and (3) multi-scale molecular simulations and quantitative analyses to elucidate the interactions between functional groups and solutes, and their dynamic behaviors within membrane pores.

(5) Cost-effective performance, scalability and commercialization. The commercialization of novel monomer-based NF membranes is governed by the synergistic interplay of multiple critical factors, including raw material cost, synthetic scalability, permeability, selectivity, long-term stability, and mechanical strength. Commercial NF membranes exhibit significantly higher overall performance in economic viability, environmental sustainability, and technological maturity compared to their laboratory-grade counterparts, primarily owing to the cost efficiency, enhanced stability, and broad industrial applicability enabled by large-scale production. In contrast, laboratory-grade NF membranes remain constrained by high material and fabrication costs, limited process scalability, poor operational stability, and narrow application scope. Consequently, closing the gap between laboratory innovation and industrial implementation demands systematic advancements (Table S1). For commercialization, the novel monomer-based NF membranes must have superior cost-effective performance to the traditionally available ones. Strategies to reduce raw material costs can be pursued through three key approaches: (1) the use of low-cost, widely available green or bio-based raw materials for the syntheses of novel monomers; (2) the combination of novel monomers and commercially available nanoparticles to synergistically increase their strengths and lower the costs; (3) the adoption of recyclable components from waste streams as raw material feedstocks. Moreover, an integrated approach to manufacture NF membranes should be developed to promote their scalability by system simplification and optimization. More crucially, enhancing the long-term stability of NF membranes not only effectively reduces system operating costs and extends the service life of membrane elements, but also ensures continuous and stable process operations and consistent effluent quality. Furthermore, it broadens their application potential in high-demand industrial sectors by minimizing the frequency of chemical cleaning and resource consumption associated with membrane replacement, thereby reducing environmental burden and aligning more closely with the principles of green and sustainable development. Therefore, controlling comprehensive costs, developing scalable fabrication processes, and enhancing the long-term stability of NF membranes are key strategies for advancing their commercial application.

In conclusion, while the latest NF membranes have demonstrated highly selective separation performance in laboratory studies, their cost-effective performance and scalability must be examined and tailored for specific or diverse wastewater treatment before commercialization. In addition, advanced characterization techniques should be integrated with artificial intelligence to guide the design and provide forward-looking solutions for the next-generation NF membranes in the field of wastewater recycling and resource recovery.

Author contributions

Wenxing Cheng: formal analysis, visualization, and writing – original draft. Qipeng Zhao: conceptualization, supervision, funding acquisition, project administration, and writing – review and editing. Huaqiang Chu: project administration, supervision, funding acquisition, and writing – review and editing. Xuefei Zhou: funding acquisition. Yalei Zhang: funding acquisition. Tai-Shung Chung: funding acquisition and writing – review and editing.

Conflicts of interest

There are no conflicts to declare.

Nomenclatures

[AEMIm][Cl]	1-Aminopropyl-3-methylimidazolium chloride
[Bmim][BF4]	1-Butyl-3-methylimidazolium tetrafluoroborate
18C6	Bis(aminobenzo)-18-crown-6
Ad	Adamantane-1,3-diamine
ADSS	3-((2-Aminoethyl) dimethylammonio) propane-1-sulfonate (sulfobetaine)
AFM-IR	Atomic force infrared spectroscopy
Am7CD	Heptakis(6-deoxy-6-amino)-β-cyclodextrin
APBA	3-Aminophenylboronic acid
Arg	L-Arginine
B. subtilis	*Bacillus subtilis*
BAC	Benzalkonium chloride
BAF	9,9-Bis(4-aminophenyl)fluorene
BAIE	1,2-Bis(*N*-aminoethylimidazoline)ethane
BBD	Bis(2-hydroxyethyl)-bipyridine-diium derivative
bisAPAF	2,2-Bis(3-amino-4-hydroxyphenyl)-hexafluoro-propane
BPA	Bisphenol A
BPPZ	2,4-(4-Hydroxyphenyl)-2,3-phthalazin-1-one
BAHPF	9,9-Bis(3-amino-4- hydroxyphenyl)fluorene
BSA	Bovine serum albumin
CA	Contact angle
CBB	Coomassie brilliant blue R250
CC	Cyanuric chloride
CD	Cyclodextrin
CHDA	1,4-Cyclohexanediamine
COFs	Covalent organic frameworks
–CO–NH–	Amide bonds
–CO–O–	Ester bonds
CR	Congo red
CTAC	Hexadecyltrimethylammonium chloride
CTAT	Hexadecyltrimethylammonium toluene-*p*-sulphonate
CTC	Chlortetracycline hydrochloride
Cyclen	1,4,7,10-Tetraazacyclododecane
DA	Dopamine
DAIB	Diaminoethyl imidazole bromide
DATB	3,3′-Diamine-Tröger's base
DFT	Density functional theory
DHDP	4,4′-Dihydroxydiphenylmethane
DHTAB	3,5-Dimethylhydrazide-benzyl trimethyl ammonium bromide
DMAP	4-Dimethylaminopyridine
DMAP	4-Dimethylaminopyridine
DMF	Dimethylformamide
DMSO	Dimethyl sulfoxide
DPD	Dissipative particle dynamics
DTAB	Dodecyl trimethyl ammonia bromide
DTAB	Dodecyl trimethyl ammonia bromide
DAB14C4	Diamino-dibenzo 14-crown-4
E. coli	*Escherichia coli*
EB	Evans blue
EDTP	Quaternizing *N*,*N*,*N*′,*N*′-tetrakis(2-hydroxypropyl)ethylenediamine
EPIP	Piperazine-2-carboxylic acid ethyl ester dihydrochloride
$FeCl_3$	Ferric chloride
FPEI	Perfluoro-functionalized polyethyleneimine
FRR	Flux recovery rate
FTIR	Fourier transform infrared spectroscopy
GRT	Girard reagent T
HA	Humic acid
HCl	Acidic chloride
IEP	Isoelectric point
ILs	Ionic liquids
IM-N	1-(3-Aminopropyl)imidazole
IP	Interfacial polymerization
IPC	Isophthaloyl chloride
KM	Kanamycin
LbL	Layer-by-layer
LP-IP	Liquid-phase interfacial polymerization
MC	Malonyl chloride
MD	Molecular dynamics
MeOH	Methanol
MF	Microfiltration
ML	Maltitol
MOFs	Metal–organic frameworks
MPD	M-phenylenediamine
MPIP	Piperazine-2-carboxylic acid methyl ester dihydrochloride
MWCO	Molecular weight cut off
MWs	Molecular weights
–N+	Quaternary ammonium
NF	Nanofiltration
Ng	Naringenin dihydrochalcone
–NH–	Secondary amine
$–NH_2$	Primary amine groups
NIPS	Non-solvent induced phase separation
NMP	*N*-Methyl-2-pyrrolidone
NP-10	Nonylphenol polyoxyethylene ether
NTSC	Naphthalene-1,3,6-trisulfonyl chloride
–OH	Hydroxyl groups
OSN	Organic solvent nanofiltration
PAA	Polyallylamine
PAH	Poly(allylamine hydrochloride)
PEI	Polyethyleneimine
PEPB	4,4′-(1-Phenylethylidene)bisphenol
PES	Polyethersulfone
PES	Polyethersulfone
PIP	Piperazine
PMDETA	*N*,*N*,*N*′,*N*′,*N*″-pentamethyldiethylenetriamine
PNIPAM	Poly(*N*-isopropylacrylamide)
PSf	Polysulfone
PSS	Poly(sodium 4-styrenesulfonate)
Pt	Phloretin
PVA	Polyvinyl alcohol

PVDF	Polyvinylidene fluoride
Pz	Phlorizin
QAEP	Quaternized diaminoethylpiperzine
QE	Quercetin
QEDTP	Bis-quaternary ammonium salt
QSPIP	Quaternized-spiral piperazine
QTDEA	Quaternary diethanolamine monomer
QTHIM	Quaternized tetrahydroxyethyl imidazolium
Ra	Roughness
rFB-IP	Reverse flexible-chain binding IP
RO	Reverse osmosis
Rq	Root mean square roughness
S. aureus	*Staphylococcus aureus*
SA	Sodium alginate
SBI	Tetramethyl-1,1′-spirobisindane-6,6′diol
SBVI	Sulfobetaine vinylimidazole
SDBS	Sodium dodecylbenzene sulfonate
SDS	Sodium dodecyl sulfate
SECM	Scanning electrochemical microscopy
$-SO_3H$	Sulfonic acid group
SPVA	Sulfonated polyvinyl alcohol
ST	Streptomycin
St	Stevioside
TA	Tannic acid
TAD	1,4,7,10-Tetraazacyclododecane
TAEA	Tris(2-aminoethyl)amine
TBB	1,3,5-Tris(bromomethyl)benzene
TEM	Transmission electron microscopy
TET	1,3,5-Tri(hydroxyethyl) benzyl triamine
TETA	Triethylenetetramine
Tg	Triaminoguanidine hydrochloride
TIPS	Thermal induced phase separation
TMAO	Trimethylamine *N*-oxide
TMC	1,3,5-Benzenetricarbonyl trichloride
TPC	Terephthaloyl chloride
TPEI	Trimethylamine *N*-oxide-based polyethylenimine
TrOCs	Trace organic contaminants
UF	Ultrafiltration
VP-IP	Vapor-phase interfacial polymerization
ε-PL	ε-Polylysine

Data availability

Data are available upon reasonable request.

Supplementary information (SI) is available. See DOI: https://doi.org/10.1039/d5cs00787a.

Acknowledgements

This work is funded by the National Natural Science Foundation of China (No. 52270076). Prof. Zhao would like to thank the financial aid from the Fundamental Research Funds for the Central Universities (22120250217). Prof. Chung is also grateful for the financial support from Yushan Scholarship Program.

References

1 S. Qu, S. Liang, M. Konar, Z. Zhu, A. S. F. Chiu, X. Jia and M. Xu, *Environ. Sci. Technol.*, 2018, **52**, 673–683.
2 Y. She, J. Chen, Q. Zhou, L. Wang, K. Duan, R. Wang, S. Qu, M. Xu and Y. Zhao, *Environ. Sci. Technol.*, 2024, **58**, 1119–1130.
3 O. A. Kazi, W. Chen, J. G. Eatman, F. Gao, Y. Liu, Y. Wang, Z. Xia and S. B. Darling, *Adv. Mater.*, 2023, **35**, 2300913.
4 P. Sarkar, C. Wu, Z. Yang and C. Y. Tang, *Chem. Soc. Rev.*, 2024, **53**, 4374–4399.
5 S. Wu, L. E. Peng, Z. Yang, P. Sarkar, M. Barboiu, C. Y. Tang and A. G. Fane, *Nano-Micro Lett.*, 2024, **17**, 91.
6 K. Wang, X. Wang, B. Januszewski, Y. Liu, D. Li, R. Fu, M. Elimelech and X. Huang, *Chem. Soc. Rev.*, 2022, **51**, 672–719.
7 S. Shao, F. Zeng, L. Long, X. Zhu, L. E. Peng, F. Wang, Z. Yang and C. Y. Tang, *Environ. Sci. Technol.*, 2022, **56**, 12811–12827.
8 Z. Qiu, J. Chen, J. Zeng, R. Dai and Z. Wang, *Water Res.*, 2023, **247**, 120774.
9 D. Yu, X. Xiao, C. Shokoohi, Y. Wang, L. Sun, Z. Juan, M. J. Kipper, J. Tang, L. Huang, G. S. Han, H. S. Jung and J. Chen, *Adv. Funct. Mater.*, 2023, **33**, 2211983.
10 S.-L. Zhang, B.-B. Li, A.-Q. Liu, L.-X. Xie, Z.-F. Li and G. Li, *Coord. Chem. Rev.*, 2024, **507**, 215748.
11 Q. Gan, Y. Hu, C. Wu, Z. Yang, L. E. Peng and C. Y. Tang, *Environ. Sci. Technol.*, 2024, **58**, 20812–20829.
12 J. R. Werber, C. O. Osuji and M. Elimelech, *Nat. Rev. Mater.*, 2016, **1**, 16018.
13 L. Ranieri, R. Esposito, S. P. Nunes, J. S. Vrouwenvelder and L. Fortunato, *Water Res.*, 2024, **253**, 121282.
14 J. Li, S. Ren, X. Qiu, S. Zhao, R. Wang and Y. Wang, *Environ. Sci. Technol.*, 2022, **56**, 15120–15129.
15 R. Lin, Q. Zhao, H. Chu, F. Feng, X. Zhou, X. Jiang, L. Shao and Y. Zhang, *Nat. Commun.*, 2025, **16**, 9978.
16 S. Zhu, Q. Zhao, Y. Chen, M. S. Khan, C.-M. Chang, T.-S. Chung and S. B. Chen, *Environ. Sci. Technol.*, 2026, **60**, 2160–2172.
17 Z. Zhu, X. Qu, F. Dong, H. Wang and B. Wang, *J. Membr. Sci.*, 2026, **742**, 125129.
18 Q. Zhao, R. Lin, S. Zhu, B. Xu, H. Chu, X. Zhou, Y. Zhang and T.-S. Chung, *Small*, 2026, e13154.
19 C.-M. Chang, S. Zhu, F. Feng, Q. Zhao and S. B. Chen, *J. Membr. Sci.*, 2025, **736**, 124732.
20 Q. Zhao, L. Y. Ee, D. L. Zhao, C.-M. Chang, T.-S. Chung and S. B. Chen, *J. Membr. Sci.*, 2024, **695**, 122497.
21 S. Hao, L. Jiang, Y. Li, Z. Jia and B. Van der Bruggen, *Chem. Commun.*, 2020, **56**, 419–422.
22 C. Wang, M. J. Park, H. Yu, H. Matsuyama, E. Drioli and H. K. Shon, *J. Membr. Sci.*, 2022, **661**, 120926.
23 U. S. Joshi, Anuradha and S. K. Jewrajka, *J. Membr. Sci.*, 2023, **669**, 121286.
24 Y. Chai, J. Chen, X. Fang, F. Li and X. Zhang, *J. Membr. Sci.*, 2025, **713**, 123293.
25 F. Zheng and Y. Wang, *J. Membr. Sci.*, 2022, **659**, 120836.

26 Q. Li, Y. Liu, Y. Jia, Y. Ji, F. Yan, J. Li, Y. Mohammad and B. He, *J. Membr. Sci.*, 2023, **677**, 121634.
27 X. Cheng, Y. Zhang, S. Shao, C. Lai, D. Wu, J. Xu, X. Luo, D. Xu, H. Liang and X. Zhu, *Desalination*, 2023, **548**, 116266.
28 P. Ramesh, M. M. Sta Cruz, S. Karla, J. Ahn, S. Lee, P. T. Underhill and G. Belfort, *J. Membr. Sci.*, 2024, **692**, 122296.
29 T. Istirokhatun, Y. Lin, K. Kinooka, Q. Shen, P. Zhang, Y. Jia, A. Matsuoka, K. Kumagai, T. Yoshioka and H. Matsuyama, *Water Res.*, 2023, **230**, 119567.
30 H. H. Wang, J. T. Jung, J. F. Kim, S. Kim, E. Drioli and Y. M. Lee, *J. Membr. Sci.*, 2019, **574**, 44–54.
31 J. T. Jung, J. F. Kim, H. H. Wang, E. di Nicolo, E. Drioli and Y. M. Lee, *J. Membr. Sci.*, 2016, **514**, 250–263.
32 S. Xiang, P. Zhang, S. Rajabzadeh, R. R. Gonzales, Z. Li, Y. Shi, S. Zhou, M. Hu, K. Guan and H. Matsuyama, *J. Membr. Sci.*, 2023, **677**, 121639.
33 N. Chen, J. Zhao, L. Shi, A. Goto and R. Wang, *J. Membr. Sci.*, 2023, **685**, 121919.
34 M. Xiao, X. Wang, S. Kim, J. Wu, J. A. Quezada-Renteria, M. Abdelrahman, D. Jassby and E. M. V. Hoek, *Chem. Eng. J.*, 2025, **521**, 166802.
35 T. A. Otitoju, C.-H. Kim, M. Ryu, J. Park, T.-K. Kim, Y. Yoo, H. Park, J.-H. Lee and Y. H. Cho, *J. Cleaner Prod.*, 2024, **467**, 142905.
36 H. Peng and K. Li, *J. Membr. Sci.*, 2023, **680**, 121738.
37 H. Zhou, R. Dai, T. Wang and Z. Wang, *Environ. Sci. Technol.*, 2022, **56**, 17266–17277.
38 Y. Liu, S. Yuan, M. Chi, Y. Wang, G. Van Eygen, R. Zhao, X. Zhang, G. Li, A. Volodine, S. Hu, J. Zheng and B. Van der Bruggen, *Water Res.*, 2022, **227**, 119322.
39 Y. Wu, Z. Gu, C. Lu, C. Hu and J. Qu, *Water Res.*, 2023, **244**, 120478.
40 P. Cheng, T. Zhu, X. Wang, K. Fan, Y. Liu, X.-M. Wang and S. Xia, *Environ. Sci. Technol.*, 2023, **57**, 12879–12889.
41 J. Di, H. Wang, L. Zhang, Z. Chen, Y. Zhang, B. B. Mamba, M. Qiu, J. Guo and L. Shao, *Desalination*, 2024, **592**, 118167.
42 J. Yu, L. Zhang, H. Sun, R. Li, D. L. Zhao, L. Shen, H. Lin, Y. Jiao and Y. Xu, *Desalination*, 2025, **599**, 118467.
43 G. Zhao, H. Gao, Z. Qu, H. Fan and H. Meng, *Nat. Commun.*, 2023, **14**, 7624.
44 Y. Hu, L. Xu, W. Zhang and H. Wang, *Angew. Chem., Int. Ed.*, 2023, **62**, e202302168.
45 F. Zhang, J.-b Fan and S. Wang, *Angew. Chem., Int. Ed.*, 2020, **59**, 21840–21856.
46 X. Wu, T. Chen, G. Dong, M. Tian, J. Wang, R. Zhang, G. Zhang, J. Zhu and Y. Zhang, *Desalination*, 2024, **577**, 117379.
47 R. Zhang, J. Yang, J. Tian, J. Zhu and B. Van der Bruggen, *Water Res.*, 2024, **257**, 121745.
48 B. Wu, W. Fan, R. Wang, N. Wang, Y. Shen, M. Wanjiya, Y. Wu and Q.-F. An, *J. Membr. Sci.*, 2024, **698**, 122585.
49 K. Fan, Z. Mai, Y. Liu, X. Wang, Y. Huang, P. Cheng, S. Xia and H. Matsuyama, *ACS ES&T Eng.*, 2023, **3**, 1738–1747.
50 Z. Zhang, K. Fan, Y. Liu and S. Xia, *Sci. Total Environ.*, 2023, **858**, 159922.
51 Z. Sun, X. Zhu, F. Tan, W. Zhou, Y. Zhang, X. Luo, J. Xu, D. Wu, H. Liang and X. Cheng, *Desalination*, 2023, **553**, 116479.
52 X. Zhu, F. Ge, X. Kang, L. Qiu, B. Liu, J. Xu, F. Wang, D. Wu, Z. Yang, D. Xu and H. Liang, *Desalination*, 2025, **593**, 118267.
53 W. Yan, G. Ma, X. Kang, Z. Yang, F. Zhang, D. Wu, M. Song, M. Li, D. Xu and X. Zhu, *J. Membr. Sci.*, 2025, **717**, 123565.
54 R. Zhao, Y. Li, Y. Mao, G. Li, T. Croes, J. Zhu, X. You, A. Volodin, J. Zheng and B. Van der Bruggen, *Environ. Sci. Technol.*, 2022, **56**, 17998–18007.
55 R. Zhang, W. Chen, Y. Gao, H. Li, Y. Lu and Z. Zhou, *J. Membr. Sci.*, 2024, **712**, 123243.
56 Z. Zhou, Z. Rui, Y.-N. Feng, Q. Wang and T.-D. Lu, *J. Membr. Sci.*, 2025, **720**, 123771.
57 Z. Liu, Y. Huang, Y. Lv, Y. Zhou, K. Wang and H. Zhao, *ACS Appl. Mater. Interfaces*, 2025, **17**, 14477–14487.
58 Y. Bai, B. Liu, J. Li, M. Li, Z. Yao, L. Dong, D. Rao, P. Zhang, X. Cao, L. F. Villalobos, C. Zhang, Q.-F. An and M. Elimelech, *Sci. Adv.*, 2023, **9**, eadg6134.
59 C. Ding, M. Zhang, B. Lyu, Z. Guo, N. Xing, X. Pang, T. Wu, Y. Jiang, R. Zhang, A. El-Gendi, H. Wu and Z. Jiang, *J. Membr. Sci.*, 2024, **705**, 122932.
60 L. Zhang, N. Di, Z. Wang and S. Zhao, *J. Membr. Sci.*, 2023, **688**, 122129.
61 Z. Hao, X. Tian, V. Mankol, Q. Li, J. Wang, Z. Wang and S. Zhao, *J. Membr. Sci.*, 2023, **672**, 121449.
62 K. Wang, W. Fu, X.-M. Wang, C. Xu, Y. Gao, Y. Liu, X. Zhang and X. Huang, *Environ. Sci. Technol.*, 2022, **56**, 17955–17964.
63 J. Li, H. Peng, K. Liu and Q. Zhao, *Adv. Mater.*, 2024, **36**, 2309406.
64 H. Peng, K. Yu, X. Liu, J. Li, X. Hu and Q. Zhao, *Nat. Commun.*, 2023, **14**, 5483.
65 H. Peng, Y. Su, X. Liu, J. Li and Q. Zhao, *Adv. Funct. Mater.*, 2023, **33**, 2305815.
66 H. Peng and Q. Zhao, *Adv. Funct. Mater.*, 2021, **31**, 2009430.
67 T. Gu, R. Zhang, S. Zhang, B. Shi, J. Zhao, Z. Wang, M. Long, G. Wang, T. Qiu and Z. Jiang, *J. Membr. Sci.*, 2022, **659**, 120802.
68 Y. Xu, H. Peng, H. Luo, Q. Zhang, Z. Liu and Q. Zhao, *Desalination*, 2022, **526**, 115519.
69 H. Peng, Q. Tang, S. Tang, J. Gong and Q. Zhao, *J. Membr. Sci.*, 2019, **592**, 117386.
70 X. Liu, Y. Feng, Y. Ni, H. Peng, S. Li and Q. Zhao, *J. Membr. Sci.*, 2023, **667**, 121178.
71 L. Pu, Q. Xia, Y. Wang, Y. Bu, Q. Zhang and G. Gao, *J. Membr. Sci.*, 2022, **658**, 120730.
72 X. Guo, B. Zhao, Q. Ding, L. Wang, Z. Zhang, J. Li and Z. Gao, *J. Membr. Sci.*, 2024, **701**, 122740.
73 X. Guo, B. Zhao, Y. Li, L. Wang, Z. Zhang and J. Li, *J. Membr. Sci.*, 2025, **713**, 123364.
74 Z. Jiang, R. Dong, A. M. Evans, N. Biere, M. A. Ebrahim, S. Li, D. Anselmetti, W. R. Dichtel and A. G. Livingston, *Nature*, 2022, **609**, 58–64.

75 H. Chen, F. Zhao, Z. Li, J. Ge, C. Wang and L. Yang, *Desalination*, 2024, **587**, 117955.
76 P. Xu, S. Zhang, H. Li, S. Xu, Q. Liu, Z. Liu, D. Wang, H. Jiang, L. Zhuo and X. Jian, *J. Membr. Sci.*, 2024, **697**, 122537.
77 B. Alhazmi, G. Ignacz, M. Di Vincenzo, M. N. Hedhili, G. Szekely and S. P. Nunes, *Nat. Commun.*, 2024, **15**, 7151.
78 S. Hong, M. Di Vincenzo, A. Tiraferri, E. Bertozzi, R. Górecki, B. Davaasuren, X. Li and S. P. Nunes, *Nat. Commun.*, 2024, **15**, 3160.
79 Z. Wang, S. Yuan, D. Wang, N. Zhang, Y. Shen and Z. Wang, *Environ. Sci. Technol.*, 2025, **59**, 5856–5865.
80 A. C. Lingaya, M. R. Gallardo, S.-H. Huang, C.-L. Li, A. R. Caparanga and K.-R. Lee, *J. Membr. Sci.*, 2024, **706**, 122982.
81 F. Li, Y. Zhai, S. Zhao, Z. Xu, K. Chen, B. Wei, H. Sun, Y. Hou, M. Wang, P. Li and Q. J. Niu, *J. Membr. Sci.*, 2024, **701**, 122778.
82 J. Dou, S. Han, S. Lin, Z. Qi, F. Huang, X. Feng, Z. Yao, J. Wang and L. Zhang, *J. Membr. Sci.*, 2023, **671**, 121382.
83 H. Yu, L. Xu, Y. Luo, M. Guo, X. Yan, X. Jiang and L. Yu, *J. Membr. Sci.*, 2023, **675**, 121569.
84 X. Yan, H. Wan, X. Xing, J. Yang, G. Yan and G. Zhang, *J. Membr. Sci.*, 2023, **687**, 122035.
85 L. Yang, K. Chen, J. Fu, Q. Zhao, N. A. Khan, Y. Liu, X. Cheng, Z. Yu and M. Long, *J. Membr. Sci.*, 2025, **736**, 124619.
86 W. Tang, B. Li, H. Liu, T. Liang, P. Li, C. Zhao, X. Li and S. Liu, *J. Membr. Sci.*, 2023, **685**, 121976.
87 X. Zhu, Z. Sun, J. Xu, S. Xu, X. Luo, F. Tan, X. Lu, D. Wu, H. Liang and X. Cheng, *Sep. Purif. Technol.*, 2024, **328**, 125076.
88 X. Zhu, H. Qiu, W. Yan, Z. Sun, X. Kang, J. Xu, D. Wu, H. Liang, X. Cheng and D. Xu, *Desalination*, 2024, **586**, 117851.
89 X. Wei, K. Fan, P. Cheng, Y. Liu and S. Xia, *Desalination*, 2024, **573**, 117219.
90 M. Jia, W.-H. Zhang, X. Zhang, M.-J. Yin, S. Gu, X. Hu and H. Guo, *Sep. Purif. Technol.*, 2023, **317**, 123884.
91 Z. G. Abdi, J.-Y. Lai and T.-S. Chung, *Desalination*, 2023, **549**, 116365.
92 B. Zhu, R. Shao, N. Li, C. Guo, P. Liu, J. Shi, C. Min, S. Liu, X. Qian, L. Wang and Z. Xu, *J. Membr. Sci.*, 2023, **667**, 121187.
93 J. Xue, Z. Jiao, R. Bi, R. Zhang, X. You, F. Wang, L. Zhou, Y. Su and Z. Jiang, *J. Membr. Sci.*, 2019, **584**, 282–289.
94 Y. Wang, C. Bao, D. Li, J. Chen, X. Xu, S. Wen, Z. Guan, Q. Zhang, Y. Ding, Y. Xin and Y. Zou, *J. Membr. Sci.*, 2022, **661**, 120925.
95 S. Cao, A. Zhang, M. Tian, Y. Jiang, G. Dong, Y. Zhang and J. Zhu, *Sep. Purif. Technol.*, 2023, **305**, 122547.
96 H. Zeng, F. Sun, J. Zhang, Y. Wang, S. Yang and D. Xing, *J. Membr. Sci.*, 2023, **675**, 121548.
97 D. Zou, Y. Zhou, W. Yan, Y. Zhou and C. Gao, *J. Membr. Sci.*, 2022, **662**, 120954.
98 Z. Liu, Z. Wang, L. Zhao, J. Xu, J. P. Chen and Q. J. Niu, *J. Membr. Sci.*, 2024, **694**, 122406.
99 A. Alkhouzaam and M. Khraisheh, *Desalination*, 2024, **581**, 117609.
100 M. Wang, M. Li, Z. Ren, Z. Fei, Y. Hou and Q. J. Niu, *J. Membr. Sci.*, 2023, **668**, 121180.
101 S. Zhang, R. Zhang, R. Li, Z. Zhang, Y. Li, H. Deng, J. Zhao, T. Gu, M. Long, X. Wang, S. Zhang and Z. Jiang, *J. Membr. Sci.*, 2022, **663**, 121063.
102 R. Zhao, P. Jin, J. Zhu, Y. Li, G. Li, A. Volodine, Y. Liu, J. Zheng and B. Van der Bruggen, *J. Membr. Sci.*, 2023, **673**, 121477.
103 T. Qi, X. Chen, T. Lu, D. Jin, R. Xu and J. Zhong, *J. Membr. Sci.*, 2024, **706**, 122930.
104 Z. Zha, T. Li, I. Hussein, Y. Wang and S. Zhao, *J. Membr. Sci.*, 2024, **695**, 122484.
105 J. Li, S. Wang, Q. Zhu, D. Xu, Y. Wang, X. Zhang, J. Du, Q. Chen, R. Zhao, X. Hu, Y. Liu, R. Dewil, Q. Gao and B. Van der Bruggen, *Desalination*, 2025, **603**, 118680.
106 H. Li, F. Tian, H. Liu, Y. Bai, C. Zhang, J. Li and L. Dong, *Desalination*, 2024, **576**, 117389.
107 S. Tang, Y. Chen, H. Zhang, T. Zhang, P. Wang and H. Sun, *Chem. Eng. J.*, 2023, **475**, 146111.
108 T. Wu, S. Zhang, M. Zhang, M. Long, G. Wang, T. Gu, H. Deng, C. Ding, R. Zhang and Z. Jiang, *J. Membr. Sci.*, 2024, **707**, 123019.
109 M.-H. Miao, J.-K. Qiu, Z.-L. Xu, C. Lian, H.-L. Liu, J.-H. Li and Y.-J. Tang, *J. Membr. Sci.*, 2023, **687**, 122094.
110 Q. Dong, E. Wang, S. Liu, W. Wu and B. Su, *J. Membr. Sci.*, 2024, **708**, 123036.
111 T. Zhang, Q. Wang, B. Zhang, Z. Wu and Z. Wang, *J. Membr. Sci.*, 2025, **713**, 123278.
112 S. Xu, J. Liu, J. Wang, H. Lin, Q. Han, F. Liu and C. Y. Tang, *J. Membr. Sci.*, 2023, **687**, 122003.
113 D. Cheng, Y. Chen, Z. Zhang, X. Wang, M. Wang, Q. Duan, G. Gong, Y. Hu and S.-L. Li, *J. Membr. Sci.*, 2023, **685**, 121969.
114 S. Liu, F. Yang, J. Zhou, Y. Peng, E. Wang, J. Song and B. Su, *J. Membr. Sci.*, 2023, **687**, 122052.
115 L. Zhou, S. Gu, F. Xu, J. Zhang, Z. Hu, S. Li and Z. Xu, *J. Membr. Sci.*, 2025, **715**, 123504.
116 M. R. Puhan, P. Sarkar, R. Amal, G. Nagendraprasad, K. A. Reddy, B. Sutariya and S. Karan, *Adv. Mater.*, 2024, **36**, 2404164.
117 Z. G. Abdi, J.-C. Chen and T.-S. Chung, *J. Membr. Sci.*, 2024, **689**, 122197.
118 X. Lu and M. Elimelech, *Chem. Soc. Rev.*, 2021, **50**, 6290–6307.
119 X. Tong, N. Chen, Y. Sui, Y. Liu, D. Chen, Q. Miao, J. Pang, Z. Tang, X. Guo and N. Cao, *J. Membr. Sci.*, 2025, **716**, 123516.
120 Y. He, Y. Zhang, F. Liang, Y. Zhu and J. Jin, *J. Membr. Sci.*, 2023, **672**, 121444.
121 M.-B. Wu, H. Ye, Z.-Y. Zhu, G.-T. Chen, L.-L. Ma, S.-C. Liu, L. Liu, J. Yao and Z.-K. Xu, *J. Membr. Sci.*, 2022, **644**, 119942.
122 Y. Zhang, H. Wang, J. Guo, X. Cheng, G. Han, C. H. Lau, H. Lin, S. Liu, J. Ma and L. Shao, *Science*, 2023, **382**, 202–206.

123 G.-J. Zhao, L.-L. Li, H.-Q. Gao, Z.-J. Zhao, Z.-F. Pang, C.-L. Pei, Z. Qu, L.-L. Dong, D.-W. Rao, J. Caro and H. Meng, *Adv. Funct. Mater.*, 2024, **34**, 2313026.
124 S. Duan, S. Jiang, Z. Li, P. Zhang, K. Guan, P. Xu and H. Matsuyama, *Desalination*, 2025, **597**, 118393.
125 M. Q. Seah, W. J. Lau, P. S. Goh, B. S. Ooi, G. S. Lai and A. F. Ismail, *Desalination*, 2023, **545**, 116091.
126 Y. Zhang, Y. Chen, M. Wang, W. Su, H. Li, P. Li and X. Zhang, *J. Membr. Sci.*, 2023, **687**, 122020.
127 Y. Li, S. Wang, W. Wu, H. Yu, R. Che, G. Kang and Y. Cao, *J. Membr. Sci.*, 2022, **659**, 120809.
128 X. Shi, Q. Zhang, Z. Wang, Q. Bi and Y. Lin, *J. Membr. Sci.*, 2025, **720**, 123780.
129 Y. Cao, Y. Wan, C. Chen and J. Luo, *Sep. Purif. Technol.*, 2022, **292**, 120974.
130 Z. Wang, L. Bai, J. Wang, Q. Zhao, H. Liang and G. Li, *Environ. Sci. Technol.*, 2023, **57**, 10838–10848.
131 X. Zhu, W. Yan, H. Peng, Z. Yang, Z. Zhou, D. Wu, L. Qiu, D. Xu, N. Wang and F. Chen, *J. Membr. Sci.*, 2025, **736**, 124670.
132 S. Fang, K. Guan, A. Zhang, L. Dai, S. Zhou, W. Fu, M. Hu, P. Xu, P. Zhang, Z. Li, Z. Mai and H. Matsuyama, *Desalination*, 2025, **594**, 118295.
133 H. Wu, H. Zhao, Y. Lin, X. Liu, L. Wang, H. Yao, Y. Tang, L. Yu, H. Wang and X. Wang, *J. Membr. Sci.*, 2023, **672**, 121468.
134 B. Wu, N. Wang, J.-H. Lei, Y. Shen and Q.-F. An, *J. Membr. Sci.*, 2022, **643**, 120050.
135 B. Wu, N. Wang, Y. Shen, C.-G. Jin and Q.-F. An, *J. Membr. Sci.*, 2023, **666**, 121144.
136 M. Zhang, J. Yuan, Z. Yin, N. A. Khan, C. Yang, M. Long, B. Lyu, X. You, R. Zhang, A. El–Gendi, H. Wu and Z. Jiang, *J. Membr. Sci.*, 2023, **680**, 121739.
137 Z. Li, S. Peng, W. Zhang, J. Zhang, Y. Jiao, R. Li, L. Shen, H. Lin and Y. Xu, *Desalination*, 2023, **564**, 116767.
138 L. Zhang, M. Hu, Y. Zhang, J. Hou, M. Zhang, C. Gao, W. Fu, H. Hui, Q. Liu, H. Ding, Z. Qin, H. Pei and H. Matsuyama, *J. Membr. Sci.*, 2024, **693**, 122386.
139 L. Paseta, C. Echaide-Górriz, C. Téllez and J. Coronas, *Green Chem.*, 2021, **23**, 2449–2456.
140 S. Karki and P. G. Ingole, *Chem. Eng. J.*, 2024, **488**, 150883.
141 D. Yadav, S. S. Sarma, D. Kumar and P. G. Ingole, *Chem. Eng. J.*, 2025, **504**, 158695.
142 J. M. Luque-Alled, L. Martínez-Izquierdo, P. Gorgojo, C. Téllez and J. Coronas, *Chem. Eng. J.*, 2023, **470**, 144233.
143 S. Yuan, G. Zhang, J. Zheng, P. Jin, J. Zhu, J. Yang, S. Liu, P. Van Puyvelde and B. Van der Bruggen, *J. Membr. Sci.*, 2020, **610**, 118282.
144 L. Jiang, Y. Ding, A. Zhu, Q. Zhang and Q. Liu, *J. Membr. Sci.*, 2025, **713**, 123344.
145 N. Yu, T. Wang, M. Wang, N. Ullah, Q. Duan, B. Wu, G. Gong, Y. Hu and S.-L. Li, *J. Membr. Sci.*, 2025, **734**, 124452.
146 J. Hu, S. Bleus, L. Achten, Y. Li, S. Eyley, W. Thielemans, I. F. J. Vankelecom, A. Volodin, W. Dehaen and X. Yang, *J. Membr. Sci.*, 2024, **692**, 122282.
147 Z. Guo, R. Li, Y. Wang, H. Zhang, H. Wang, Y. Sun and N. Chang, *J. Membr. Sci.*, 2025, **727**, 124087.
148 Z. Liu, Y. Zhao, M. Yi, L. Liao, Y. Huang, G. Lei, G. Hu, M. Lan, H. Li and Z. Mi, *J. Membr. Sci.*, 2025, **734**, 124458.
149 Q. Li, Z. He, X. Yu, Q. Li, N. Zhang, Q. Zhang, C. Sun, Y. Liu and H. Deng, *J. Membr. Sci.*, 2025, **719**, 123751.
150 X. Luo, L. Jiang, R. Zhao, Y. Wang, X. Xiao, S. Ghazouani, L. Yu, Z. Mai, H. Matsuyama and P. Jin, *J. Hazard. Mater.*, 2024, **465**, 133059.
151 C. Liang, B. Yi, G. Geng, S. Yu, D. Wu, M. Liu and C. Gao, *Chem. Eng. J.*, 2025, **522**, 167865.
152 Y. Xie, J. Ren, P. Liu, J. Zheng, Z. Mai, Y. Liu, X. Zhu, X. Li, D. Xu and H. Liang, *Desalination*, 2025, **593**, 118243.
153 X. Wang, T. Li, M. Su, Z. Li, S. Zhang, Y. Zhang and F. Liu, *Desalination*, 2025, **615**, 119259.
154 Y. Zheng, R. Jia, Z.-L. Xu, J. Liang, R. Han, J.-Y. Dai and L. Yu, *J. Membr. Sci.*, 2024, **712**, 123229.
155 P. Xu, R. R. Gonzales, J. Hong, K. Guan, Y.-H. Chiao, Z. Mai, Z. Li, S. Rajabzadeh and H. Matsuyama, *J. Membr. Sci.*, 2023, **668**, 121251.
156 B. Wu, S.-L. Li, N. Ullah, Q. Duan, M. Wang, N. Yu, G. Gong and Y. Hu, *Sep. Purif. Technol.*, 2025, **360**, 131005.
157 N. Yang, K. Li, Y. Hao, L. Zhang, Y. Sun, L. Zhang and B. Jiang, *J. Membr. Sci.*, 2024, **695**, 122483.
158 X. Mao, N. Xu, X. Shi, H. Wen and C. Liu, *J. Membr. Sci.*, 2025, **713**, 123315.
159 C. Yang, S. Liu, Q. Zhao, X. Zhang, Z. Wang, F. Zhang and J. Jin, *J. Membr. Sci.*, 2024, **711**, 123227.
160 Y. Jiang, S. Wen, J. Zhang, B. Peng, H. Zhang and Q. Zhang, *J. Membr. Sci.*, 2025, **735**, 124525.
161 L. Ren, J. Chen, Q. Lu, C. Wang, J. Han, K. Huang, X. Pan and H. Wu, *J. Membr. Sci.*, 2020, **597**, 117641.
162 J.-M. Jin, H. Ye, T.-H. Li, M.-B. Wu, L. Liu and J. Yao, *Desalination*, 2024, **582**, 117605.
163 S. Panda, S. Kundu, P. Malik and R. Haldar, *Chem. Sci.*, 2024, **15**, 2586–2592.
164 S.-Y. Fang, J.-L. Gong, L. Tang, W.-C. Cao, J. Li, Z.-K. Tan, Q.-Y. Niu and Z.-P. Chen, *Chem. Eng. J.*, 2022, **449**, 137808.
165 F. Xiang, A. M. Marti and D. P. Hopkinson, *J. Membr. Sci.*, 2018, **556**, 146–153.
166 L. Wang, M. Fang, J. Liu, J. He, J. Li and J. Lei, *ACS Appl. Mater. Interfaces*, 2015, **7**, 24082–24093.
167 Y. Xiao, W. Zhang, Y. Jiao, Y. Xu and H. Lin, *J. Membr. Sci.*, 2021, **624**, 119101.
168 Y. Hu, Z. Chen, Y. Ding, Y. Xu, H. Lin, W. Yu, J. Teng, L. Shen, Y. Jiao and B.-Q. Liao, *Sep. Purif. Technol.*, 2023, **323**, 124343.
169 P. Zheng, L. Jiang, Q. Zhang, Q. Liu and A. Zhu, *J. Colloid Interface Sci.*, 2024, **662**, 707–718.
170 J. Luo, C. Dong, R. He, C. Liu and T. He, *Desalination*, 2023, **557**, 116596.
171 J. Luo, B. Zhou, C. Dong, R. He, Y. Zhang and T. He, *Desalination*, 2024, **574**, 117229.
172 S. Xu, R. He, J. Luo and T. He, *Desalination*, 2024, **591**, 118032.

173 Y. Liang and S. Lin, *Environ. Sci. Technol.*, 2021, **55**, 738–748.
174 Y. Yang, Y. Li, K. Goh, C. H. Tan and R. Wang, *J. Membr. Sci.*, 2022, **648**, 120337.
175 D. Scheepers, J. de Keizer, Z. Borneman and K. Nijmeijer, *J. Membr. Sci.*, 2023, **670**, 121320.
176 B. Liu, J. Chen, R. He, J. Zhu, B. Hu and T. He, *Desalination*, 2025, **597**, 118387.
177 J. Bashir, S. Ilyas, A. Asif, W. M. de Vos, A. L. Khan and F. H. Akhtar, *ACS Appl. Polym. Mater.*, 2025, **7**, 3147–3156.
178 J. Niu, T. Yan, Q. Xiong, Y. Lei, F. Zheng, A. Patabendige, Z. Pan and G. Han, *Sep. Purif. Technol.*, 2025, **355**, 129656.
179 Z. Li, F. Zhao, H. Chen, L. Yang and J. Zhang, *J. Membr. Sci.*, 2025, **713**, 123373.
180 R. He, C. Dong, S. Xu, C. Liu, S. Zhao and T. He, *Desalination*, 2022, **525**, 115492.
181 M. Yu, T.-X. Ren, X.-G. Jin, X. Tang, M.-M. Tang, X.-H. Ma and Z.-L. Xu, *Desalination*, 2024, **580**, 117561.
182 P. Bera and S. K. Jewrajka, *J. Membr. Sci.*, 2024, **692**, 122292.
183 P. Zhao, F. Guo, L. Wang, H. Zhen, N. Zhang, S. Yin, G. Zhou, X. Ruan, G. He and X. Jiang, *Desalination*, 2024, **577**, 117394.
184 D. Xu, J. Zheng, X. Zhang, D. Lin, Q. Gao, X. Luo, X. Zhu, G. Li, H. Liang and B. Van der Bruggen, *Environ. Sci. Technol.*, 2022, **56**, 1927–1937.
185 N. Ma, G. Li, Y. Liu, J. Yang, Y. He and F. Liu, *J. Membr. Sci.*, 2024, **712**, 123249.
186 M. Yi, T. D. Nguyen, H. Liu, Y. Liu, S. Xiong and Y. Wang, *Adv. Funct. Mater.*, 2023, **33**, 2213471.
187 B. Seoane, J. Coronas, I. Gascon, M. E. Benavides, O. Karvan, J. Caro, F. Kapteijn and J. Gascon, *Chem. Soc. Rev.*, 2015, **44**, 2421–2454.
188 A. Nour, W. Iqbal, J. Navarro-Alapont, J. Ferrando-Soria, P. Magarò, R. Elliani, A. Tagarelli, C. Maletta, T. F. Mastropietro, E. Pardo and D. Armentano, *ACS Sustainable Chem. Eng.*, 2024, **12**, 12014–12028.
189 J. Wang, Y. Ying, P. Guo, D. Liu, W. Zhang and Q. Yang, *J. Membr. Sci.*, 2025, **713**, 123387.
190 S.-r Chen, T. Wang, X. Zhuo, Y.-x Wang and L.-g Wu, *J. Environ. Chem. Eng.*, 2022, **10**, 108027.
191 H. E. Karahan, K. Goh, C. Zhang, E. Yang, C. Yıldırım, C. Y. Chuah, M. G. Ahunbay, J. Lee, Ş. B. Tantekin-Ersolmaz, Y. Chen and T.-H. Bae, *Adv. Mater.*, 2020, **32**, 1906697.
192 A. Khosla, Sonu, H. T. A. Awan, K. Singh, Gaurav, R. Walvekar, Z. Zhao, A. Kaushik, M. Khalid and V. Chaudhary, *Adv. Sci.*, 2022, **9**, 2203527.
193 B. Barzegar, R. Habibi and H. Aghdasinia, *Chem. Eng. J.*, 2025, **508**, 161032.
194 M. Pagliero, A. Comite, O. Soda and C. Costa, *J. Membr. Sci.*, 2022, **658**, 120752.
195 R. Li, Y. Yang, Z. Zhang, S. Lian, Q. Zhao and C. Song, *J. Membr. Sci.*, 2023, **685**, 121983.
196 R. Li, Y. Yang, Z. Zhang, S. Lian and C. Song, *J. Membr. Sci.*, 2024, **690**, 122203.
197 Y. Liu, M. Yi and Y. Wang, *J. Membr. Sci.*, 2023, **678**, 121662.
198 L.-Y. Gong, N. Zhang, J.-Y. Yu, Y.-N. Wu, C.-J. Wei, H.-L. Zhu, X.-L. Cao and L.-F. Liu, *Desalination*, 2025, **614**, 119117.
199 Z. Wang, Y. Gao, J. Zhang, Z. Peng, X.-M. Wang, S. Liu and X. Huang, *ACS ES&T Eng.*, 2024, **4**, 1113–1122.
200 L. Shen, R. Cheng, M. Yi, W.-S. Hung, S. Japip, L. Tian, X. Zhang, S. Jiang, S. Li and Y. Wang, *Nat. Commun.*, 2022, **13**, 500.
201 Y. Ye, N. Qiu, Z. Qiu, J. Wang, Y. He and F. Liu, *J. Membr. Sci.*, 2024, **694**, 122426.
202 M. Long, L. Yang, T. Wu, M. Zhang, S. Zhang, D. An, Y. Zheng, R. Zhang and Z. Jiang, *J. Membr. Sci.*, 2024, **700**, 122729.
203 J. Pang, H. Wang, C. Zhang, W. Fan, Y. Feng, L. Yu, L. Fan, R. Wang, Z. Kang and D. Sun, *Sep. Purif. Technol.*, 2023, **323**, 124497.
204 Y. Sun, J. Zhong, Z. Lin, R. Sun, L. Chen, Z. Jiang and J. Pang, *J. Membr. Sci.*, 2023, **666**, 121179.
205 S. Hao, L. Liu, J. Xiao, J. Wang, Y. Xu and Y. Hu, *J. Membr. Sci.*, 2024, **707**, 122994.
206 Y. Liang, Y. Zhu, C. Liu, K.-R. Lee, W.-S. Hung, Z. Wang, Y. Li, M. Elimelech, J. Jin and S. Lin, *Nat. Commun.*, 2020, **11**, 2015.
207 R. Jia, X.-G. Jin, Z.-L. Xu, L.-K. Wu, Y.-H. Tong, H.-X. Li, H.-H. Ping, X.-H. Ma and S.-J. Xu, *J. Membr. Sci.*, 2024, **712**, 123235.
208 R. Jia, H.-X. Li, Z.-L. Xu, X.-G. Jin, L.-K. Wu, H.-H. Ping, X.-H. Ma and S.-J. Xu, *J. Membr. Sci.*, 2025, **726**, 124048.
209 M. Wang, M. Li, Z. Fei, J. Li, Z. Ren and Y. Hou, *Desalination*, 2022, **544**, 116131.
210 H. Geng, X. Huo, Z. Jing, Z. Shi, H. Wang and N. Chang, *J. Membr. Sci.*, 2025, **713**, 123369.
211 X. Zhang, H.-M. Cui, Y. Gao, Z.-W. Yan, X. Yan, Y. Chen, X.-J. Guo and W.-Z. Lang, *Desalination*, 2023, **558**, 116617.
212 Y. Liu, W. Fang, Z. Yue, Y. Wang, Y. Zhu, J. Jin and L. Jiang, *Nat. Water*, 2025, **3**, 430–438.
213 X. Han, Z. Wang and J. Wang, *J. Membr. Sci.*, 2022, **651**, 120453.
214 Y. Li, S. Wang, H. Li, G. Kang, Y. Sun, H. Yu, Y. Jin and Y. Cao, *J. Membr. Sci.*, 2022, **643**, 120056.
215 D. T. T. Huyen, S. S. Ray and Y.-N. Kwon, *Desalination*, 2024, **572**, 117118.
216 G. Liu, Z. Pu, C. Matindi, Z. Cui, H. Wang, J. Yang and J. Li, *J. Membr. Sci.*, 2025, **713**, 123292.
217 Q. Peng, R. Wang, Z. Zhao, S. Lin, Y. Liu, D. Dong, Z. Wang, Y. He, Y. Zhu, J. Jin and L. Jiang, *Nat. Commun.*, 2024, **15**, 2505.
218 Q. Gan, L. E. Peng, Z. Yang, P.-F. Sun, L. Wang, H. Guo and C. Y. Tang, *Environ. Sci. Technol.*, 2023, **57**, 1819–1827.
219 K. Dong, X. Liu, H. Dong, X. Zhang and S. Zhang, *Chem. Rev.*, 2017, **117**, 6636–6695.
220 L. Yung, H. Ma, X. Wang, K. Yoon, R. Wang, B. S. Hsiao and B. Chu, *J. Membr. Sci.*, 2010, **365**, 52–58.
221 D. Zheng, D. Hua, A. Yao, Y. Hong, X. Cha, X. Yang, S. Japip and G. Zhan, *J. Membr. Sci.*, 2021, **636**, 119551.

222 K. Ma, X. Li, X. Xia, Y. Chen, Z. Luan, H. Chu, B. Geng and M. Yan, *J. Membr. Sci.*, 2023, **673**, 121486.
223 J. Bai, W. Lai, L. Gong, L. Xiao, G. Wang, L. Shan and S. Luo, *J. Membr. Sci.*, 2022, **641**, 119882.
224 B.-B. Guo, C. Liu, C.-Y. Zhu, J.-H. Xin, C. Zhang, H.-C. Yang and Z.-K. Xu, *Nat. Commun.*, 2024, **15**, 2282.
225 X.-G. Jin, X. Tang, T.-X. Ren, J. Wang, P. Zheng, X.-H. Ma and Z.-L. Xu, *J. Membr. Sci.*, 2024, **696**, 122536.
226 C. Liu, J. Yang, B.-B. Guo, S. Agarwal, A. Greiner and Z.-K. Xu, *Angew. Chem., Int. Ed.*, 2021, **60**, 14636–14643.
227 B. He, H. Peng, Y. Chen and Q. Zhao, *J. Membr. Sci.*, 2020, **608**, 118202.
228 Q.-F. An, W.-D. Sun, Q. Zhao, Y.-L. Ji and C.-J. Gao, *J. Membr. Sci.*, 2013, **431**, 171–179.
229 Y. Wang, H. Chang, S. Jiang, J. Chen, J. Wang, H. Liang, G. Li and X. Tang, *J. Membr. Sci.*, 2023, **677**, 121615.
230 Y. Fang, B. Jiang, Y. Hao, N. Yang, L. Zhang, C. Zhang, Y. Sun, X. Xiao and L. Zhang, *J. Membr. Sci.*, 2023, **678**, 121689.
231 M. Zhang, X. You, K. Xiao, Z. Yin, J. Yuan, J. Zhao, C. Yang, R. Zhang, H. Wu and Z. Jiang, *J. Membr. Sci.*, 2022, **657**, 120673.
232 Z. Zhai, K. Chen, H. Yang, Y. Huang, H. Lan, X. Jie, Q. J. Niu and Y. Zhao, *Desalination*, 2022, **539**, 115941.
233 C.-M. Chang, Q. Zhao and S. B. Chen, *J. Membr. Sci.*, 2024, **697**, 122571.
234 X. Guo, B. Zhao, Y. Li, L. Wang, Z. Zhang and J. Li, *J. Membr. Sci.*, 2025, **723**, 123928.
235 P. Dou, L. Liu, Q. Sun, D. Meng, J. Du, A. Yao, X. Ding, A. A. Al-Thuraya and J. Liu, *ACS Nano*, 2025, **19**, 22442–22453.
236 H. Zhao, L. Zhang, H. Hui, H. Pei and X. Li, *J. Membr. Sci.*, 2026, **738**, 124866.
237 H. Ding, M. Huang, Y. Liu, L. Zhang, H. Pei and X. Li, *J. Membr. Sci.*, 2025, **728**, 124102.
238 F. Yan, Z. Wang and M. Wang, *J. Membr. Sci.*, 2025, **734**, 124430.
239 Y. Li, C. Deng, H. Hu, Y. Wang, Z. Qi, C. Chen, C. Zhou and L. Shen, *J. Membr. Sci.*, 2026, **738**, 124784.
240 T. Qi, X. Wei, X. Chen, T. Lu, D. Jin and J. Zhong, *J. Membr. Sci.*, 2025, **736**, 124662.
241 Y. Zhang, Y. Fan, G. Zhou, Y. Cao, J. Wang, X. Jiang, N. Zhang and S. Yin, *J. Membr. Sci.*, 2024, **693**, 122351.
242 H. Chen, F. Zhao, X. Zhang, H.-D. Park, Z. Li and L. Yang, *J. Membr. Sci.*, 2024, **707**, 122992.
243 F. Soyekwo, C. Liu, X. Mao and R. Nie, *J. Membr. Sci.*, 2024, **707**, 122940.
244 B. Yuan, M. Wang, M. Wu, D. Yang, K. Zhang, S. Zhao, Y. Zhang, P. Hu, M. You, S. Zhao, K. Chen, X. Zhang, J. Jiang, X. Lou and Q. J. Niu, *J. Membr. Sci.*, 2024, **701**, 122743.
245 L. Shi, S. Liu, W.-S. Hung, W. Shi, X. Lu and C. Wu, *J. Membr. Sci.*, 2023, **668**, 121252.
246 Y. Qian, H. Wu, S.-P. Sun and W. Xing, *J. Membr. Sci.*, 2020, **611**, 118286.
247 W.-H. Yu, Z.-Q. Gan, J.-R. Wang, Y. Zhao, J. Han, L.-F. Fang, X.-Z. Wei, Z.-L. Qiu and B.-K. Zhu, *J. Membr. Sci.*, 2021, **639**, 119756.
248 Y. Zeng, L. Wang, L. Zhang and J. Q. Yu, *J. Membr. Sci.*, 2018, **546**, 225–233.
249 Y. Zhang, Z. Hao, I. Hussein, Z. Wang and S. Zhao, *Adv. Funct. Mater.*, 2024, **34**, 2315750.
250 L. Wang, Y. Lin, Y. Tang, D. Ren and X. Wang, *J. Membr. Sci.*, 2021, **634**, 119405.
251 H. Peng, X. Liu, Y. Su, J. Li and Q. Zhao, *Angew. Chem., Int. Ed.*, 2023, **62**, e202312795.
252 T. Huang, B. A. Moosa, P. Hoang, J. Liu, S. Chisca, G. Zhang, M. AlYami, N. M. Khashab and S. P. Nunes, *Nat. Commun.*, 2020, **11**, 5882.
253 S. Wang, Z. Wang, S. Zhu, S. Liu, F. Zhang and J. Jin, *J. Membr. Sci.*, 2023, **675**, 121540.
254 A. He, Z. Jiang, Y. Wu, H. Hussain, J. Rawle, M. E. Briggs, M. A. Little, A. G. Livingston and A. I. Cooper, *Nat. Mater.*, 2022, **21**, 463–470.
255 Y. Gao, Y. Zhao, X.-M. Wang, C. Tang and X. Huang, *Environ. Sci. Technol.*, 2022, **56**, 14038–14047.
256 J. Huang, Y. Zhang, J. Guo, Z. Yang, Y. Bai, G. Gao, J. Zhu, B. B. Mamba, H. Wang and L. Shao, *J. Membr. Sci.*, 2024, **711**, 123216.
257 H. Zhen, M. Wu, Z. Yuan, Z. Qi, Y. Meng, X. Zu, D. Liu, G. He and X. Jiang, *J. Membr. Sci.*, 2023, **672**, 121445.
258 Y.-F. Mi, G. Xu, Y.-S. Guo, B. Wu and Q.-F. An, *J. Membr. Sci.*, 2020, **601**, 117795.
259 H. Zhang, F. Xie, Z. Zhao, N. U. Afsar, F. Sheng, L. Ge, X. Li, X. Zhang and T. Xu, *ACS Appl. Mater. Interfaces*, 2022, **14**, 10782–10792.
260 A. Zhang, J. Zhu, S. Han, Y. Zhang and B. Van der Bruggen, *J. Membr. Sci.*, 2022, **662**, 120987.
261 S.-L. Li, G. Chang, Y. Huang, K. Kinooka, Y. Chen, W. Fu, G. Gong, T. Yoshioka, N. B. McKeown and Y. Hu, *Angew. Chem., Int. Ed.*, 2022, **61**, e202212816.
262 J. Huang, Y. Zhang, J. Guo, F. Yang, J. Ma, Y. Bai, L. Shao, S. Liu and H. Wang, *Nat.Sustainability*, 2024, **7**, 901–909.
263 X. Geng, J. Wang, Y. Ding, W. Zhang, Y. Wang and F. Liu, *J. Membr. Sci.*, 2021, **632**, 119385.
264 X. Zhu, X. Cheng, J. Xing, T. Wang, D. Xu, L. Bai, X. Luo, W. Wang, G. Li and H. Liang, *Desalination*, 2020, **474**, 114197.
265 J. Cheng, Z. Li, X. Bao, R. Zhang, S. Yin, W. Huang, K. Sun and W. Shi, *J. Membr. Sci.*, 2022, **657**, 120675.
266 A. Szymczyk and P. Fievet, *J. Membr. Sci.*, 2005, **252**, 77–88.
267 X. Zhai, S. Lin, X. Li and Z. Wang, *Environ. Sci. Technol.*, 2024, **58**, 15874–15884.
268 X. Zhai, Y.-L. Wang, R. Dai, X. Li and Z. Wang, *Environ. Sci. Technol.*, 2022, **56**, 14069–14079.
269 W. Liu, X.-M. Wang, D. Li, Y. Gao, K. Wang and X. Huang, *Environ. Sci. Technol.*, 2025, **59**, 5848–5855.
270 R. Wang and S. Lin, *J. Membr. Sci.*, 2021, **620**, 118809.
271 L. Lin, T. M. Weigand, M. W. Farthing, P. Jutaporn, C. T. Miller and O. Coronell, *J. Membr. Sci.*, 2018, **564**, 935–944.
272 F. Wang, Z. Yang and C. Y. Tang, *ACS ES&T Eng.*, 2022, **2**, 2023–2033.
273 X. Li, C. Li, K. Goh, T. H. Chong and R. Wang, *J. Membr. Sci.*, 2022, **652**, 120466.

274 T. Huang, T. Puspasari, S. P. Nunes and K.-V. Peinemann, *Adv. Funct. Mater.*, 2020, **30**, 1906797.
275 C. Zhang, S. Chen, Y. Zhao and J. Meng, *J. Membr. Sci.*, 2024, **694**, 122411.
276 M. C. Y. Wong, L. Lin, O. Coronell, E. M. V. Hoek and G. Z. Ramon, *J. Membr. Sci.*, 2016, **500**, 124–135.
277 C. Jiang, L. Tian, Y. Hou and Q. J. Niu, *J. Membr. Sci.*, 2019, **586**, 192–201.
278 H. Wen, Z. Liu, J. Xu and J. P. Chen, *Desalination*, 2024, **591**, 117967.
279 Y. Li, Y. Zhao, H. Wang and M. Wang, *Desalination*, 2019, **468**, 114081.
280 M. S. Sajna, T. Elmakki, S. Zavahir, H. Tariq, A. Abdulhameed, H. Park, H. K. Shon and D. S. Han, *Desalination*, 2024, **592**, 118148.
281 Y.-T. Shi, X. Meng, L. Yao and M. Tian, *Desalination*, 2021, **517**, 115239.
282 Z. H. Foo, D. Rehman, A. T. Bouma, S. Monsalvo and J. H. Lienhard, *Environ. Sci. Technol.*, 2023, **57**, 6320–6330.
283 Z. Yan, X. Chen, H. Chang, H. Pang, G. Fan, K. Xu, H. Liang and F. Qu, *Water Res.*, 2024, **254**, 121340.
284 K. Chen, F. Li, T. Wei, H. Zhou, T. Zhang, S. Zhao, T. Xie, H. Sun, P. Li and Q. J. Niu, *J. Membr. Sci.*, 2023, **684**, 121882.
285 X. Tian, D. Ji, H. Feng, W. Lin, C. Wang, L. Wei, W. Shu and C. Xiao, *J. Membr. Sci.*, 2025, **713**, 123310.
286 O. Setiawan, Y.-H. Huang, Z. G. Abdi, W.-S. Hung and T.-S. Chung, *J. Membr. Sci.*, 2023, **668**, 121269.
287 B. Yuan, Y. Zhang, P. Qi, D. Yang, P. Hu, S. Zhao, K. Zhang, X. Zhang, M. You, J. Cui, J. Jiang, X. Lou and Q. J. Niu, *Nat. Commun.*, 2024, **15**, 471.
288 Z. Pan, Y. Lei, F. Zheng, J. Zhan and G. Han, *J. Membr. Sci.*, 2024, **711**, 123172.
289 Y. Fan, H. Tian, K. Wang, G. Zhou, J. Wang, G. Li, Y. Cao, Y. Wang, X. Jiang and W. Kou, *Sep. Purif. Technol.*, 2025, **358**, 130276.
290 J. Wang, W. Wang, Y. Yan, Y. Liu, G. Zhang, J. Li and Y. Wu, *J. Membr. Sci.*, 2025, **722**, 123858.
291 Y. Huang, J. Wang, L. Xue, M. Chen, F. Huang and C. Gao, *Sep. Purif. Technol.*, 2025, **367**, 132871.
292 S. Zhao, Z. Zhao, X. Zhang, Z. Zha, T. Tong, R. Wang and Z. Wang, *Environ. Sci. Technol.*, 2024, **58**, 5174–5185.
293 Y. Liang, R. Pan, B. Yang, X. Li, M. Wang, Z. Cui, B. He and F. Yan, *J. Membr. Sci.*, 2026, **738**, 124740.
294 P. Xu, K. Guan, Y.-H. Chiao, Z. Mai, Z. Li, M. Hu, P. Zhang, R. R. Gonzales and H. Matsuyama, *J. Membr. Sci.*, 2023, **688**, 122133.
295 A. Hu, Y. Liu, X. Wang, S. Xia and B. Van der Bruggen, *Water Res.*, 2025, **268**, 122677.
296 W. Gong, L. Bai and H. Liang, *Desalination*, 2024, **590**, 117974.
297 K. Fan, Z. Zhang, Y. Liu, W. Xu, X. Wang, T.-Y. Zhang and S. Xia, *Environ. Sci. Technol.*, 2025, **59**, 2875–2885.
298 P. Marchetti, M. F. Jimenez Solomon, G. Szekely and A. G. Livingston, *Chem. Rev.*, 2014, **114**, 10735–10806.
299 P. Vandezande, L. E. M. Gevers and I. F. J. Vankelecom, *Chem. Soc. Rev.*, 2008, **37**, 365–405.
300 G. M. Shi, Y. Feng, B. Li, H. M. Tham, J.-Y. Lai and T.-S. Chung, *Prog. Polym. Sci.*, 2021, **123**, 101470.
301 Z.-Y. Wang, R. Feng, W.-J. Wang, Y.-X. Sun, S.-N. Tao, Y.-M. Wang, Y.-F. Chen, Z.-J. Fu, X.-L. Cao, S.-P. Sun and W. Xing, *Adv. Membr.*, 2021, **1**, 100007.
302 Z. F. Gao, A. Naderi, W. Wei and T.-S. Chung, *J. Membr. Sci.*, 2020, **616**, 118582.
303 W. Song, E. Wang, Y. Peng, R. Che, Q. Zhang, H. Li and B. Su, *J. Membr. Sci.*, 2025, **720**, 123770.
304 W. Fu, Y. Huang, L. Deng, J. Sun, S.-L. Li and Y. Hu, *J. Membr. Sci.*, 2022, **655**, 120583.
305 J.-B. Li, C.-Y. Zhu, B.-B. Guo, C. Liu, J.-H. Xin, C. Zhang, J. Wu, L. Zhang, H.-C. Yang and Z.-K. Xu, *J. Membr. Sci.*, 2024, **693**, 122342.
306 J. Choi, K. Choi, Y. Kwon, D. Kim, Y. Yoo, S. G. Im and D.-Y. Koh, *Nat. Commun.*, 2024, **15**, 2800.
307 Z. Liu, H. Wen, S. Jiang, J. Xu and J. P. Chen, *Desalination*, 2025, **597**, 118316.
308 Z. Li, H. Zhen, Y. Jia, W. Xiao, X. Li, X. Wu, T. Li, G. He and X. Jiang, *J. Hazard. Mater.*, 2024, **480**, 136356.
309 Y. Liu, K. Wang, Z. Zhou, X. Wei, S. Xia, X.-M. Wang, Y. F. Xie and X. Huang, *Environ. Sci. Technol.*, 2022, **56**, 15220–15237.
310 J. Chen, T. Wang, R. Dai, Z. Wu and Z. Wang, *Environ. Sci. Technol.*, 2024, **58**, 9416–9426.
311 H. Zhou, Z. Qiu, J. Zeng, R. Dai and Z. Wang, *J. Membr. Sci.*, 2023, **688**, 122125.
312 B. Liang, X. He, J. Hou, L. Li and Z. Tang, *Adv. Mater.*, 2019, **31**, 1806090.
313 S. Xie, Z. Yu, L. Chen, J. Du, J. Li, W. Yuan, X. Li and J. Lin, *Desalination*, 2024, **591**, 118056.
314 O. Setiawan, Z. G. Abdi, M. Weber, W.-S. Hung and T.-S. Chung, *J. Membr. Sci.*, 2023, **685**, 121942.
315 X. Wang, T. Li, Z. Li, M. Su, S. Zhang and F. Liu, *J. Membr. Sci.*, 2025, **729**, 124147.
316 D. Hu, Y. Liu, J. Wu and Y. Wang, *J. Membr. Sci.*, 2026, **740**, 124924.
317 Y. Liu, Q. Cen, K. Fan, A. Hu, X. Yuan and S. Xia, *J. Membr. Sci.*, 2024, **693**, 122358.
318 Y.-S. Guo, Y.-L. Ji, B. Wu, N.-X. Wang, M.-J. Yin, Q.-F. An and C.-J. Gao, *J. Membr. Sci.*, 2020, **593**, 117441.
319 T. Tong, X. Liu, T. Li, S. Park and B. Anger, *Environ. Sci. Technol.*, 2023, **57**, 7129–7149.
320 Z. Cao, Y. Hu, H. Zhao, B. Cao and P. Zhang, *Water Res.*, 2022, **222**, 118945.
321 L. Zheng, H. Zhong, Y. Wang, N. Duan, M. Ulbricht, Q. Wu, B. Van der Bruggen and Y. Wei, *Water Res.*, 2024, **250**, 121023.
322 L. Zheng, Q. Wu, M. Ulbricht, H. Zhong, N. Duan, B. Van der Bruggen and Y. Wei, *Water Res.*, 2024, **258**, 121671.
323 S. Zhao, Z. Liao, A. Fane, J. Li, C. Tang, C. Zheng, J. Lin and L. Kong, *Desalination*, 2021, **499**, 114857.
324 L. Liu, Y. Liu, X. Chen, S. Feng, Y. Wan, H. Lu and J. Luo, *J. Membr. Sci.*, 2023, **668**, 121205.

325 S. Li, J. Luo, X. Hang, S. Zhao and Y. Wan, *J. Membr. Sci.*, 2019, **582**, 264–273.
326 L. Liu, X. Chen, S. Feng, Y. Wan and J. Luo, *ACS Appl. Mater. Interfaces*, 2022, **14**, 36132–36142.
327 J. Rolf, T. Cao, X. Huang, C. Boo, Q. Li and M. Elimelech, *Environ. Sci. Technol.*, 2022, **56**, 7484–7511.
328 X. Zhang, F. He, Z. Yang, M. Xie, H. Ren, D. Wu, J. Xu, C. Luo and L. Bai, *Desalination*, 2023, **558**, 116642.
329 S. Li, H. Meng, H. Wang, J. S. Vrouwenvelder and Z. Li, *Water Res.*, 2022, **219**, 118554.
330 T. Huang, Z. Su, K. Hou, J. Zeng, H. Zhou, L. Zhang and S. P. Nunes, *Chem. Soc. Rev.*, 2023, **52**, 4173–4207.
331 H. Liu, Z. Wang, H. Wang, Z. Liu, J. Yang, H. Zhang, H. Liang and L. Bai, *Water Res.*, 2024, **267**, 122528.
332 R. Ma, X. Lu, C. Wu, S. Zhang, S. Zheng, K. Ren, J. Gu, H. Wang and H. Shen, *J. Membr. Sci.*, 2022, **660**, 120886.
333 S. Mazinani, A. Al-Shimmery, Y. M. J. Chew and D. Mattia, *J. Membr. Sci.*, 2022, **644**, 120137.
334 S. Wang, Z.-Y. Wang, J.-Z. Xia and X.-M. Wang, *J. Membr. Sci.*, 2021, **620**, 118830.
335 W. Shang, W. Liu, W. Wang, N. K. Khanzada, J. Guo, M. Li, X. Li, J.-Y. Lao, S. Y. Jeong, C. Y. Tso, F. Sun and A. K. An, *Desalination*, 2023, **555**, 116524.
336 A. Ilyas, D. Madhav, I. Nulens, K. V. Agrawal, C. Van Goethem and I. F. J. Vankelecom, *J. Membr. Sci.*, 2024, **700**, 122721.
337 J. Ding, H. Wu and P. Wu, *Chem. Eng. J.*, 2020, **396**, 125199.
338 Y. Shen, J. Zhou, B. Wu, M. Ge, N. Wang, Y. Zhao, Q.-F. An and B. V. d Bruggen, *J. Membr. Sci.*, 2023, **675**, 121571.
339 Y. Liu, J. Ran, Q. Guo, L. Gao, S. Yin, S. Li, X. Jiang, N. Zhang and G. Zhou, *Desalination*, 2024, **583**, 117649.
340 Q. Wang, W. Lin, S. Chou, P. Dai and X. Huang, *Water Res.*, 2023, **236**, 119943.
341 Y. Su, H. Peng, Y. Hu, S. Li, J. Rao and Q. Zhao, *J. Membr. Sci.*, 2024, **697**, 122591.
342 I. M. Hsieh, A. K. Thakur and M. Malmali, *Desalination*, 2021, **509**, 115046.
343 I. A. Khan, Y. S. Lee and J.-O. Kim, *Desalination*, 2023, **549**, 116313.
344 K. Huang, K. P. Reber, M. D. Toomey, H. Haflich, J. A. Howarter and A. D. Shah, *Environ. Sci. Technol.*, 2019, **53**, 8167–8176.
345 K. Huang, K. P. Reber, M. D. Toomey, J. A. Howarter and A. D. Shah, *Environ. Sci. Technol.*, 2021, **55**, 2575–2584.
346 A. Wang, S. Huo, J.-P. Croué and C. Liu, *Water Res.*, 2023, **241**, 120159.
347 D. Wu, J. Martin, J. R. Du, Y. Zhang, D. Lawless and X. Feng, *J. Membr. Sci.*, 2015, **487**, 256–270.
348 Y. Cao, J. Luo, C. Chen and Y. Wan, *Chem. Eng. J.*, 2021, **425**, 131791.
349 D. L. Zhao, W. S. Yeung, Q. Zhao and T.-S. Chung, *J. Membr. Sci.*, 2020, **604**, 118039.
350 J. Lee, Y. Shin, C. Boo and S. Hong, *J. Membr. Sci.*, 2023, **666**, 121142.
351 S.-L. Gao, J.-K. Qiu, Z.-L. Xu, C. Lian, H.-L. Liu, J.-H. Li and Y.-J. Tang, *J. Membr. Sci.*, 2024, **694**, 122412.
352 M.-H. Miao, J.-K. Qiu, Z.-L. Xu, C. Lian, H.-L. Liu, J.-H. Li and Y.-J. Tang, *J. Membr. Sci.*, 2024, **699**, 122653.
353 B.-N. Dong, L.-Y. Gong, L. Xia, N. Zhang and L.-F. Liu, *J. Membr. Sci.*, 2024, **693**, 122379.
354 M. Ji, Z. Wang, Y. Zhu, L. Shan, Y. Lu, Y. Zhang, Y. Zhang and J. Jin, *J. Membr. Sci.*, 2022, **645**, 120189.
355 K. H. Lasisi, T. F. Ajibade and K. Zhang, *J. Membr. Sci.*, 2022, **661**, 120909.
356 L. Yu, K. Li, Y. Zhang, J. Wang and G. Zhang, *J. Membr. Sci.*, 2022, **648**, 120381.
357 W. Lai, L. Liu, J. Bai, L. Xiao, Y. Jiao, Y. Yang, L. Shan and S. Luo, *Chem. Eng. J.*, 2023, **460**, 141708.
358 H. Ivnitsky, D. Minz, L. Kautsky, A. Preis, A. Ostfeld, R. Semiat and C. G. Dosoretz, *J. Membr. Sci.*, 2010, **360**, 165–173.
359 R. Xu, W. Qin, B. Zhang, X. Wang, T. Li, Y. Zhang and X. Wen, *Chem. Eng. J.*, 2020, **395**, 125087.
360 Q. Zeng, D. L. Zhao, L. Shen, H. Lin, N. Kong, L. Han, C. Chen, J. Teng, C. Tang and T.-S. Chung, *Chem. Eng. J.*, 2023, **474**, 145579.
361 Z. Huang, D. Ling Zhao, L. Shen, H. Lin, C. Chen, Y. Xu, B. Li, J. Teng, L. Han and T.-S. Chung, *Sci. Bull.*, 2024, **69**, 125–140.